THE APPLICATION OF SCET TO HEAVY QUARKONIUM PHYSICS

by

Xiaohui Liu

B.S., University of Science and Technology of China, 2004

M.S., University of Pittsburgh, 2005

Submitted to the Graduate Faculty of

the Arts and Sciences in partial fulfillment

of the requirements for the degree of

PhD in Physics and Astronomy

University of Pittsburgh

2011

UNIVERSITY OF PITTSBURGH

DEPARTMENT OF PHYSICS AND ASTRONOMY

This dissertation was presented

by

Xiaohui Liu

It was defended on

April 12th 2011

and approved by

Adam Leibovich, Associate Professor

Joseph Boudreau, Associate Professor

Anthony Duncan, Professor

Ira Rothstein, Carnegie Mellon University Professor

Eric Swanson, Associate Professor

Dissertation Director: Adam Leibovich, Associate Professor

THE APPLICATION OF SCET TO HEAVY QUARKONIUM PHYSICS

Xiaohui Liu, PhD

University of Pittsburgh, 2011

In this thesis we explore various heavy quarkonium decay and production processes in certain kinematic regime close to phase space boundaries. Our traditional understanding of heavy quarkonium physics is rooted in the nonrelativistic QCD (NRQCD) formalisms. However close to certain phase space boundaries, NRQCD factorization theorems for quarkonium production or decay break down. This is mainly due to the occurrence of very energetic jet states which are not properly included in the framework of NRQCD, which result in large perturbative and non-perturbative corrections. Discrepancies between NRQCD predictions and experimental results have been observed. Thus in these regions we utilize the soft collinear effective theory (SCET) to derive factorization theorems in which the collinear degrees of freedom will be included correctly meanwhile shape functions describing the internal motion of the heavy quarkonium will arise naturally. Large logarithmic corrections due to several well-separated scales are summed up using renormalization group equations (RGEs). Combining SCET with fixed order NRQCD calculations, we obtain results with better agreement with the experimental data.

TABLE OF CONTENTS

LIST OF TABLES

LIST OF FIGURES

viii

PREFACE

I would like to show my gratitude to a lot of people at this point.

First to my advisor, Prof. Leibovich, for your kindness and inspirational guidance these years, which leads me to this exciting field of effective theories. And to those professors in physics department from both U. Pitt and CMU, for presenting me the wonderful world of physics: from small to large, from perturbative to non-perturbative, from particles to strings, from lower dimensions to extra dimensions, from textbook field theories to the most frontier Ads/CFT.

Also to all my friends who share fun with me all these years in this city, especially to Botao and Qingqing, who help me a lot in my most early and most last days in Pittsburgh, respectively.

Last to C.C.

1.0 INTRODUCTION

The past several decades were fascinating epochs for physicists. Since the 1960s a series of tremendous successes have been achieved in exploring the physical phenomena on length scales less than 10^{-13}cm, which opens up a whole new and colorful subatomic world. Nowadays it is clear that the subatomic world (but still within a domain larger than the Planck length scale) is dominated by three fundamental interactions: strong, weak and electromagnetic, which can be described to a remarkably high accuracy by the Standard Model (SM) of particle physics. The most fundamental constituents comprising the SM are elementary particle fields: three generations of quark fields (top, bottom and etc.), three generations of leptons (electron, electron neutrino and etc.) alongside the gauge bosons (photon, gluon and etc.) carrying the fundamental interactions and a Higgs boson sometimes called the God particle, yet to be detected. Among those particles, free leptons were observed by experiments a long time ago while no isolated quarks or gluons have ever been detected. This phenomenon is known as color confinement, a special feature of the strong nuclear force which quarks and gluons participate in but leptons do not. Color confinement states that no color charged particles like quarks can be isolated singularly. The quarks are glued together by surrounding gluons to form different states of mesons or baryons, collectively called hadrons. The existence of the quarks and gluons can be inferred from the properties of the mesons and baryons. A summary of the properties for the quark sector in the SM is listed in Table 1.

The color confinement hypothesis is believed to be a consequence of the non-abelian characters of quantum chromodynamics (QCD), the sector of the SM relevant for the strong interactions among quarks. A short review on QCD will be given in the next section. According to QCD, mesons and bayons are bound states made up of quark-anti-quark pair

and three quarks in color-singlet configurations respectively. A direct application of QCD to these bound states is very tough due to the nonperturbative structure at low energy, as we will see that the interactions between quarks and gluons become so strong at low energy that QCD can not be understood in a perturbative manner based on a power series expansion of the QCD coupling constant. The situation becomes even more challenging for hadrons containing one or more heavy quarks (bottom or charm quark, whereas top quark is too heavy to form a bound state), where the entanglement of different well seperated energy scales, including the kinematic energy scales set by experiments, adds more complications to the problem. Exploiting QCD perturbative calculations in a brute force manner turns out to be unpractical at high orders. Seemingly desperate though that may be, however, accurate descriptions of QCD are crucial in understanding the nature of hadrons or hunting for new physics beyond the SM. At this point, by excluding the relatively ultraviolet (UV) degrees of freedom, various effective theories have been constructed for different purposes as approximations of QCD in different low energy domains [1, 2, 3, 5, 6, 7, 8]. The absence of UV modes can be compensated by a set of local operators built entirely out of the low energy degrees of freedom in the effective theories. The effective theories need not be renormalizable, however the non-renormalizable terms will be suppressed. Those effective theories could greatly simplify our calculations while still maintaining accuracy to an extent that we demand.

Table 1: A summary of the quark properties in the SM. [4] All quark masses are specified in $\overline{\text{MS}}$ scheme. For the light quarks, the renormalization scale is chosen to be $\mu = 2\text{GeV}$.

name(symbol)	electric charge (e)	mass (mc^2)
up (u)	2/3	$2.49^{+0.81}_{-0.79}\text{MeV}$
down (d)	$-1/3$	$5.05^{+0.75}_{-0.95}\text{MeV}$
charm (c)	2/3	$1.27^{+0.07}_{-0.11}\text{GeV}$
strange (s)	$-1/3$	$104^{+26}_{-34}\text{MeV}$
top (t)	2/3	$171.2^{+2.1}_{-2.1}\text{GeV}$
bottom (b)	$-1/3$	$4.20^{+0.17}_{-0.07}\text{GeV}$

In this thesis, we focus on the applications of one effective theory of QCD, soft collinear

effective theory [5, 6, 7, 8], to several heavy quarkonium decay and production processes. The thesis is organized as follows:

In the rest of this chapter, we will briefly review some basic properties of QCD for self-consistency and introduce the NRQCD, an effective theory designed for mesons composed of two heavy quarks. We will address the successes and difficulties in applying QCD or NRQCD. Also we will review some experiments that inspire the emergence of the SCET. Chapter 2 presents an introduction to the SCET formalisms that will be elaborately used throughout the thesis. Some achievements and novel results of SCET will also be presented in this chapter. Chapter 3 and Chapter 4 are devoted to the study of J/ψ production in e^+e^- annihilation and J/ψ production in Υ decay, the main original work of this thesis. Some relevant work can be found in Ref. [56, 79]. Factorization theorems will be derived in the framework of SCET. We will show how to sum up the large logarithmic corrections using RGEs in SCET. Following that, a chapter on conclusion will be given.

1.1 REVIEW OF QCD

In this section, we give a short review on QCD, the non-abelian $SU(3)_c$ sector of the SM. At the Lagrangian level, QCD is formulated in terms of quarks and gluons given by

$$\mathcal{L}_{\text{QCD}} = -\frac{1}{2}\text{Tr}\left[G_{\mu\nu}G^{\mu\nu}\right] + \sum_i^{n_f} \bar{q}_i \left(i\slashed{D} - m_i\right) q_i, \tag{1.1}$$

in a renormalizable form similar to quantum electromagnetics (QED). In this equation, the four-component dirac spinors q_i are the quark fields, with i traversing all six flavors listed in Table 1. Each spinor is in the fundamental representation of $SU(3)_c$. The generators of the fundamental representation are denoted as T^a obeying $[T^a, T^b] = if^{abc}T^c$ and being normalized to $\text{Tr}[T^aT^b] = 1/2\delta^{ab}$. The gauge field tensor $G_{\mu\nu} = \partial_\mu A_\nu - \partial_\nu A_\mu + ig_s[A_\mu, A_\nu]$ with $A_\mu = \sum_{a=1}^8 A_\mu^a T^a$ the gluon fields living in the adjoint representation of $SU(3)_c$ group and g_s is the strong coupling parameter. The interactions between quarks and gluons are embedded in the covariant derivative $D_\mu = \partial_\mu + ig_s A_\mu$.

The QCD Lagrangian density in Eq. (1.1) is invariant under the gauge transformation $U(x) = \exp[iT^a\theta^a(x)]$

$$q_i(x) \rightarrow U(x)q_i(x)\,, \tag{1.2}$$

$$A_\mu \rightarrow U(x)A_\mu U^{-1}(x) + \frac{i}{g_s}\left(\partial_\mu U(x)\right)U^{-1}(x)\,. \tag{1.3}$$

The gauge invariance brings such redundancy to the theory, which acts as more an obstacle than an advantage in quantizing QCD. An elegant and convenient approach to quantizing QCD was given by Faddeev and Popov [9] using the functional path integral formalism

$$Z = \int \mathcal{D}A_\mu^a \mathcal{D}\bar{q}_i \mathcal{D}q_i\, e^{i\int \mathrm{d}^4 x \mathcal{L}_{\mathrm{QCD}}[A_\mu^a, q_i, \bar{q}_i]}\,. \tag{1.4}$$

At this stage the integral in the equation above is not well defined in the sense that we are integrating over all possible field configurations including fluctuations obtained by gauge transformations[1]. We are not allowed to integrate over the unphysical fluctuations along gauge symmetry directions, which will overcount the result when we perform the integration Z and in our case there are an infinite number of duplicates. Mathematically, the gauge transformation defines an equivalence relation on the gauge field configuration space. Any two fields differing only by a gauge transformation are physically equivalent to each other and fall into the same equivalence class. Intuitively, the functional integral in Eq. (1.4) can be factorized into a product of an integral over all possible equivalence classes satisfying some given gauge condition ($F[A^a] = \omega$) and an integral over all possible gauge transformaions which only contributes to an overall factor and drops off safely. In general, a gauge transformation corresponds to a change of variables in the integral over the equivalence classes which gives rise to the Faddeev-Popov determinant $\det[\delta F[A^a]/\delta\theta^b]$. As a consequence, two extra terms must be added to the Lagrangian for deriving Feynman rules [2]

$$\mathcal{L}_{\mathrm{fix}} = -\frac{1}{2\xi}F^2\,,$$

$$\mathcal{L}_{\mathrm{ghost}} = -\bar{\eta}_a\frac{\delta F[A^a]}{\delta\theta^b}\eta^b\,. \tag{1.5}$$

---

[1]In addition, the integrand is also strongly oscillatory which can be resolved by Wick rotating to Euclidean space.

[2]A third extra term $\mathcal{L}_{CP} = \theta\epsilon^{\mu\nu\rho\sigma}G_{\mu\nu}^a G_{\rho\sigma}^a$ may also be added to the Lagrangian without violating gauge symmetry or renormalizability. However this term violates CP. It can contibute to the neutron electric dipole moment and experiments shows that $\theta \ll 10^{-9}$ leading to the strong CP problem.

The first is the gauge fixing term with $F[A^a]$ some specified gauge choice. Convenient choices of F are the covariant gauge $F[A^a] = \partial \cdot A^a$ and the physical gauge $F[A^a] = n \cdot A^a$. The parameter ξ can be chosen arbitrarily since the dependence of ξ will eventually cancel in any gauge invariant calculations. The covariant gauge with $\xi = 1$ corresponds to the Feynman gauge. Keeping ξ explicit serves as a useful check on the arithmetic. The second term in Eq. (1.5) is the ghost density in which η_a are the unphysical ghost fermions that anticommute and only show up in loops. The existence of the ghost term is crucial in covariant gauges for maintaining gauge invariance and unitarity of the S-matrix in QCD.

The QCD Feynman rules are summarized in fig. 1. From the Feynman rules we can see that unlike the charge neutral photon in QED, the force-carrying gluons in QCD carry color charges and have tree- and four-point self interactions. This fact has a profound impact.

In QED, the electric charge grows with the energy scale (Landau pole problem) due to the screening effect by the surrounding polarized virtual e^+e^- pairs generated in the vacuum. On the contrary, in QCD, since the gluons carry color charges, they introduce anti-screening effects that overcome the screening produced by the quarks. As a result, the strong running coupling $\alpha_s = g_s^2/(4\pi)$ decreases at short distance or equivalently at high energy but increases at low energy scale, which is known as asymptotic freedom [10]

$$\mu \frac{\mathrm{d}}{\mathrm{d}\mu} \alpha_s(\mu) = \beta(\alpha_s) = -2\alpha_s(\mu) \left(\frac{\alpha_s(\mu)}{4\pi} \beta_0 + \left(\frac{\alpha_s(\mu)}{4\pi} \right)^2 \beta_1 + \dots \right), \tag{1.7}$$

with $\beta(\alpha_s)$ being negative as a reflection of the anti-screening effect. Calculated perturbatively, $\beta_0 = 11C_A/3 - 2n_f/3$ and $\beta_1 = 34C_A^2/3 - 10C_A n_f/3 - 2C_F n_f$. Quantum effects have generated an intrinsic energy scale, Λ_{QCD}, in QCD at which the inverse strong coupling $\alpha_s^{-1}(\Lambda_{\mathrm{QCD}}) \to 0$. To the first order accuracy, Eq. (1.7) gives

$$\Lambda_{\mathrm{QCD}}^2 = \frac{\mu^2}{e^{4\pi/(\beta_0 \alpha_s(\mu))}}. \tag{1.8}$$

Asymptotic freedom has long been tested against experiments. The fact that the strong coupling runs with energy scale in a way predicted by QCD is demonstrated by experiments as can be seen in fig. 2. Experimentally Λ_{QCD} is found to be around 200MeV. The discovery of asymptotic freedom was a triumph of QCD as a field theory for the strong interactions.

5

$$i \xrightarrow{\quad p \quad} j \qquad = \quad \delta_{ij}\frac{i}{\not{p}-m+i\epsilon}$$

$$\overset{a}{\underset{\mu}{}} \overset{q}{\text{0000000000}} \overset{b}{\underset{\nu}{}} \qquad = \quad \delta_{ab}\frac{-ig^{\mu\nu}}{q^2+i\epsilon}$$

$$i \xrightarrow{\qquad\qquad} j \qquad = \quad ig_s T^a_{ij}\gamma^\mu \qquad (\mu, a)$$

$$\nu,b,p \quad\quad \rho,c,q \qquad = \quad g_s f^{abc}\left[g^{\mu\nu}\left(k-p\right)^\rho + g^{\nu\rho}\left(p-q\right)^\mu + g^{\rho\mu}\left(q-k\right)^\nu\right] \qquad (\mu,a,k)$$

$$\rho,c \quad\quad \nu,b \qquad = \quad -ig_s\left[f^{abe}f^{cde}\left(g^{\mu\rho}g^{\nu\sigma}-g^{\mu\sigma}g^{\nu\rho}\right) + (b\leftrightarrow c,\nu\leftrightarrow\rho) + (c\leftrightarrow d,\rho\leftrightarrow\sigma)\right] \qquad (\mu,a)(\sigma,d)$$

$$a,k \quad\quad c \qquad = \quad -g_s f^{abc}k^\mu \qquad (\mu,b)$$

$$a \xrightarrow{\quad k \quad} b \qquad = \quad \delta_{ab}\frac{i}{k^2+i\epsilon} \tag{1.6}$$

Figure 1: QCD Feynman rules in covariant gauge.

It explains the validity of the parton picture of deep inelastic scattering [12] and provides plausibility for color confinement.

However in practice, asymptotic freedom is like a double-edged sword. On the one side it ensures that we are safe to calculate quantities such as parton level cross sections perturbatively in QCD at sufficiently large energy scales; on the other side it implies that the way
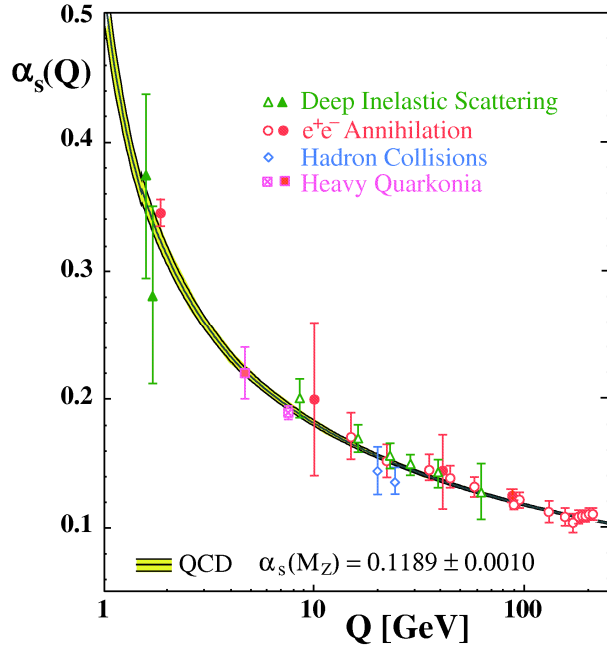
Figure 2: Experimental tests of asymptotic freedom [11]. The theoretical curve is based on a 4-loop approximation in QCD.

quarks and gluons hadronize is purely nonperturbative. Hence the predictive power based on perturbation methods for real processes in nature involving hadrons remains questionable. There still exist subtleties even in applying fully perturbative calculations at the parton level. In the situation that some energy scale $\sqrt{s}$ is much larger than the quark mass m, the calculations beyond leading order (LO) are always plagued by infrared (IR) divergences owing to the existence of many degenerate states produced by emitting soft and collinear particles. Those difficulties lead to the concepts of factorization and IR safe quantities.

Factorization is a way that in certain cases we can disentangle the soft (low energy) effects from the temporaneously localized hard (high energy) processes and write quantities such as cross sections σ as convolutions of partonic kernels $\hat{\sigma}_i$ and universal hadronic wave functions $\phi_{i/H}$ to all orders

$$\sigma \sim \sum_{\text{partons } i} \hat{\sigma}_i(x, \mu) \otimes \phi_{i/H}(x, \mu) . \tag{1.9}$$

7

Some IR divergences are absorbed by the wave functions $\phi_{i/H}$. The hard kernels $\hat{\sigma}_i$ and the evolutions of the hadronic functions can be calculated perturbatively while the soft hadronic functions are non-perturbative and have to be determined via measurements or lattice QCD simulations.

IR safe quantities satisfy the condition

$$\sigma\left(\frac{s}{\mu^2},\frac{m^2}{\mu^2},\alpha_s(\mu)\right) = \sigma\left(\frac{s}{\mu^2},0,\alpha_s(\mu)\right)\left\{1+\mathcal{O}\left(\left(\frac{m^2}{s}\right)^a\right)\right\},a>0\,,\qquad(1.10)$$

where m represents the mass of the light quark or some IR regulator for massless gluon. There exist subtle cancellations between IR divergences from virtual corrections and real emissions for IR safe quantities, for instance the hadronic total cross section of e^+e^- annihilation. In practice we are always interested in applying perturbation methods to compute quantities free of IR singularites. For less inclusive processes, the cancellation may be imperfect in some regions, especially near certain phase space boundaries and results in large Sudakov logarithms of the form $\alpha_s^n \log^{2n-m}\tau$ with $\tau \ll 1$ spoiling perturbative calculations. Therefore in order to use asymptotic freedom consistently, we must sum up these logarithms by reorganizing the perturbation series.

In QCD, factorization and IR safety can be proved or disproved, process to process, rigorously in the language of the Landau equation [13], Coleman-Norton theorem [14], reduced diagram, pinch surface and IR power counting. The proofs are not easy. For a review on this subject, see [15]. In the rest of this thesis, you will see that effective theories provide powerful tools for deriving factorization theorems and summing up large logarithms.

1.2 THE SUCCESSES AND THE DIFFICULTIES OF NRQCD

Studies of the heavy quarkonium (a bound state of heavy quark-anti-quark $Q\bar{Q}$ pair) spectrum suggested that the quarkonium kinematics can be described in a nonrelativistic picture characterized by the heavy quark velocity $v \ll 1$. This introduces a hierarchy of energy scales: the heavy quark mass $M_Q \gg \Lambda_{\text{QCD}}$, setting the scale for $Q\bar{Q}$ creation or annihilation, the momentum $M_Q v$, which is the inverse of the bound state typical size, and the kinetic

energy $M_Q v^2$, fixing the interaction time between the two heavy constituents inside $Q\bar{Q}$ bound states. The difficulties in understanding the physics of quarkonia originate from the entanglement of those multiple energy scales.

To smooth away the complexities, the effective theory NRQCD [3] was designed to systematically keep track of this scale hierarchy based on a double power expansion in the strong coupling α_s and the velocity parameter v. Starting from the Lagrangian $\mathcal{L}_{\mathrm{QCD}}$ in Eq. 1.1, NRQCD is constructed by integrating out relativistic heavy quarks, as well as gluons and light quarks with momenta of order M_Q from QCD. The effects due to removing the relativistic modes can be compensated by adding nonrenormalizable local terms to the NRQCD Lagrangian restricted by the symmetries of the effective theory. For practical purposes, a redefinition of the heavy quark fields in Eq. (1.1) through a unitary transformation, named the Foldy-Wouthuysen-Tani transformation, is useful for deriving the NRQCD Lagrangian

$$q_i \rightarrow \exp\left(-i\boldsymbol{\gamma}\cdot\boldsymbol{D}/(2m_Q)\right)q_i\,. \tag{1.11}$$

The NRQCD Lagrangian is written in terms of two-component Pauli spinors

$$\mathcal{L}_{\mathrm{NRQCD}} = \psi^\dagger\left(iD_t + \frac{\boldsymbol{D}^2}{2M_Q}\right)\psi + \chi^\dagger\left(iD_t - \frac{\boldsymbol{D}^2}{2M_Q}\right)\chi + \mathcal{L}_{\mathrm{light}} + \delta\mathcal{L}\,, \tag{1.12}$$

where ψ (χ) is the spinor field that annihilates (creates) a heavy quark (anti-quark). $\mathcal{L}_{\mathrm{light}}$ is identical to $\mathcal{L}_{\mathrm{QCD}}$ by turning off the mass terms and $\delta\mathcal{L}$ is the correction term whose exact form up to dimension $d = 6$ can be found in [3].

The NRQCD factorization formula shows that the inclusive production cross section or the decay rate for heavy quarkonium state H can be written as

$$d\sigma(H) = \sum_n d\sigma(n, Q\bar{Q})\langle\mathcal{O}(n, H)\rangle\,. \tag{1.13}$$

Here $d\sigma(n, Q\bar{Q})$ is the cross section or the decay rate for $Q\bar{Q}$ pair which can be calculated using perturbative QCD. The way how the $Q\bar{Q}$ pair evolves into state H is encoded in various nonperturbative matrix elements $\langle\mathcal{O}(n, H)\rangle$. $\langle\mathcal{O}(n, H)\rangle$ are universal and known as the NRQCD matrix elements, each scaling differently with the velocity v. Provided that v is sufficiently small, the series (1.13) can be truncated at a given order in v. Only a finite number of the matrix elements contribute, which ensures the predictive power of NRQCD.

A series of scaling rules for specific matrix elements can be found in [16] and [17]. The values for the matrix elements can be extracted from experiments. The heavy $Q\bar{Q}$ pair need not be in a color-singlet state and the sum is over all possible color, spin and angular momentum configurations. The presence of color-octet states is necessary for absorbing logarithmic infrared divergences [3].

The operators in Eq. (1.13) can not be mixed 2-fermion operators involving χ and ψ, since such an operator annihilates a $Q\bar{Q}$ pair and gives birth to light partons with energies of order M_H which have been integrated out of this effective theory. However the annihilation of $Q\bar{Q}$ pair can be related to the imaginary parts of $Q\bar{Q} \to Q\bar{Q}$ amplitudes through the optical theorem. Therefore, the operators relevant in Eq. (1.13) are the 4-fermion operators in the NRQCD Lagrangian with the general form

$$\mathcal{O}(n, H) = \chi^\dagger \Gamma_n \psi a_H^\dagger a_H \psi^\dagger \Gamma'_n \chi \,, \tag{1.14}$$

where Γ_n and Γ'_n contain information of spin, color and intrinsic dynamics. $a_H^\dagger a_H$ is the projection operator. In heavy quarkoniom H decay, the operator is a unit operator. In production processes, it projects onto states in the far future that contain H and other light partons

$$a_H^\dagger a_H = \sum_X |H + X\rangle\langle H + X| \,. \tag{1.15}$$

A set of the lowest dimension (dimension 6) operators is listed below

$$\begin{aligned}
\mathcal{O}_1\left({}^1S_0\right) &= \chi^\dagger \psi a_H^\dagger a_H \psi^\dagger \chi \\
\mathcal{O}_8\left({}^1S_0\right) &= \chi^\dagger T^a \psi a_H^\dagger a_H \psi^\dagger T^a \chi \\
\mathcal{O}_1\left({}^3S_1\right) &= \chi^\dagger \sigma^i \psi a_H^\dagger a_H \psi^\dagger \sigma_i \chi \\
\mathcal{O}_8\left({}^3S_1\right) &= \chi^\dagger \sigma^i T^a \psi a_H^\dagger a_H \psi^\dagger \sigma_i T^a \chi \,.
\end{aligned} \tag{1.16}$$

Here the subscripts denote the color configurations.

NRQCD enjoyed its successes in analyzing various ψ and Υ production channels [17, 18, 19]. Before the invention of NRQCD, quarkonium productions were studied using the
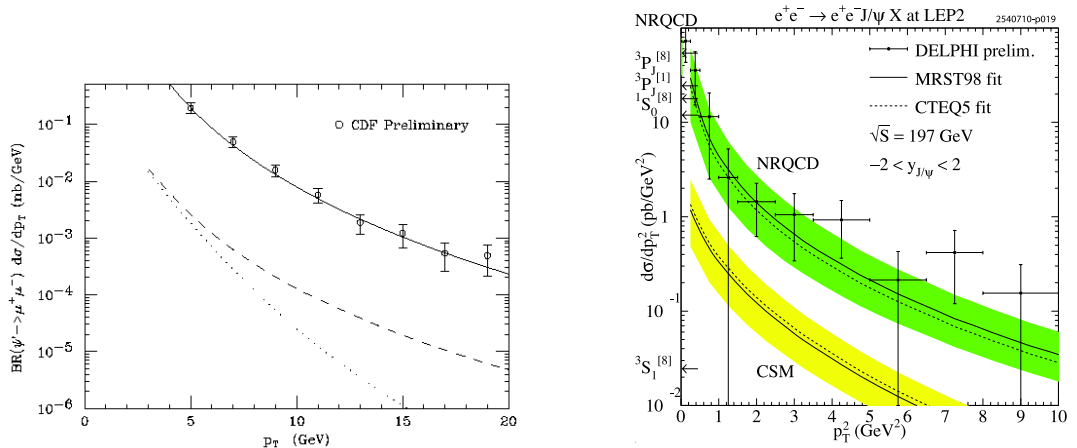
Figure 3: Comparison between the experimental measurements of cross section differential in p_T spectrum, color-singlet model and NRQCD predictions for ψ' production at Tevatron (left, dotted line: LO color singlet model; dashed line: fragmentation and LO; solid curve: color octet mechanism fragmentation) [18] and $\gamma\gamma$ production of J/ψ (right) [19]. The data favor the NRQCD predictions.

color-singlet model, which coincides with Eq. (1.13) by excluding the color-octet contributions. Remarkable discrepencies between color-singlet model predictions and experimental measurements were observed. For instance, the color-singlet prediction based on a fragmentation approximation underestimates the CDF measurements of direct ψ' production cross section [20] by more than an order of magnitude. The same story seems to happen in the $\gamma\gamma$ production of the J/ψ by the DELPHI collaboration [21] while in this case a complete next to leading order (NLO) calculation is needed to draw conclusions. By introducing the color octet mechanism, NRQCD opens up the possibilities to solve those problems [18, 19]. As we can see from fig. 3, the experimental data seem to favor the NRQCD predictions. A similar situation occurs to the Υ production p_T spectrum at Tevatron [17].

Though NRQCD is capable of handling the differential cross sections, the framework is severely challenged by the experimental polarization measurements for heavy quarkonium production at Tevatron [22] and RHIC [23]. As first predicted by Cho and Wise [24], the inclusive ψ' production at the Tevatron at sufficiently large p_T is dominated by gluon fragmentation. The fragmenting gluon is almost on shell and thus nearly 100% transversely polarized. The spin symmetry [3] of the nonrelativistic heavy quarks implies that the ψ'

11

produced through a fragmenting gluon to a color octet configuration is predominantly transversely polarized, inheriting the spin of the gluon. The same argument holds for other $J^{PC} = 1^{--}$ state quarkonium. The polarization can be infered from measuring the angular distribution in $\psi\prime \to l^+l^-$, which behaves as $1 + \alpha\cos^2\theta$, with $\alpha = 1$ corresponding to totally transversely polarized. The argument was demonstrated quantitatively by explicit calculations in NRQCD [25, 26, 27, 28] predicting a rise in α with increasing p_T. However this feature was not captured by the experiemnts; instead, the present data tend to favor negative α at large p_T, deviating from the NRQCD prediction at the 3σ level. Some efforts have been devoted to resolve this disparity, there is no satisfactory solution to the polarization problem as of yet. The most recent review involving this subject can be found in [29].

NRQCD has also been applied to study heavy quarkonium decay. In fig. 4, we show the result extracted from [30] for radiative Upsilon decay $\Upsilon \to \gamma X$ spectrum with data from CLEO. The theoretical curves are based on the calculations of the NRQCD factorization formalism along with photon fragmentation. In the low range $z = E_\gamma/M_b < 0.3$, the dominant contribution is from fragmentation in which the photon is emitted through final state light quarks splitting [32]. The α^2 suppression in fragmention is compensated by a double logarithmic enhancement leading to a contribution at least the same order as the lowest order direct production. The photon spectrum is well described by the direct production in the intermediate range of the spectrum $0.3 < z < 0.7$ using the NRQCD formula, in which the photon comes from the heavy quark directly. Clearly from fig. 4, the spectrum at large values of $z > 0.7$ is poorly understood under the scheme of NRQCD. Similar problem arises in the spectrum of the J/ψ production in Υ decay [33] as shown in fig. 5: the enhancement predicted by NRQCD near the kinematic end-point is not observed in data.

The problems near the end-point may be alleviated by replacing the NRQCD matrix elements by hadronic shape functions accounting for the internal soft dynamics in the heavy meson. The shape functions arise due to the resummation of certain operator matrix elements of higher order in v. Shape functions have effects only in a small region near the end-point and act as a realization of the phenomenological idea of the "Fermi motion" of the heavy quarks inside the bound state. However shape functions are not sufficient for solving all problems, and we need an intermediate theory to deal carefully with extra degrees of freedom that
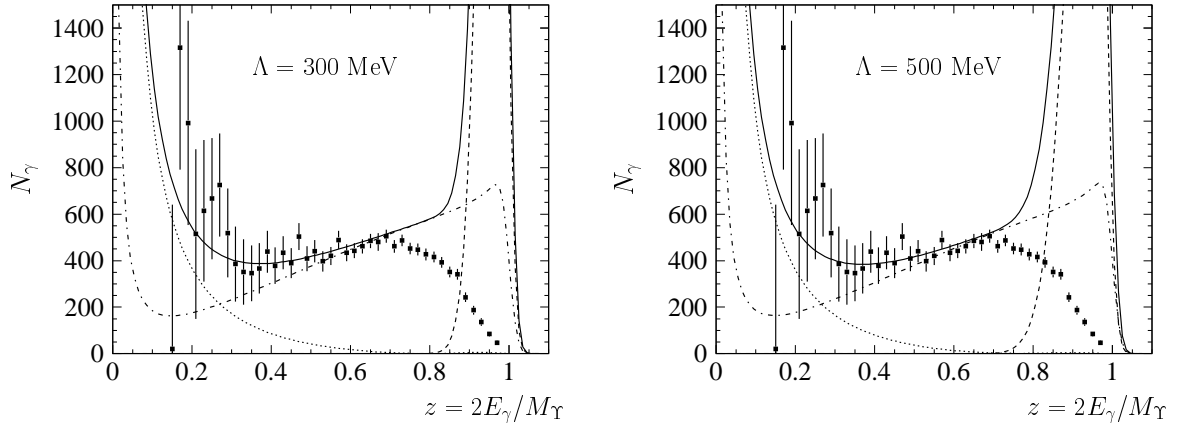
Figure 4: Comparison of the theoretical spectrum (solid line) for $\Lambda_{\mathrm{QCD}} = 300$ MeV (left) and $\Lambda_{\mathrm{QCD}} = 500$ MeV (right) with data of CLEO [31]. The dashed line shows the direct, the dotted line the fragmentation contribution. The spectrum predicted by the NRQCD(direct production and fragmentation, without hadronization models) is indicated by the dash-dotted curvature.

emerge near the end-point.

The main reason for the breakdown of NRQCD formalism near the end-point is because this effective theory does not contain the correct degrees of freedom. The collinear fields that emerge in certain phase space region are missing from the NRQCD framework. Recently it has been understood that the suitable effective theory that can correctly describe the physics in this regime is a combined one incorporating both NRQCD for the heavy quarks and the soft collinear effective theory (SCET) [5, 6, 7, 8] for the highly energetic collinear modes. We now turn to an introduction of SCET in the following chapter.
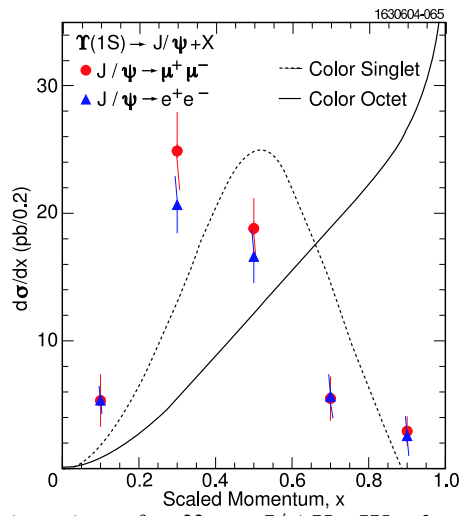
Figure 5: Differential cross sections in x for $\Upsilon \to J/\psi X$. We show the theoretical expectations based on the color-octet (solid line) and color-singlet (dashed line) models.

2.0   SOFT COLLINEAR EFFECTIVE THEORY

Soft collinear effective theory (SCET) is an effective QCD framework suitable for studying phenomena involving interactions among highly energetic collinear particles as well as the ones between collinear and soft or ultrasoft (usoft) degrees of freedom. The situation typically occurs on the phase space boundaries in heavy meson decay cases like Υ decay or collision experiments at large energy, for instance at the LHC. SCET was first developed to resum Sudakov logarithms. It is constructed by realizing that in addition to the hard scale set by the b quark mass m_b and the usoft scale Λ_{QCD}, another scale $\sqrt{m_b \Lambda_{\mathrm{QCD}}}$ of the order of the collinear particle offshellness plays an important role in this region. The naive expansion in powers of $\Lambda_{\mathrm{QCD}}/m_b$ fails due to the existence of this intermediate scale. SCET saves the predictive power of perturbative QCD by including the collinear scale $\sqrt{m_b \Lambda_{\mathrm{QCD}}}$. It provides us with a systematic way to power count as well as a convenient tool to derive factorization thereoms. Usually, in SCET a two-step matching is needed: from the hard scale to the collinear scale and then from the collinear to the (u)soft physics. For more complicated cases, extra matching procedures may be needed. Through matching, hadronic shape functions and jet functions for collinear fields emerge naturally.

This chapter serves as a systematic review of SCET. Conventions and techniques used in the rest of this thesis will be explained here. Some calculations will be presented in detail. Therefore, this chapter could be tedious. For humanitarian considerations, this chapter is divided into several sections.

2.1 PHYSICAL DEGRESS OF FREEDOM

First we identify the relevant physical degrees of freedom used to formulate SCET. It will be convenient to work in the light-cone coordinate system due to the presence of relativistic particles with small invariant mass. The light-cone coordinate system includes two light-cone directions that satisfy

$$n^2 = \bar{n}^2 = 0, \quad n \cdot \bar{n} = 2 \,. \tag{2.1}$$

For particles moving along the $\pm z$-axis, the associated light-cone directions can be chosen as $n = (1, 0, 0, 1)$ and $\bar{n} = (1, 0, 0, -1)$. Any four vector can be decomposed into these two light-cone directions plus the transverse direction

$$p^\mu = \frac{n \cdot p}{2} \bar{n}^\mu + \frac{\bar{n} \cdot p}{2} n^\mu + p_\perp^\mu \,. \tag{2.2}$$

Thus we denote an arbitrary vector using the notation $p = (p^+, p^-, p_\perp) \equiv (n\cdot p, \bar{n}\cdot p, p_\perp)$, with the first two being the light-cone components along $\bar{n}$ and n respectively and the third entry the transverse component. For highly relativistic particles, the three light-cone components of the momentum are widely separated in scale. Taking the collinear mode moving in the $+z$-direction as an example, its momentum components scale as

$$\text{coll} : p_c = (p_c^+, p_c^-, p_c^\perp) \sim Q(\lambda^2, 1, \lambda) \,, \quad m_c^2 = p_c^2 \sim Q^2 \lambda^2 \,, \tag{2.3}$$

with Q being the large scale like the b quark mass in Upsilon or B meson decay. Here we have introduced a small power counting parameter $\lambda \sim p_\perp/Q$ which plays a similar role as the velocity parameter v in NRQCD. The physical degrees of freedom showing up in SCET can be categorized according to the way their momenta scale in λ. In addition to the collinear mode, we also have soft and usoft modes in SCET, whose momenta scale as

$$\begin{aligned}
\text{soft} &: p_s \sim Q(\lambda, \lambda, \lambda) \,, \quad p_s^2 \sim Q^2 \lambda^2 \,, \\
\text{usoft} &: p_{us} \sim Q(\lambda^2, \lambda^2, \lambda^2) \,, \quad p_{us}^2 \sim Q^2 \lambda^4 \,.
\end{aligned} \tag{2.4}$$

We note that the (non)necessity of different types of fields could be different case by case, which is identified by studying the kinematics of the particular process that we are interested in.
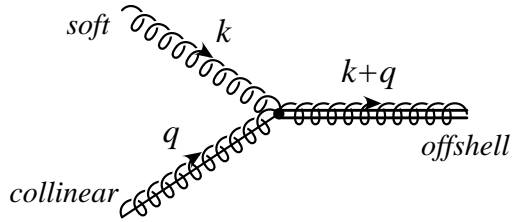
Figure 6: The interaction of a soft and collinear gluon with momenta $k \sim Q(\lambda, \lambda, \lambda)$ and $q \sim Q(\lambda^2, 1, \lambda)$ respectively, to produce an offshell gluon with momentum $k + q \sim Q(\lambda, 1, \lambda)$. [8]

2.2 SCET$_{\mathrm{I}}$ AND SCET$_{\mathrm{II}}$

We emphasize that the size of the parameter λ depends on the type of problem we are considering. For example, in inclusive decays the typical size of the parameter is $\lambda \sim \sqrt{\Lambda_{\mathrm{QCD}}/Q}$. In exclusive processes, on the other hand, one typically has the transverse momentum of the energetic hadron scale as $p_\perp \sim \Lambda_{\mathrm{QCD}}$, therefore $\lambda \sim \Lambda_{\mathrm{QCD}}/Q$. These two different parameter sizes introduce two different types of effective theory, SCET$_{\mathrm{I}}$ and SCET$_{\mathrm{II}}$ [34], respectively. In SCET$_{\mathrm{II}}$, there exist no usoft modes because such degrees of freedom would correspond to color fields with virtuality of order $\Lambda_{\mathrm{QCD}}^2/Q$, which do not appear in QCD due to confinement.

From the momentum scaling rules, we notice that a collinear field can interact with a usoft mode locally without being knocked off its mass shell too much. However there are no local interactions between collinear and soft fields, since interactions of this kind will kick the collinear mode offshell by an order of $Q^2\lambda \gg Q^2\lambda^2$. Therefore to construct SCET$_{\mathrm{II}}$ directly from QCD, one must integrate out this far offshell mode. An example for a triple gluon vertex with a collinear and soft gluon is shown in fig. 6, in which an offshell gluon with momentum $p \sim Q(\lambda, 1, \lambda)$ is produced and should be integrated out of the theory [8].

Alternatively, SCET$_{\mathrm{II}}$ can be obtained more conveniently by treating it as a low energy effective theory of SCET$_{\mathrm{I}}$, by integrating out fluctuations around the order of $\sqrt{Q\Lambda_{\mathrm{QCD}}}$ [34]. The soft mode in SCET$_{\mathrm{II}}$ is nothing but the usoft degrees of freedom in SCET$_{\mathrm{I}}$ and we will

see that via a field redefinition all usoft modes can be decoupled from the collinear ones and factorized into the so-called usoft Wilson lines. Thus the matching from SCET_I to SCET_II can simply be achieved by lowering the size of the parameter λ from $\sqrt{\Lambda_\text{QCD}/Q}$ to Λ_QCD/Q and replacing the usoft Wilson lines with the soft ones [34].

We note that the decoupling of the usoft and collinear fields is crucial for this matching procedure to be trivial. When matching off the mass shell, extra modes such as the soft-collinear messenger [35] or a particular choice of the infrared regulator [36] should be introduced in order to correctly reproduce all the infrared structures of QCD in SCET_II, since the offshellness spoils the decoupling theorem.

2.3 SCET LAGRANGIAN AND POWER COUNTING

In this section we turn to the construction of the SCET Lagrangian focusing on the SCET_I case. We start from the quark sector in the QCD Lagrangian in Eq. (1.1).

We first remove the large momentum fluctuations by defining a new field $q_{n,p}$

$$q(x) = \sum_{\tilde{p}} e^{-i\tilde{p}\cdot x} q_{n,p} \, . \tag{2.5}$$

Here we split the momentum q carried by the collinear quark into a large part and residual momentum

$$p^\mu = \tilde{p}^\mu + k^\mu \, , \quad \text{with} \quad \tilde{p}^\mu = \frac{1}{2} p^- n^\mu + p_\perp^\mu \, , \tag{2.6}$$

where the momenta scaling like $\mathcal{O}(1)$ and $\mathcal{O}(\lambda)$, denoted by $\tilde{p}$, are treated as the large parts while the residual momenta k^μ representing the fluctuation of an order $\lambda^2 \sim \Lambda_\text{QCD}$ are dynamical. In principle, by the scaling rule the label momentum can not be zero, $\tilde{p} \neq 0$. The new field $q_{n,p}$ is labeled by its large momentum and the direction of motion.

We further project out the large components $\xi_{n,p}$ and the small components $\chi_{\bar{n},p}$ of the newly defined Dirac field $q_{n,p}$, using projection operators

$$\xi_{n,p} = \frac{\slashed{n}\slashed{\bar{n}}}{4} q_{n,p} \, , \quad \chi_{\bar{n},p} = \frac{\slashed{\bar{n}}\slashed{n}}{4} q_{n,p} \, . \tag{2.7}$$

18

The Lagrangian for massless collinear quarks can be expressed in terms of $\xi_{n,p}$ and $\chi_{\bar{n},p}$

$$\mathcal{L} = \sum_{\tilde{p},\tilde{p}'} e^{i(\tilde{p}'-\tilde{p})\cdot x} \left\{ \bar{\xi}_{n,p'} \frac{\slashed{\bar{n}}}{2} \left(in\cdot D\right)\xi_{n,p} + \bar{\chi}_{\bar{n},p'} \frac{\slashed{n}}{2}\left(\bar{n}{\cdot}p + i\bar{n}\cdot D\right)\chi_{\bar{n},p} \right.$$
$$\left. + \bar{\xi}_{n,p'}\left(\slashed{p}_\perp + i\slashed{D}_\perp\right)\chi_{\bar{n},p} + \bar{\chi}_{\bar{n},p'}\left(\slashed{p}_\perp + i\slashed{D}_\perp\right)\xi_{n,p} \right\} . \tag{2.8}$$

In this equation, the derivatives ∂_μ acting on the fermonic field $\chi_{\bar{n},p}$ scale as the residual momenta $k^\mu \sim \lambda^2$. Thus the kinetic terms for $\chi_{\bar{n},p}$ is suppressed relative to $\bar{n}{\cdot}p$ and $p_\perp$. As a result the small components $\chi_{\bar{n},p}$ are not dynamical but auxiliary and we can eliminate them at tree level using the equation of motion

$$\chi_{\bar{n},p}(x) = \frac{1}{\bar{n}{\cdot}p + i\bar{n}\cdot D}\left(\slashed{p}_\perp + i\slashed{D}_\perp\right)\frac{\slashed{\bar{n}}}{2}\xi_{n,p}(x) . \tag{2.9}$$

The inverse operator is understood to solve the equation of motion in a perturbative way. Replacing the auxiliary field $\chi_{\bar{n},p}$ in Eq. (2.8) by $\xi_{n,p}$ using the equation above gives the Lagrangian for the collinear quarks in SCET

$$\mathcal{L}_\xi = \sum_{\tilde{p}\tilde{p}'} e^{i(\tilde{p}'-\tilde{p})\cdot x} \bar{\xi}_{n,p'}\left\{ in\cdot D + \left(\slashed{p}_\perp + i\slashed{D}_\perp\right)\frac{1}{\bar{n}{\cdot}p + i\bar{n}\cdot D}\left(\slashed{p}_\perp + i\slashed{D}_\perp\right)\right\}\frac{\slashed{\bar{n}}}{2}\xi_{n,p} . \tag{2.10}$$

The overall phase is highly oscillatory compared with the slowly varying fields, which enforces the conservation of the label momenta since

$$\int \mathrm{d}^4 x\, e^{i(p'-p)\cdot x} = \delta^{(3)}_{\tilde{p}',\tilde{p}} \int \mathrm{d}^4 x\, e^{i(k'-k)\cdot x} . \tag{2.11}$$

We pause here and switch to discuss the power counting rules for the fields appearing in SCET. The rules can be obtained by demanding that in equations

$$\int \mathrm{d}^4 x\, e^{ip\cdot x}\langle 0|\mathrm{T}[q(x)\bar{q}(0)]|0\rangle = \frac{i\slashed{p}}{p^2 + i\epsilon} ,$$
$$\int \mathrm{d}^4 x\, e^{iq\cdot x}\langle 0|\mathrm{T}[A^\mu(x)A^\nu(0)]|0\rangle = \frac{i}{q^2 + i\epsilon}\left(-g^{\mu\nu} + \eta\frac{q^\mu q^\nu}{q^2}\right) , \tag{2.12}$$

the scaling of the components on the right hand side agree with the ones on the left. For instance for collinear fermonic fields, the right hand scales as λ^{-2}. On the left hand side, we have, from the commutation relation, $x_c^+ \sim 1$, $x_c^- \sim \lambda^{-2}$ and $x_c^\perp \sim \lambda^{-1}$ hence $\mathrm{d}^4 x_c \sim \lambda^{-4}$. Therefore $\xi_{n,p}$ has to scale as λ to make the scaling on both sides agree. The power counting rules in λ for SCET fields are summarized in Table 2. There is some freedom in choosing

Table 2: Power counting rules for SCET fields.

Type	momenta	fields	field scaling
collinear	$p_c^\mu \sim Q(\lambda^2, 1, \lambda)$	$\xi_{n,p}$	λ
		$(A_{n,q}^+, A_{n,q}^-, A_{n,q}^\perp)$	$(\lambda^2, 1, \lambda)$
usoft	$p_{us}^\mu \sim Q(\lambda^2, \lambda^2, \lambda^2)$	q_{us}	λ^3
		A_{us}^μ	λ^2
soft	$p_s^\mu \sim Q(\lambda, \lambda, \lambda)$	q_s	$\lambda^{3/2}$
		A_s^μ	λ

the scaling rule for the collinear gauge field. The rule used in SCET is preferred due to the advantage that as long as A_c^μ scales the same way as a collinear momentum there are no interactions that will scale as λ^{-1}.

Now we return to the discussion about the SCET Lagrangian to determine the interactions between fermonic fields and different types of gauge bosons in the effective theory. From Table 2, we can see that the soft gluons can not appear in the Lagrangian in Eq. (2.10) since it will cause inconsistency in power counting. For instance, there is no way to maintain the power counting rules as well as the conservation law of the label momenta in Eq. (2.10) for terms involving both soft and collinear modes. Meanwhile the usoft gluons only contribute to the first term in Eq. (2.10), which leads to interactions of the same form as the ones in QCD among quarks and gluons. Other usoft contributions are relatively suppressed according to power counting rules.

The collinear gluon fields can be manipulated in the same manner as the collinear quarks. We extract the large momentum by defining a new field $A_c^\mu(x) = \sum_{\tilde{q}} e^{-i\tilde{q}\cdot x} A_{n,q}^\mu(x)$. Plugging the collinear gluons into Eq. (2.10), we get a compact form for the fermonic Lagrangian

$$\mathcal{L}_\xi = \bar{\xi}_{n,p'} \left\{ in \cdot D + \left(\mathcal{P}_\perp + g_s \mathcal{A}_{n,q_1}^\perp \right) \frac{1}{\bar{\mathcal{P}} + g_s \bar{n} \cdot A_{n,q_2}} \left(\mathcal{P}_\perp + g_s \mathcal{A}_{n,q_3}^\perp \right) \right\} \frac{\bar{\slashed{n}}}{2} \xi_{n,p}, \qquad (2.13)$$

where we have introduced a projection operator $\mathcal{P}^\mu = \frac{1}{2} n^\mu \bar{\mathcal{P}} + \mathcal{P}_\perp^\mu$ [7] with $\bar{\mathcal{P}} = \bar{n} \cdot \mathcal{P}$. The operator acts on all the collinear fields to its right and projects out the sum of large label

20

momenta on fields minus the sum of large labels on conjugate fields. The derivatives $\bar{n} \cdot \partial$ and $\partial_\mu^\perp$ in Eq. (2.10) can be replaced by the projection operator since

$$i\partial^\mu e^{-i\tilde{p}\cdot x} q_{n,p}(x) = e^{-i\tilde{p}\cdot x} \left(\mathcal{P}^\mu + i\partial^\mu \right) q_{n,p}(x). \tag{2.14}$$

The summation on the label momenta is always implied. We are free to change variables on the labels as long as we keep the label momenta conserved, which is enforced by the overall phase. The covariant derivative $in \cdot D$ contains both collinear and usoft gluon contributions and this term is identical to the large energy effective theory Lagrangian [37]. Eq. (2.13) can be further simplified using collinear Wilson lines. We stick to this form (2.13) at this moment since it is more straightforward to give the Feynman rules and wait to talk about the Wilson lines in the following chapters.

We expand the Lagrangian (2.13) to leading order in λ and up to $\mathcal{O}(g_s^2)$ to derive some of the Feynman rules in SCET_I

$$\begin{aligned}
\mathcal{L}_\xi &= \bar{\xi}_{n,p'} \left\{ in \cdot \partial + \mathcal{P}_\perp \frac{1}{\bar{\mathcal{P}}} \mathcal{P}_\perp + g_s n \cdot A_{us} \right. \\
&\quad + g_s \left(n \cdot A_{n,q} + \mathcal{P}_\perp \frac{1}{\bar{\mathcal{P}}} \mathcal{A}_{n,q}^\perp + \mathcal{A}_{n,q}^\perp \frac{1}{\bar{\mathcal{P}}} \mathcal{P}_\perp - \mathcal{P}_\perp \frac{1}{\bar{\mathcal{P}}} \bar{n} \cdot A_{n,q} \frac{1}{\bar{\mathcal{P}}} \mathcal{P}_\perp \right) \\
&\quad + g_s^2 \left(\mathcal{A}_{n,q'}^\perp \frac{1}{\bar{\mathcal{P}}} \mathcal{A}_{n,q}^\perp - \mathcal{P}_\perp \frac{1}{\bar{\mathcal{P}}} \bar{n} \cdot A_{n,q'} \frac{1}{\bar{\mathcal{P}}} \mathcal{A}_{n,q}^\perp \right. \\
&\quad \left. \left. - \mathcal{A}_{n,q'}^\perp \frac{1}{\bar{\mathcal{P}}} \bar{n} \cdot A_{n,q} \frac{1}{\bar{\mathcal{P}}} \mathcal{P}_\perp + \mathcal{P}_\perp \frac{1}{\bar{\mathcal{P}}} \bar{n} \cdot A_{n,q'} \frac{1}{\bar{\mathcal{P}}} \bar{n} \cdot A_{n,q} \frac{1}{\bar{\mathcal{P}}} \mathcal{P}_\perp \right) \right\} \frac{\slashed{\bar{n}}}{2} \xi_{n,p}. \tag{2.15}
\end{aligned}$$

The Feynman rules are shown in fig. 7. We notice that at leading order, the interaction between usoft and collinear quarks only comes from the $g_s n \cdot A_{us}$ term that will eventually be eliminated by a field re-definition as we will show later in this chapter.

The SCET_II Lagrangian is the same as Eq. (2.13) after turning off the usoft interaction term. Extra terms for regulating the IR divergence may be added to the Lagrangian to reproduce all the IR divergences of QCD [36].

The collinear gluon Lagrangian can be found in [8] including the gauge fixing term and ghost term. We list here only the term for collinear gluons ignoring the ghosts.

$$\mathcal{L}_g = \frac{1}{2g_s^2} Tr \left\{ \left[i\mathcal{D}^\mu + g_s A_{n,q}^\mu, \, i\mathcal{D}^\nu + g_s A_{n,q'}^\nu \right] \right\}^2 + \frac{1}{\xi} Tr \left\{ \left[i\mathcal{D}, A_{n,q}^\mu \right] \right\}, \tag{2.16}$$

$$(\tilde{p},k) \qquad = \quad i\,\frac{\slashed{n}}{2}\,\frac{\bar{n}\cdot p}{n\cdot k\,\bar{n}\cdot p + p_\perp^2 + i\epsilon}$$

$$\mu\,,A \qquad = \quad ig\,T^A\,n_\mu\,\frac{\slashed{\bar{n}}}{2}$$

$$\mu\,,A \qquad = \quad ig\,T^A\left\{ n_\mu + \frac{\gamma_\mu^\perp \slashed{p}_\perp}{\bar{n}\cdot p} + \frac{\slashed{p}'_\perp \gamma_\mu^\perp}{\bar{n}\cdot p'} - \frac{\slashed{p}'_\perp \slashed{p}_\perp}{\bar{n}\cdot p\,\bar{n}\cdot p'}\bar{n}_\mu \right\}\frac{\slashed{\bar{n}}}{2}$$

$$\mu\,,A \quad \nu\,,B \qquad = \quad \frac{ig^2\,T^A T^B}{\bar{n}\cdot(p-q)}\left\{ \gamma_\mu^\perp\gamma_\nu^\perp - \frac{\gamma_\mu^\perp \slashed{p}_\perp}{\bar{n}\cdot p}\bar{n}_\nu - \frac{\slashed{p}'_\perp \gamma_\nu^\perp}{\bar{n}\cdot p'}\bar{n}_\mu + \frac{\slashed{p}'_\perp \slashed{p}_\perp}{\bar{n}\cdot p\,\bar{n}\cdot p'}\bar{n}_\mu\bar{n}_\nu \right\}\frac{\slashed{\bar{n}}}{2}$$

$$+ \frac{ig^2\,T^B T^A}{\bar{n}\cdot(q+p')}\left\{ \gamma_\nu^\perp\gamma_\mu^\perp - \frac{\gamma_\nu^\perp \slashed{p}_\perp}{\bar{n}\cdot p}\bar{n}_\mu - \frac{\slashed{p}'_\perp \gamma_\mu^\perp}{\bar{n}\cdot p'}\bar{n}_\nu + \frac{\slashed{p}'_\perp \slashed{p}_\perp}{\bar{n}\cdot p\,\bar{n}\cdot p'}\bar{n}_\mu\bar{n}_\nu \right\}\frac{\slashed{\bar{n}}}{2}$$

Figure 7: Feynman rules involve collinear quark to leading order in λ in SCET$_\mathrm{I}$ [6] : collinear quark (dashed line) is labeled by $\tilde{p}$ and residual momentum k. We present the soft gluon by a spring line and the collinear gluon by a spring with a straight line going through.

where $i\mathcal{D}$ including usoft gluons will be defined in Eq. (2.20). The propagator for the collinear gluon has the same form as the one in QCD. Only the $n \cdot A_{us}$ component of the usoft gauge field can appear to leading order in λ in the interactions with collinear gluons and, in Feynman gauge, the four-gluon vertex in the usoft-collinear interactions vanishes. This observation will help us show that the collinear fields can decouple from the usoft degrees of freedom using field redefinitions at leading order in the following chapters.

2.4 GAUGE TRANSFORMATIONS

Gauge symmetries are important in applying effective theories, since they set strong constraints on the forms of the operators that we can construct out of the fields in the effective theories. In SCET, there are three classes of gauge transformations in correspondance with three different types of gauge bosons. We denote the gauge transformations as $U(x) = \exp(i\theta^a(x)T^a)$ and in QCD the fields transform as shown in Eq. (1.2). In SCET, gauge transformations are categorized into usoft, soft and collinear by requiring that their derivatives scale the same way as the corresponding gauge fields: $\partial_\mu U_{us}(x) \sim Q\lambda^2$, $\partial_\mu U_s(x) \sim Q\lambda$ and $\partial_\mu U_c(x) \sim Q(\lambda^2, 1, \lambda)$. Other scalings put fields way off their mass shells so are not allowed due to power counting which can be seen easily from Lagrangian (2.13). For instance, we consider the kinetic term for collinear fermions in the Lagrangian (2.13) under arbitrary gauge transformations

$$\bar{\xi}_{n,p'} in \cdot \partial \xi_{n,p} \to \bar{\xi}_{n,p'} in \cdot \partial \xi_{n,p} - \bar{\xi}_{n,p'} \left[n \cdot \partial \theta^a(x) T^a \right] \xi_{n,p} . \tag{2.17}$$

The square bracket in the second term indicates that the derivative acts on $\theta^a(x)$ only. The Lagrangian can not be invariant under transformations other than usoft and collinear without changing the species of the gauge fields.

We investigate the gauge transformations in SCET$_\mathrm{I}$. The gauge field is decomposed into collinear and usoft $A^\mu = A^\mu_c + A^\mu_{us}$. Under the usoft transformation $U_{us}(x)$ we have (taking scaling into consideration)

$$A^\mu_c + A^\mu_{us} \to U_{us} A^\mu_c U^\dagger_{us} + U_{us} A^\mu_{us} U^\dagger_{us} + \frac{i}{g_s} U_{us} \partial^\mu U^\dagger_{us} , \tag{2.18}$$

and under the collinear transformation $U_c(x)$ we have

$$\begin{aligned} A^\mu_c + A^\mu_{us} &\to U_c A^\mu_c U^\dagger_c + \frac{i}{g_s} U_c \left(\partial^\mu - ig_s A^\mu_{us} \right) U^\dagger_c \\ &\to U_c A^\mu_c U^\dagger_c + \frac{i}{g_s} \left[U_c, [D^\mu_{us} U^\dagger_c] \right] + A^\mu_{us} \end{aligned} \tag{2.19}$$

Here the covariant derivative is defined as $iD_{us} = i\partial + g_s A^c_{us}$ containing only the usoft gluons. The inner square bracket again sets the range that the derivative is active. The commutator here is defined as $[A, [BC]] = A[BC] - [B(CA)]$. We can see that under a collinear

transformation, the usoft gluons with a wavelength of the order $1/(Q\lambda^2)$ are fixed since it can not resolve the relatively fast local change, therefore the usoft gluons act like classical background fields. The background fields provide a slowly varying color background for the collinear fields to live in. Thus under a usoft transformation, the collinear fields experience global color rotations. In the presence of soft gluons, soft gauge transformations appear. However, the collinear and usoft fields can not transform under this gauge transformation since it will take them far off their mass shells. The same arguments hold for quarks.

To factorize out the large momentum components in the collinear transformations, we use the same trick as for the collinear fields to define $U_c(x) = \sum_{\tilde{Q}} e^{-i\tilde{Q}\cdot x}\mathcal{U}_Q$, where $\partial^\mu \mathcal{U}_Q \sim Q\lambda^2$ and $\sum_{\tilde{Q}} \mathcal{U}_{Q+r}\mathcal{U}^\dagger_{-Q+r'} = \delta^{(3)}_{\tilde{r}\tilde{r}'}$ with (r, r') fixed. We use the projector $\mathcal{P}$ to project out the large label momenta and throw away the power suppressed terms in λ. In this way, the usoft covariant derivative iD^μ_{us} in Eq. (2.19) is replaced by

$$i\mathcal{D}^\mu = \bar{\mathcal{P}}\frac{n^\mu}{2} + \mathcal{P}^\mu_\perp + in \cdot D_{us}\frac{\bar{n}^\mu}{2}. \tag{2.20}$$

Only the $n \cdot A_{us}$ component of the usoft gluon field contributes, the others are suppressed by powers of λ.

We list all of the SCET gauge transformations in Table 3. We note that, for instance, in SCET_I under usoft or collinear gauge symmetries the combination $A_{us} + A_c$ transforms the same way as the gauge field in QCD (2.18) and (2.19). This is not true for the collinear and usoft fermions, since the small components of the collinear quark spinor have been integrated out via equation of motion (2.9) to build the effective Lagrangian while gauge fields have not.

2.5   WILSON LINES

To see that the Lagrangian (2.13) is invariant under gauge transformations, we introduce an important building block in SCET, the Wilson lines. Similar to the three different gauge transformations in SCET, there are three types of Wilson lines in SCET corresponding to collinear, usoft and soft.

Table 3: Gauge transformations for the collinear, soft, and usoft fields. The p labels on collinear fields are fixed, while Q and R are summed over. For simplicity labels on the soft fields are suppressed here.

	Collinear $\mathcal{U}_R$	Soft U_s	Usoft U_{us}
$\xi_{n,p}$	$\mathcal{U}_{p-Q}\,\xi_{n,Q}$	$\xi_{n,p}$	$U_{us}\,\xi_{n,p}$
$A_{n,p}^\mu$	$\mathcal{U}_Q\,A_{n,R}^\mu\,\mathcal{U}_{Q+R-p}^\dagger + \frac{1}{g_s}\left[\mathcal{U}_Q,\left[i\mathcal{D}^\mu\,\mathcal{U}_{Q-p}^\dagger\right]\right]$	$A_{n,p}^\mu$	$U_{us}\,A_{n,p}^\mu\,U_{us}^\dagger$
q_s	q_s	$U_s\,q_s$	$U_{us}\,q_s$
A_s^μ	A_s^μ	$U_s\left(A_s^\mu + \frac{1}{g_s}\mathcal{P}^\mu\right)U_s^\dagger$	$U_{us}\,A_s^\mu\,U_{us}^\dagger$
q_{us}	q_{us}	q_{us}	$U_{us}\,q_{us}$
A_{us}^μ	A_{us}^μ	A_{us}^μ	$U_{us}\left(A_{us}^\mu + \frac{i}{g_s}\partial^\mu\right)U_{us}^\dagger$

The one built out of the collinear gauge field, as expected, is the collinear Wilson line. The collinear Wilson line is important in building operators like $\bar{\phi}_{us}\psi_c$. Since the collinear fields are populating near $n \cdot x \sim 0$ while the usoft fields are far away in $\bar{n}$ direction, we need a Wilson line to link them to conserve gauge invariance which gives $\bar{\phi}_{us}(\infty\bar{n})W(\infty\bar{n},x)\psi_c(x)$.

The necessity of the collinear Wilson line can also be infered from the fact that, unlike QCD, the SCET Lagrangian should be non-local in the x^+ direction since we integrate out the small components of the fermion spinor along the light-cone direction. Though the separation is of order $1/Q$, the nonlocal contribution to the SCET Langrangian is enhanced by $p_\perp \sim Q\lambda$. The non-locality is disguised in (2.13) by the expansion in λ and the operator $1/\bar{\mathcal{P}}$. To see this more explicitly, we consider the equation of motion (2.9), in the light-cone gauge $\bar{n} \cdot A = 0$ for simplicity,

$$
\begin{aligned}
\chi_{\bar{n},p}(x) &= \frac{1}{\bar{n}\cdot p + i\bar{n}\cdot\partial}\left[(\not{p}_\perp + i\not{D}_\perp)\frac{\not{\bar{n}}}{2}\xi_{n,p}\right](x) \\
&= -i\int_{-\infty}^0 ds\, e^{-is(\bar{n}p+i\epsilon)}\left[(\not{p}_\perp + i\not{D}_\perp)\frac{\not{\bar{n}}}{2}\xi_{n,p}\right](x+s\bar{n}). \quad (2.21)
\end{aligned}
$$

25

To get the second line, a $+i\epsilon$ prescription has been applied on the denominator in the first line. Plugging the equation above into the QCD Lagrangian, we find in light-cone gauge the SCET Lagrangian to all orders in λ (without usoft quarks) containing a term of the form

$$\mathcal{L} \supset i \int_{-\infty}^{0} \mathrm{d}s\, e^{-is(\bar{n}p+i\epsilon)} \left[\bar{\xi}_{n,p'} \left(\slashed{p}'_{\perp} + i\overleftarrow{\slashed{\mathcal{D}}}^{\dagger}_{\perp} \right) \right](x) \left[\left(\slashed{p}_{\perp} + i\slashed{\mathcal{D}}_{\perp} \right) \frac{\bar{\slashed{n}}}{2} \xi_{n,p} \right](x+s\bar{n}). \quad (2.22)$$

Now we see explicitly that we have two parts in the Lagrangian sitting at two space-time points separated along the light-cone direction $\bar{n}$ by s. The size of the separation could be found in the overall phase which has its support over a range of order $s \sim 1/Q$. An expansion of this term around x to leading order in λ or s ($s\bar{n} \cdot \partial \xi_{n,p} \sim \lambda^2$) would reproduce the Lagrangian we found in Eq. (2.13) in the light-cone gauge. In arbitrary gauges, the Wilson line

$$\begin{aligned} W(x, x+s\bar{n}) &= P \exp\left[ig_s \int_{x+s\bar{n}}^{x} \mathrm{d}t\, \bar{n}\cdot A(t\bar{n}) \right] \\ &= P \exp\left[ig_s \int_{-\infty}^{x} \mathrm{d}t\, \bar{n}\cdot A(t\bar{n}) \right] P \exp\left[-ig_s \int_{-\infty}^{x+s\bar{n}} \mathrm{d}t\, \bar{n}\cdot A(t\bar{n}) \right] \\ &\equiv W(x) W^{\dagger}(x+s\bar{n}). \end{aligned} \quad (2.23)$$

has to be inserted to link the two different space-time points x and $x+s\bar{n}$ for maintaining the gauge invariance of the Lagrangian, which gives

$$\mathcal{L} \supset i \int_{-\infty}^{0} \mathrm{d}s\, e^{-is(\bar{n}p+i\epsilon)} \left[\bar{\xi}_{n,p'} \left(\slashed{p}'_{\perp} + i\overleftarrow{\slashed{\mathcal{D}}}^{\dagger}_{\perp} \right) W \right](x) \left[W^{\dagger} \left(\slashed{p}_{\perp} + i\slashed{\mathcal{D}}_{\perp} \right) \frac{\bar{\slashed{n}}}{2} \xi_{n,p} \right](x+s\bar{n}). \quad (2.24)$$

To leading order in λ power counting, only the $\bar{n} \cdot A_c$ component of the collinear gluon contributes to the Wilson line, which is named the collinear Wilson line W_c.

Under arbitrary collinear gauge transformations, the collinear Wilson line transforms as

$$W_c \rightarrow U_c(x) W_c(x) U_c(x - \infty\bar{n}), \quad (2.25)$$

therefore, Eq. (2.24) is manifestly gauge invariant and in fact each piece in the square bracket is collinear gauge invariant independently as long as the collinear gauge fields have no support at infinity and hence $U_c^{\dagger}(x - \infty\bar{n}) = 1$. In general, this situation is satisfied since collinear gluons with large $\bar{n}\cdot q \sim Q$ only smear over a distance of order $1/Q$ in $\bar{n}$ direction. Eq. (2.24) can be expanded in λ in several different ways. On one hand, we could firstly expand

$W_c(x, x + s\bar{n})$ to leading order in λ by turning the integration over full momenta to one over the residual momenta $\int \mathrm{d}^4 q \to \sum_{\tilde{q}} \int \mathrm{d}^4 k$

$$
\begin{aligned}
W_c(x, x + s\bar{n}) &= \sum_{\text{perms}} \exp\left[-\frac{g_s}{(2\pi)^4} \int \mathrm{d}^4 q \frac{\bar{n} \cdot A_c(q)}{\bar{n} \cdot q + i\epsilon} e^{-iq \cdot x}\right] \\
&\times \sum_{\text{perms}} \exp\left[-\frac{g_s}{(2\pi)^4} \int \mathrm{d}^4 q' \frac{\bar{n} \cdot A_c^*(q')}{\bar{n} \cdot q' - i\epsilon} e^{iq' \cdot (x + s\bar{n})}\right] \\
&= \sum_{\text{perms}} \exp\left[-g_s \frac{\bar{n} \cdot A_{n,q}(x)}{\bar{n} \cdot q + i\epsilon}\right] \\
&\times \sum_{\text{perms}} \exp\left[-g_s \frac{\bar{n} \cdot A_{n,-q'}(x)}{\bar{n} \cdot q' - i\epsilon} e^{is\bar{n}q'}\right].
\end{aligned}
\tag{2.26}
$$

In the last equation, a sum over the label momentum is implied and $A_{n,-q} = A_{n,q}^*$. Inserting the equation into Eq. (2.24), expanding around x to leading order in λ and performing the integration over s recovers the Lagrangian in Eq. (2.13) order by order in g_s with the help of the projector $\mathcal{P}$. On the other hand, we have

$$
i \int_{-\infty}^{0} \mathrm{d}s \, \left[\bar{\xi}_{n,p'} \left(\not{p}'_\perp + i\overleftarrow{\not{\mathcal{D}}}^\dagger_\perp\right) W_c\right](x) \, e^{-is(\bar{n}p + i\epsilon)} \left[e^{-is\bar{n} \cdot \partial} W_c^\dagger(x)\right] \left[(\not{p}_\perp + i\not{\mathcal{D}}_\perp) \frac{\not{\bar{n}}}{2} \xi_{n,p}\right](x) \tag{2.27}
$$

Integrating over s yields a manifestly gauge-invariant Lagrangian in the hybrid momentum-position space representation [7]

$$
\bar{\xi}_{n,p'} \left\{ \left(\mathcal{P}_\perp + g_s \mathcal{A}_{n,q}^\perp\right) W_n(x) \frac{1}{\bar{\mathcal{P}}} W_n^\dagger(x) \left(\mathcal{P}_\perp + g_s \mathcal{A}_{n,q'}^\perp\right) \right\} \frac{\not{\bar{n}}}{2} \xi_{n,p}(x), \tag{2.28}
$$

where

$$
W_n \equiv \left[\sum_{\text{perms}} \exp\left(-g_s \frac{1}{\bar{\mathcal{P}}} \bar{n} \cdot A_{n,q}(x)\right)\right], \tag{2.29}
$$

and under the collinear gauge transformation $\mathcal{U}_Q$, the Wilson line W_n goes like

$$
W_n \to \mathcal{U}_Q W_n. \tag{2.30}
$$

as a consequence of Eq. (2.25) with the boundary condition that $U_c^\dagger(x - \infty \bar{n}) = 1$.

From the equivalence of Eq. (2.28) and (2.13), we can infer that $W_n \bar{\mathcal{P}}^{-1} W_n^\dagger = (\bar{\mathcal{P}} + g_s \bar{n} \cdot A)^{-1}$. This can be generalized to $W_n f(\bar{\mathcal{P}}) W_n^\dagger = f(\bar{\mathcal{P}} + g_s \bar{n} \cdot A)$ [7] which is nice since the

relation ensures that gauge invariant combinations of the $\bar{n} \cdot A_{n,q}$ components only appear in the collinear Wilson line W_n.

As we mentioned in the previous sections, at leading order the usoft fields can decouple from the collinear modes through field re-definitions. The decoupling simplifies the factorization theorem in SCET and is realized by using the usoft Wilson line denoted as Y.

The usoft Wilson line can be obtained by considering an on-shell collinear field propagates within a background full of usoft gluons as depicted in fig. 8 and fig. 9. For the collinear quark case, the Feynman rules in fig. 7 gives

$$\xi_{n,p} \to Y \xi_{n,p} = \sum_{\text{perms}} \exp\left[-g_s \frac{n \cdot A_{us}^a T^a}{n \cdot k}\right] \xi_{n,p} \,. \tag{2.31}$$

Here the quark spinor ξ turns into a field which no longer interacts with the usoft gluons. All the interactions have been factored into the overall exponential which defines the usoft Wilson line. Expressed in a path-ordered form the usoft Wilson line is given by

$$Y(x) = P \exp\left[i g_s \int_{-\infty}^{x} \mathrm{d}s \, n \cdot A_{us}^a(sn) T^a\right] \,, \tag{2.32}$$

where we have shown explicitly that, for the quark sector, the usoft Wilson line is in the fundamental representation. We note that this form corresponds to a $+i\epsilon$ prescription in the denominator of Eq. (2.31). The position of the poles determined by the sign of $i\epsilon$ term has physical consequences. Different prescriptions correspond to different physical processes. The prescription used here, for instance, is related to the usoft gluons attached to a incoming quark from $-\infty$ to x. For a systematic analysis on the structures of the usoft Wilson lines, see [38].

This decoupling statement holds true at the level of Lagrangian at lowest order in λ, since one can prove that under such a field re-definition, the term involving the interactions between usoft gluons and collinear quarks transforms as

$$Y^\dagger i n \cdot D_{us} Y = i n \cdot \partial \,. \tag{2.33}$$

And we will see that no extra usoft terms will arise once we re-define the gluon field in a similar manner. However beyond leading order, the situation is complicated by the emergence
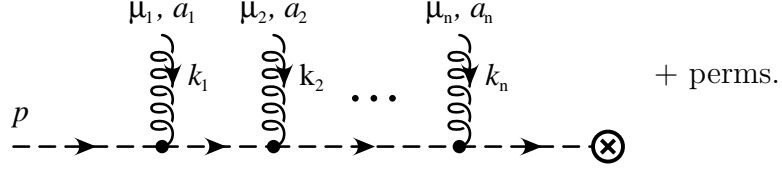
Figure 8: The usoft gluons (spring lines) attached to a collinear quark line can be summed up into a path-ordered exponential. [8]
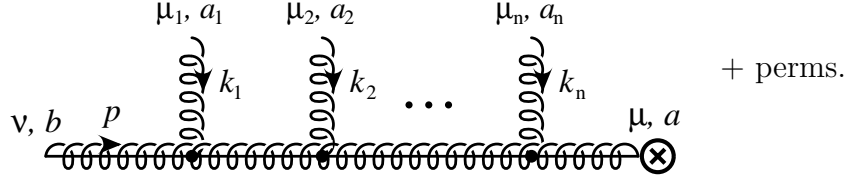
Figure 9: The usoft gluons attached to a collinear gluon can be summed up into a path-ordered exponential. [8]

of subleading couplings of usoft gluons and quarks and the decoupling theorem may not be proved simply with the aid of the usoft Wilson line.

The collinear gauge fields can be treated in the same way. A suitable choice of gauge makes the calculation [8] similar to the collinear quark case, which yields

$$A_{n,p}^{a,\mu} \rightarrow \mathcal{Y}^{ab} A_{n,p}^{b,\mu} = \sum_{\text{perms}} \exp\left[-g_s \frac{n \cdot A_{us}^c (-if^{cab})}{n \cdot k}\right] A_{n,p}^{b,\mu}. \tag{2.34}$$

Similar to the quark fields, at this lowest order in λ, the gauge fields do not couple to usoft gluons. All usoft gluons are summed up into the exponential in the adjoint representation. In the position space the usoft Wilson line is given by the path-ordered exponential

$$\mathcal{Y}^{ab}(x) = P \exp\left[ig_s \int_{-\infty}^{x} \mathrm{d}s n \cdot A_{us}^c (sn)(-if^{cab})\right]. \tag{2.35}$$

Also a $+i\epsilon$ prescription should be utilized in performing the Fourier transformation. The

Table 4: Gauge transformations for the collinear, soft, and usoft Wilson lines W_n, S, and Y.

	Collinear $\mathcal{U}_Q$	Soft U_s	Usoft U_{us}
W_n	$\mathcal{U}_Q W_n$	W_n	$U_{us} W_n U_{us}^\dagger$
S	S	$U_s S$	$U_{us} S U_{us}^\dagger$
Y	Y	Y	$U_{us} Y$

adjoint representation can be related to the fundamental one by the equation $T^b \mathcal{Y}^{ba} = Y T^a Y^\dagger$. Therefore we find the field re-definitions

$$\xi_{n,p} \to Y \xi_{n,p}, \quad A_{n,q}^\mu \to Y A_{n,q}^\mu Y^\dagger, \quad W_n \to Y W_n Y^\dagger. \tag{2.36}$$

By modifying the SCET Lagrangian (2.13) and (2.16) using the redefined fields listed above, we can easily see that the usoft contributions have been completely removed from the SCET Lagrangian and no couplings of usoft gluons to collinear modes exist. Therefore we can claim that at leading order in power counting, all interactions of usoft gluons and collinear fields can be factored into the usoft Wilson line Y defined with respect to the direction of the collinear particles.

The soft Wilson line plays a similar role as the usoft one in decoupling the soft and collinear sectors. The decoupling theorem is proved in [8] or can be obtained in a neat way by matching SCET$_\text{I}$ onto SCET$_\text{II}$ [34]. The soft Wilson line is obtained simplify by replacing the usoft gluons by the soft ones, which gives, in the path-ordered form,

$$S(x) = P \exp \left[i g_s \int_{-\infty}^x \mathrm{d}s n \cdot A_s(sn) \right], \tag{2.37}$$

in the fundamental or adjoint represention for quarks or gluons respectively.

We conclude this section by listing the transformation rules for the Wilson lines under different types of gauge transformations in Table. 4 and emphasize that Wilson lines are important building blocks in constructing gauge invariant operators in SCET.

2.6 REPARAMETERIZATION INVARIANCE

The SCET Lagrangian that we have discussed so far is derived by tree-level matching from QCD. In general, loop effects can not only modify the coefficients of the operators but introduce new terms that satisfy the gauge symmetries. The worst case is that radiative corrections develop extra kinetic terms for collinear particles and thus the kinetic Lagrangian can only be defined order by order. However once we impose new symmetries in SCET, we will see that these operators are forbidden and the SCET Lagrangian is not renormalized as long as we take a matching scheme obeying all symmetries and the power counting rules.

In addition to the constraints from gauge symmetries, the SCET operators are also required to be reparameterization invariant [39]. The requirement for reparameterization invariance comes from the fact that we have redundancy in defining the light-cone coordinates. In SCET, any choice of the light-cone vectors $\bar{n}$ and n are equally good and has no physical consequence as long as they satisfy the conditions in Eq. (2.1) and keep the scaling of the collinear momenta unchanged. Therefore we can have three types of reparameterization transformations

$$
\begin{aligned}
\text{Type}_\text{I} : \quad & n \to n + \Delta^\perp \,, \\
\text{Type}_\text{II} : \quad & \bar{n} \to \bar{n} + \epsilon^\perp \,, \\
\text{Type}_\text{III} : \quad & n \to e^\alpha n \,, \quad \bar{n} \to e^{-\alpha}\bar{n} \,,
\end{aligned}
\tag{2.38}
$$

where $\Delta^\perp$, $\epsilon^\perp$ and α are parameters with $\Delta^\perp \sim \lambda$, $\epsilon^\perp \sim 1$ and $\alpha \sim 1$ to preserve the scaling of the collinear momenta .

Some transformation rules can be found in Table. 5. Using the parameterization invariance, one can show that the Lagrangian (2.28) is the most general form at leading power counting order, satisfying both gauge symmetries and reparameterization invariance [39]. Therefore the form of the kinetic term is entirely fixed [39] and acquires no anomalous correction.

Table 5: A summary of the reparameterization transformation rules in the SCET. [39]

Type$_\text{I}$	Type$_\text{II}$	Type$_\text{III}$
$n \to n + \Delta^\perp$	$n \to n$	$n \to e^\alpha n$
$\bar{n} \to \bar{n}$	$\bar{n} \to \bar{n} + \epsilon^\perp$	$\bar{n} \to e^{-\alpha}\bar{n}$
$\xi_n \to \left(1 + \frac{1}{4}\slashed{\Delta}^\perp \slashed{\bar{n}}\right)\xi_n$	$\xi_n \to \left(1 + \frac{1}{2}\slashed{\epsilon}^\perp \frac{1}{\bar{n}\cdot\mathcal{D}}\slashed{\mathcal{D}}^\perp\right)\xi_n$	$\xi_n \to \xi_n$
$n\cdot\mathcal{D} \to n\cdot\mathcal{D} + \Delta^\perp\cdot\mathcal{D}^\perp$	$n\cdot\mathcal{D} \to n\cdot\mathcal{D}$	$n\cdot\mathcal{D} \to e^\alpha n\cdot\mathcal{D}$
$\bar{n}\cdot\mathcal{D} \to \bar{n}\cdot\mathcal{D}$	$\bar{n}\cdot\mathcal{D} \to \bar{n}\cdot\mathcal{D} + \epsilon^\perp\cdot\mathcal{D}^\perp$	$\bar{n}\cdot\mathcal{D} \to e^{-\alpha}\bar{n}\cdot\mathcal{D}$
$W_n \to W_n$	$W_n \to \left[\left(1 - \frac{1}{\bar{n}\cdot\mathcal{D}}\epsilon^\perp\cdot\mathcal{D}^\perp\right)\right]W_n$	$W_n \to W_n$

2.7   ZERO BIN SUBTRACTION

When we analyze physical processes, we always need to deal with different kinds of integrals, such as loop integrals in higher order corrections or phase space integrals. In SCET these integrals involve a sum over the large momentum labels along with an integral over the residual momenta, which, in practice, one always turns into an integration over full momenta $p = \tilde{p} + k$ using

$$\sum_{\tilde{p}} \int \mathrm{d}^n k = \int \mathrm{d}^n p \qquad (2.39)$$

to avoid the explicit summations. However this substitution is problematic since it includes bins where the large label $\tilde{p} = 0$. In SCET, collinear modes can be distinguished from usoft fields through their large label momenta. When the label momenta vanish, however, the momenta of the collinear particles will scale the same way as the usoft momenta and the fields should essentially be regarded as usoft. The conversion from summation to integral overcounts the contributions from this overlapped zero bin region and must be carefully subtracted in order to reproduce the infrared structure of the full theory [40]

$$\sum_{\tilde{p}\neq 0} \int \mathrm{d}^n k F[p,k] = \int \mathrm{d}^n p \left(F[p] - F_\text{sub}[0]\right) . \qquad (2.40)$$
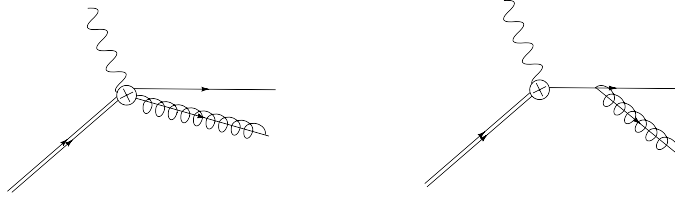
Figure 10: Real emission of a collinear gluon in SCET.

Here the subtraction is performed at the integrand level.

We emphasize that zero bin subtraction is crucial for SCET or other effective theories, such as NRQCD, to faithfully reproduce the infrared physics. It is related to the end-point sigularities that will spoil our naive expectations for the factorization theorem. For instance, in deep-inelastic-scattering (DIS) near the end-point $x \to 1$, both initial and final state partons share features of collinear degrees of freedom. In a certain frame (Breit frame), they propagate in opposite light cone directions, n and $\bar{n}$, and communicate with each other through emitting or absorbing soft gluons. A naive expectation for the amplitude in this frame takes the form $I_n + I_{\bar{n}} + I_s$ corresponding to the factorization $\sigma \sim f_{i/p} \cdot J_n \cdot S$. However the correct total amplitude is given by $I_n + I_{\bar{n}} - I_s$, which can be reproduced in SCET only when one performs zero bin subtraction correctly to yield $\sigma \sim f_{i/p}/S \cdot J_{\bar{n}}/S \cdot S = f_{i/p} \cdot J_{\bar{n}} \cdot S^{-1}$.

We use a trivial example to highlight the zero bin subtraction scheme by considering a heavy quark decaying into a light one. The SCET operators contributing to the process take the form

$$\sum_i \sum_\omega C_i(\omega) \bar{\xi}_n W_n \delta_{\omega, \bar{\mathcal{P}}^\dagger} \Gamma_i^\mu h_v \,, \tag{2.41}$$

where ξ_n is the collinear light quark and Γ_i^μ are Dirac structures. The overall coefficients are determined order by order in perturbation theory by matching with QCD. h_v is the field annihilating a heavy quark with velocity v. The dynamics for h_v can be described by heavy quark effective theory. Here we have not factorized out the usoft Wilson line, therefore the collinear field ξ still can emit or absorb usoft gluons.

33

We focus on the real emission of collinear gluons in $d = 4 - 2\epsilon$ dimension. The Feynman diagrams are shown in fig. 10. A naive implementation of the Feynman rules in fig. 7 gives that

$$|\mathcal{M}|^2 = g_s^2 C_F |\mathcal{M}|_0^2 \frac{1}{q_{g\xi}^2} \left(\frac{4\bar{n}\cdot q}{\bar{n}\cdot k} + (2 - 2\epsilon)\frac{n \cdot q}{n \cdot q_{g\xi}} \right) , \qquad (2.42)$$

where q and k are momenta for the collinear quark and gluon respectively. The total momentum for the collinear quark-gluon system is denoted as $q_{g\xi}$. $\mathcal{M}_0$ is the tree level $1 \rightarrow 2$ amplitude. When $\bar{n}\cdot q$ or $\bar{n} \cdot k$ goes to zero, the momenta scale like $Q(\lambda^2, \lambda^2, \lambda^2)$ rather than $Q(\lambda^2, 1, \lambda)$. These zero bin contributions should be subtracted to avoid double counting. By power counting (including the power counting for the phase space), the zero bin contribution from the collinear quark is suppressed by a power of λ^2 since $\bar{n}\cdot q \sim Q\lambda^2$, therefore the only term that needs to be subtracted comes from the collinear gluon, which gives

$$|\mathcal{M}|^2_{\text{zero}} = g_s^2 C_F |\mathcal{M}|_0^2 \frac{1}{q_{g\xi}^2} \left(\frac{4\bar{n}\cdot q_{g\xi}}{\bar{n} \cdot k} \right) , \qquad (2.43)$$

with $k \sim Q\lambda^2$. The purely collinear contribution is given by the difference between the naive matrix element or the element without a zero bin subtraction and the zero bin matrix element

$$|\mathcal{M}|^2_{\text{coll}} = g_s^2 C_F |\mathcal{M}|_0^2 \frac{1}{q_{g\xi}^2} \left(\frac{4\bar{n}\cdot q}{\bar{n} \cdot k} + (2 - 2\epsilon)\frac{n \cdot q}{n \cdot q_{g\xi}} - \frac{4\bar{n}\cdot q_{g\xi}}{\bar{n} \cdot k} \right) , \qquad (2.44)$$

which reproduces the infrared structure of QCD after including usoft radiation effects. A more careful analysis reveals that the zero bin contribution only comes from the cross term in fig. 10. Others are either vanishing or suppressed by powers of λ. A similar procedure should be carried out for loop integrations, and in the current case the net effect of the zero bin subtraction is simply to convert the infrared poles into the ultraviolet ones in dimensional regularization since the integrals are scaleless.

We note that under certain circumstances similar to what we discussed above, the zero-bin contributions can be factored into zero-bin Wilson lines by field re-definitions just like we

did for decoupling usoft and collinear particles [41, 42]. The zero-bin Wilson line is defined as

$$W_{n,0} = P \exp\left[ig_s \int_{-\infty}^{x} \mathrm{d}s \, n \cdot A_{n,0}(sn) \right],$$ (2.45)

which is identical to the usoft Wilson line. Under such factorization the purely collinear matrix elements can be related to the naive one,

$$\langle 0|W_n^\dagger \xi_n|\xi\rangle_{\mathrm{coll}} = \frac{\langle 0|W_n^\dagger \xi_n|\xi\rangle}{\langle 0|W_{\bar{n},0}^\dagger W_{n,0}|0\rangle}.$$ (2.46)

This factorization offers the explanation for the form of the DIS cross section near $x = 1$.

2.8 APPLICATIONS OF SCET

SCET has achieved some successes in understanding physical problems involving scales spanned over hard, collinear and (u)soft regions that typically arise near the phase space boundaries. The predictive power is based on the factorization theorem provided by SCET, which allows us to disentangle the contributions from different scales with accuracies up to a given power in λ. Without loss of generality, the factorization theorem can be written as an overall hard coefficient multiplied by the convolution of a collinear jet function (or jet functions) with a (u)soft shape function[1]

$$\mathrm{d}\sigma = H(p_h, \mu) \prod_{n_i} J_{n_i}(p_h k_s, \mu) \otimes S(k_s, \mu),$$ (2.47)

where the hard coefficient H encodes the short distance physics obtained from matching QCD onto SCET, while the collinear jet functions J_{n_i} describe the behavior of the jet like particles in different n_i directions obtained by further matching SCET onto purely (u)soft effective theory. The jets in different light-cone directions communicate with each other only through the (u)soft function S, since in the effective theory the degrees of freedom relate to the momenta that will cause onshell singularites in QCD, and according to the Coleman and Norton theorem [14], only classically allowed processes can occur. Each piece in (2.47)

---

[1] Here the jet functions are purely collinear with zero bin subtracted.

depends on a scale μ and the dependences give the renormalization group equations (RGEs) in SCET

$$\mu \frac{\mathrm{d}}{\mathrm{d}\mu} H(\mu) = \gamma_H(\mu) H(\mu) \,, \tag{2.48}$$

$$\mu \frac{\mathrm{d}}{\mathrm{d}\mu} J_{n_i}(\mu) = \gamma_{J_{n_i}}(\mu) J_{n_i}(\mu) \,, \tag{2.49}$$

$$\mu \frac{\mathrm{d}}{\mathrm{d}\mu} S(\mu) = \gamma_S(\mu) S(\mu) \,, \tag{2.50}$$

while in principle the physical quantity σ can not. Therefore we must have the relation

$$\gamma_H + \sum_{n_i} \gamma_{J_{n_i}} + \gamma_S = 0 \,, \tag{2.51}$$

hold order by order.

As we mentioned, SCET was invented to resum large Sudakov logarithms near phase space boundaries in Ref. [5], as an example, the authors showed that in B meson inclusive radiative decay near the photon spectrum end-point, the large logarithmic corrections can be resumed in an elegant way. Later on, SCET found its power in proving the factorization theorem for exclusive processes. For instance, in Ref. [43], the authors derived the factorization for $B \to D\pi$ to all orders in α_s up to corrections suppressed by factors of $1/m_c$, $1/m_b$ and $1/E_\pi$, based on the observation that no collinear gluons couple to the $B - D$ system and the decoupling of (u)soft gluons to the pion at leading order in λ in SCET. Some other exclusive factorizations for B-meson decaying to light particles, like $B \to \pi\pi$, have also been established under the framework of SCET.

Other than B physics, SCET has been useful in investigating heavy quarkonium systems. Based on the factorization theorem (2.47), SCET helps solve the puzzle that arises in the spectrum of the Upsilon radiative decay near the photon maximum energy region as we mentioned in section 1.2.

In Refs. [44], the authors showed that for $\Upsilon \to \gamma X$ decay the factorization theorem (2.47) near the end-point can be derived using the leading order gauge and reparameterization invariant SCET operators in λ with the help of NRQCD for both color singlet and octet configurations. Heavy quarkonium structure functions arise naturally in SCET to take the place

36

of the NRQCD matrix elements[2]. The enhancement near the phase boundary is removed by resumming the leading large Sudakov logarithms using the RGEs (2.48) and applying some simple model for the color octet structure functions. Their result married with the NRQCD prediction in the intermediate region and fragmentation approximation in the small z region is shown in fig. 11. We can see that the SCET prediction (solid line) is consistent with the data.

Due to its soft-collinear features, SCET is also a generic tool for characterizing the jet events on hadron colliders. It has been used to study jet shapes and jet algorithms in Ref. [45] where a factorization theorem for jet shape distributions is proved and the jet functions for angularity jet shapes are calculated to one loop order and resummed. Their results are in good agreement with the Monte Carlo simulations. Another result based on SCET is the conjecture of an exact formula for the infrared singularities of dimensionally regularized scattering amplitudes in massless perturbative QCD to all orders in α_s [46]. The anomalous-dimension matrix they proposed for an n-jet operator in SCET in the color-space is of the form

$$\Gamma = \sum_{i,j} \frac{T_i \cdot T_j}{2} \gamma_{\mathrm{cusp}}(\alpha_s) \log \frac{\mu^2}{-s_{ij}} + \sum_i \gamma^i(\alpha_s), \tag{2.52}$$

where the sums run over the external jets and the explanation of the symbols can be found in [46]. Their derivation comes from the observation that in SCET the infrared poles of onshell amplitudes are in one-to-one correspondence to the ultraviolet singularities of operator matrix elements. Their results have been demonstrated to three loop order.

More recently, SCET has started to draw attention in physical processes initiated by proton-proton collisions at hadron colliders. For instance, a procedure was developed by employing SCET to generate fully exclusive events [47]. SCET has been realized to be a perfect tool to naturally incorporate both the parton distribution functions and the energetic initial state radiation effects via different sorts of beam functions [48, 49, 50, 51]. In Ref. [48], the authors studied the color octet inclusive J/ψ photoproduction $\gamma p(g) \to J/\psi(c\bar{c}) + X$ when the J/ψ meson almost reaches its maximum energy. In this case, the final jet like particles X come from the initial gluon radiation introducing the p_T-independent gluon beam function

---

[2]The color singlet structure functions are essentially the NRQCD matrix elements.

for the first time. Later on, the beam functions of the same type arose from systematic studies in proton-(anti)proton collisions at the LHC or Tevatron with experimental restrictions on the hadronic final states [49]. Similar to [48], it was shown that the factorization does not yield standard parton distribution functions but instead the beam functions for the so-called isolated Drell-Yan cross section. The beam functions was found to be related to standard parton distribution functions by $\mathcal{B}_{i/p} = \sum_j \mathcal{I}_{ij} \otimes f_{j/p}$ with $\mathcal{I}_{ij}$ calculated perturbatively in SCET and, unlike the standard parton distribution functions, the beam functions evolve in the same way as collinear jets. Other types of beam functions with p_T-dependence emerge when one considers the transverse momentum distribution of a system with a large total invariant mass m in the small p_T ($\Lambda_{\text{QCD}} \ll p_T \ll m$) region [50, 51]. The large logarithmic corrections of the form $\log (p_T^2/m^2)$ due to multiple radiation need to be summed. Conventionally the summation is performed in the impact parameter b space following the seminal Collins-Soper-Sterman approach in which a suitable prescription is needed to avoid Landau poles associated with impact parameter integrations. However in the SCET approach [51], the factorization is performed solely in the momentum space with no reference to the impact parameter b [3] and the non-perturbative contributions indicated by the appearance of the Landau poles are encoded in terms suppressed by Λ_{QCD}/p_T. Therefore the Landau poles can be avoided in the SCET approach. The power suppressed terms can also be studied in a systematic way in SCET. For p_T-dependent beam functions [51], the authors only considered the cases where the final states contain only color-neutral objects. It would be interesting to extend their results to study the production of final states with color charges (at parton level).

Similar situations occur when one considers double differential decay rates, $B \to XK\gamma$ for instance [52], in which a novel fragmenting jet function arises instead of the standard parton fragmentation function. The fragmenting jet function provides extra information on the invariant mass of the jet from which a detected hadron fragments. The fragmenting jet functions were calculated in [53] and [54].

---

[3]Though the matching from the beam functions to the parton distribution functions must be executed in the impact parameter space, after matching one can perform a fourier transformation to entirely remove the dependence on the impact parameter.

2.9 SUMMARY

In this chapter, we gave a short review on some basic constituents of SCET for the purpose of setting the fundamentals for the rest of this thesis. We conclude this chapter by outlining the general procedures in applying SCET

- Constructing all possible SCET operators $\mathcal{O}_i$ relevant to the problem of interest. The operators should satisfy SCET gauge invariance as well as reparameterization invariance. The operators should carry the correct quantum numbers including color configuration, parity, etc. The series of the operators can be truncated up to a desired power counting in λ.

- Matching. The QCD amplitudes can be recovered through a summation of these operators $\sum_i C_i \mathcal{O}_i$ with C_i being the Wilson coefficients. The Wilson coefficients are obtained by a procedure called matching. The matching is performed at some hard scale Q. When matching beyond tree level, one has to perform loop integrals. It will be very convenient to use dimensional regularization for loop integrals since in SCET the integrations are often scaleless, and thus zero, and in dimensional regularization the contributions to the Wilson line come from the region where all loop momenta scale as Q as a result of the asymptotic expansion of loop integrals near threshold [55].

- Deriving the factorization theorem. If we are lucky enough, the physical quantities can be factored into collinear and (u)soft pieces with the help of the decoupling of (u)soft and collinear degrees of freedom.

- Running. A typical problem suitable for SCET involves several well separated scales: hard, collinear and (u)soft. Those scales are linked by RGEs. By running from one scale to another, large Sudakov logarithms are summed up to a desired order.
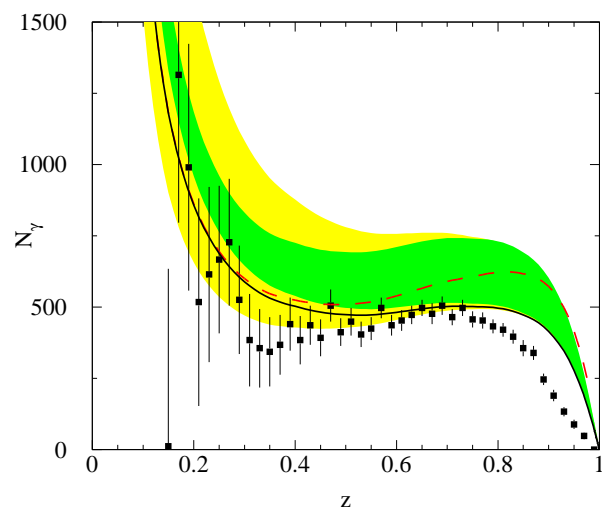
Figure 11: The inclusive photon spectrum compared with data [31]. The interpolated resummed theoretical prediction is presented by the solid curve including color singlet, color octet and fragmentation contributions. The variations are caused by different choices of α_s, m_b, fragmentation function and the collinear scale. [44]

3.0 J/ψ PRODUCTION IN LEPTON ANNIHILATION

Starting in this chapter, we begin to discuss the application of SCET to heavy quarkonium physics. As we have seen in section 1.2, the behavior of quarkonium production or decay spectrum can not be understood entirely in NRQCD. Additional help from SCET is necessary in certain kinematic regime for making reasonable theoretical predictions. In the current chapter, we will investigate inclusive J/ψ production in lepton annihilation $e^+e^- \to J/\psi + X$ by using SCET. In a recent paper, the Sudakov logarithms in the color-octet contribution were summed by combining NRQCD with SCET at the endpoint. However, to be consistent, the color-singlet contributions must also be summed in the endpoint region. This chapter is based on Ref. [56], in which we sum the leading logarithms in the color-singlet contribution to the J/ψ production cross section. We find that the color-singlet cross section is suppressed near the endpoint compared to the fixed-order NRQCD prediction.

3.1 INTRODUCTION

Bound states of heavy quarks and antiquarks have been of great interest since the discovery of the J/ψ [57]. In particular the production of quarkonium is an interesting probe of both perturbative and nonperturbative aspects of QCD dynamics. Production requires the creation of a heavy $Q\bar{Q}$ pair with energy greater than $2m_Q$, a scale at which the strong coupling constant is small enough that perturbation theory can be used. However, hadronization probes much smaller mass scales of order $m_Q v^2$, where v is the typical velocity of the quarks in the quarkonium. For J/ψ, $m_Q v^2$ is numerically of order $\Lambda_{\rm QCD}$ so the production process is sensitive to nonperturbative physics as well.

Many phenomenological problems can be understood well enough by using the Non-Relativistic Quantum Chromodynamics (NRQCD) [58, 59]. NRQCD provides a generalized factorization theorem that includes nonperturbative corrections to the color-singlet model. All infrared divergences can be factored into nonperturbative matrix elements, so that infrared safe calculations of inclusive decay rates are possible [3]. However, there are some predictions of NRQCD in conflict with the data, in particular the predicted polarization of J/ψ at the Fermilab Tevatron [60, 61] and more recently the production rate of J/ψ associated with extra c and $\bar{c}$ quarks (both inclusive and exclusive) at the B factories [62, 63]. In particular, Belle reports a large cross section for J/ψ produced along with open charm [62],

$$\frac{\sigma(e^+e^- \rightarrow J/\psi c\bar{c})}{\sigma(e^+e^- \rightarrow J/\psi X)} = 0.59^{+0.15}_{-0.13} \pm 0.12 \,.$$

The predicted ratio from leading order color-singlet production mechanisms alone is about 0.2 [64, 65] and a large color-octet contribution makes this ratio even smaller. In addition to the inclusive measurements, Belle reports a cross section for exclusive double charmonium production which exceeds previous theoretical estimates. Recent attempts to address the latter problem can be found in Ref. [66].

The inclusive J/ψ production at the B factories is another potential conflict between experimental observations and theoretical predictions using NRQCD [67, 68]. Leading order NRQCD calculations predict that for most of the range of allowed energies prompt J/ψ production should be dominated by color-singlet production mechanisms, while color-octet contributions dominate when the J/ψ energy is nearly maximal. Furthermore, as pointed out in Ref. [69], color-octet processes predict a dramatically different angular distribution for the J/ψ. Writing the differential cross section as

$$\frac{d\sigma}{dp_\psi \, d\cos\theta} = S(p_\psi)[1 + A(p_\psi)\cos^2\theta] \,, \tag{3.1}$$

where p_ψ is the J/ψ momentum and θ is the angle of the J/ψ with respect to the axis defined by the e^+e^- beams, one finds the color-singlet mechanism gives $A(p_\psi) \approx 0$ except for large p_ψ, where $A(p_\psi)$ becomes large and negative. On the other hand, color-octet production predicts $A(p_\psi) \approx 1$ at the end-point. The significant enhancement of the cross section accompanied by the change in angular distribution were proposed as a distinctive signal of

color-octet mechanisms in Ref. [69]. It was expected that these effects would be confined to J/ψ whose momentum is within a few hundred MeV of the maximum allowed.

However, experimental results do not agree with these expectations. The cross section data as a function of momentum does not exhibit any enhancement in the bins closest to the endpoint. On the other hand, the total cross section measured by the two experiments exceeds predictions based on the color-singlet model alone. The total prompt J/ψ cross section, which includes feeddown from ψ' and χ_c states but not from B decays, is measured to be $\sigma_{tot} = 2.52 \pm 0.21 \pm 0.21$ pb by BaBar, while Belle measures $\sigma_{tot} = 1.47 \pm 0.10 \pm 0.13$ pb. Estimates of the color-singlet contribution range from $0.4 - 0.9$ pb [64, 70, 65, 71]. Furthermore, $A(p_\psi)$ is measured to be consistent with 1 (with large errors) for $p_\psi > 2.6\,\text{GeV}$ (Belle) and $p_\psi > 3.5\,\text{GeV}$ (BaBar).

The NRQCD factorization formalism claims that the differential J/ψ cross section can be written as

$$d\sigma(e^+e^- \to J/\psi + X) = \sum_n d\hat{\sigma}(e^+e^- \to c\bar{c}[n] + X)\langle \mathcal{O}_n^{J/\psi}\rangle, \qquad (3.2)$$

where $d\hat{\sigma}$ is the inclusive cross section for producing a $c\bar{c}$ pair in a color and angular momentum state labeled by $[n] = {}^{2S+1}L_J^{(i)}$. In this notation, the spectroscopic notation for angular momentum quantum numbers is standard and $i = 1(8)$ for color-singlet (octet) production matrix elements. The short-distance coefficients are calculable in a perturbation series in α_s. The long-distance matrix elements $\langle \mathcal{O}_n^{J/\psi}\rangle$ are vacuum matrix elements of four-fermion operators in NRQCD [58]. These matrix elements scale as some power of the relative velocity $v \ll 1$ of the c and $\bar{c}$ quarks as given by the NRQCD power-counting rules.

At lowest order in v the only term in Eq. (3.2) is the color-singlet contribution, $[n] = {}^3S_1^{(1)}$, which scales as v^3. The coefficient for this contribution starts at $O(\alpha_s^2)$ [72]. There are two different contributions to the leading-order color-singlet, depending on what else is produced along with the J/ψ: $e^+e^- \to J/\psi + g + g$ and $e^+e^- \to J/\psi + c + \bar{c}$. Away from the kinematic endpoint $E_{max} = (s + M_\psi^2)/(2\sqrt{s})$, where s is the center-of-mass energy squared, color-octet contributions also start at $O(\alpha_s^2)$. Since the color-octet contributions are suppressed by $v^4 \sim 0.1$ relative to the leading color-singlet contributions, they are negligible throughout most of the allowed phase-space at leading order in perturbation theory.

The theoretical situation becomes more interesting, however, near the endpoint. The lowest-order, color-singlet term approaches a constant[1]

$$\lim_{z \to 1} \frac{d\hat{\sigma}[^3S_1^{(1)}]}{dz\,d\cos\theta} = \frac{64\pi\alpha^2\alpha_s^2 e_c^2}{27s^2 m_c}(1+r)\left(\frac{1+r}{1-r} - \cos^2\theta\right).$$ (3.3)

where $r = 4m_c^2/s$, and $z = E_{c\bar{c}}/E_{c\bar{c}}^{max}$ with $E_{c\bar{c}}^{max} = \sqrt{s}(1+r)/2$, while the lowest-order, color-octet piece is singular (proportional to a delta function). Physically, when the J/ψ emerges with close to the maximal energy, it is recoiling against an energetic gluon jet with energy of order M_Υ but invariant mass of order $M_\Upsilon\sqrt{\Lambda_{\rm QCD}/M_\psi}$. The degrees of freedom needed to describe this inclusive jet have been integrated out of NRQCD, and thus cannot be described by the effective field theory. The effective theory that correctly describes this kinematic regime is a combination of NRQCD for the heavy degrees of freedom, and SCET [5, 6, 7, 8] for the light energetic degrees of freedom. Furthermore, the renormalization group equations of SCET will sum the large kinematic preturbative corrections that appear near corners of phase space.

In a previous paper [73] the combination of NRQCD and SCET was used to sum the large kinematic logarithms (Sudakov logarithms) that arise in the color-octet contribution near the endpoint. For the color-octet contribution, there are also large non-perturbative contributions at the endpoint [74] that must also be summed into a non-perturbative shape function. Since the shape function is unknown, in Ref. [73] the shape function was modeled. Since it is universal, it is possible that it could be extracted from another process (such as J/ψ photoproduction [48]). With the summation of the perturbative corrections and the simple model chosen, a good fit to the data was obtained.

However, to be consistent, the color-singlet contribution should also be summed in the endpoint region. This is the goal of the present chapter. The kinematic logarithms in the $J/\psi + c + \bar{c}$ color-singlet contribution are small, since the mass of the charm quark acts as a cutoff. However, we would expect that the summed $J/\psi + g + g$ color-singlet rate would be suppressed relative to the unsummed rate. This would help alleviate the discrepancy with the open charm data. However, we would not expect a very large suppression except right

---

[1]The $J/\psi c\bar{c}$ contribution goes to zero before the kinematic endpoint, due to the non-zero mass of the charm quarks. It therefore does not contribute to the endpoint contribution given in Eq. (3.3).

near the endpoint, and thus do not expect that this will be a solution to the J/ψ + open charm question. This will be confirmed in our analysis in this thesis. The remainder of the chapter is organized as follows. In Sec 3.2 a factorization theorem for J/ψ production near the endpoint is developed. Then in Sec 3.3 the Sudakov logarithms are summed, including mixing with the $J/\psi + q + \bar{q}$ final state. In Sec 3.4 the phenomenology of the J/ψ production is investigated, and finally we conclude in Sec 3.5. A similar treatment of nonperturbative and perturbative endpoint corrections to the color-singlet and color-octet contributions in the inclusive decay $\Upsilon \to X + \gamma$ can be found in Refs. [44, 75], and we will rely on some of the results from these papers. Similar results have been previously reported in Ref. [76].

3.2   FACTORIZATION

In this section, we will derive a factorization theorem for $e^+e^- \to J/\psi + X$ near the kinematic endpoint, where the rate can be factored into a hard coefficient, a collinear jet function and an ultrasoft shape function. The derivation is quite similar to Refs. [8, 44, 73, 75, 48, 77]. We begin by briefly reviewing the kinematics of the process in the e^+e^- center of mass (COM) frame[73]. In the COM frame, the virtual photon has momentum $q^\mu = \sqrt{s}/2(n^\mu + \bar{n}^\mu)$ with the lightlike vectors defined as $\bar{n}^\mu = (1, 0, 0, 1)$ and $n^\mu = (1, 0, 0, -1)$. The J/ψ is moving in the z-direction with four-velocity

$$v^\mu = \frac{1}{2}\left(\frac{M_\psi}{x\sqrt{s}}n^\mu + \frac{x\sqrt{s}}{M_\psi}\bar{n}^\mu \right). \tag{3.4}$$

Here M_ψ is the J/ψ mass and $x = (E_\psi + p_\psi)/\sqrt{s}$. The $c\bar{c}$ pair has momentum $p_{c\bar{c}}^\mu = Mv^\mu + \ell^\nu = Mv^\mu + \Lambda^\mu{}_\nu\hat{\ell}^\nu$, where $M = 2m_c$ and ℓ^ν is the residual momentum of the $c\bar{c}$ pair inside the J/ψ. In the J/ψ rest frame, $\hat{\ell}^\mu$ has components of $O(\Lambda_{\rm QCD})$, which get boosted in the COM frame to ℓ^μ scaling as $\bar{n}\cdot\ell \sim M_\psi\Lambda_{\rm QCD}/(x\sqrt{s}), n\cdot\ell \sim x\sqrt{s}\Lambda_{\rm QCD}/M_\psi$ and $\ell_\perp \sim \Lambda_{\rm QCD}$. The momentum of the gluon jets is

$$p_X^\mu = \frac{\sqrt{s}}{2}\left[\left(1 - \frac{r}{\hat{x}}\right)n^\mu + (1 - \hat{x})\bar{n}^\mu \right] - \ell^\mu, \tag{3.5}$$

where $\hat{x} = xM/M_\psi$. In the end point region the NRQCD factorization formula breaks down because NRQCD does not include appropriate collinear modes. When $1 - x \sim \Lambda_{\text{QCD}}/M$, the jet is no longer highly virtual. Since $m_X^2/E_X^2 \sim \Lambda_{\text{QCD}}/M \ll 1$, the gluon jet is composed of energetic particles with small invariant mass that must be included explicitly in the effective theory. Hence, a new factorization theorem is needed to handle the end point, which can be derived using a combination of NRQCD for the heavy quark degrees of freedom and SCET [5, 6, 7, 8] that includes the collinear physics.

SCET has collinear degrees of freedom whose momentum scales as $\bar{n} \cdot p \sim Q$, $n \cdot p \sim \lambda^2 Q$, and $p^\perp \sim \lambda Q$, soft degrees of freedom whose momentum scales as λ and ultrasoft (usoft) degrees of freedom whose momentum scales as λ^2. Heavy quark fields in SCET are the same as in NRQCD when considering quarkonium. For $e^+ e^- \rightarrow J/\psi + X$, Q is of order $\sqrt{s}$, while $\lambda \sim \sqrt{1 - x} \sim \sqrt{\Lambda_{\text{QCD}}/M}$. To the order we are working, operators will contain usoft, collinear quarks and gluons and heavy quark fields. Soft fields do not enter to the order we are interested and are neglected.

We match QCD onto SCET at the scale Q by evaluating matrix elements in QCD at the scale Q and expanding in powers of λ. Each order in λ is reproduced in the effective theory by the product of SCET operators and Wilson coefficients. All the dependence on the large scale Q shows up in the Wilson coefficients. We must include all SCET operators that can contribute to the process under consideration at each order of λ. These operators must respect the symmetries of the effective theory. For $e^+ e^- \rightarrow J/\psi + X$, the operators must be invariant under both collinear and usoft gauge transformations [8]. Lorentz invariance is realized in the effective theory by additional constraints on the operators, from RPI [39] introduced in the previous chapter.

In the collinear sector of SCET there is a collinear fermion field $\xi_{n,p}$, a collinear gluon field $A_{n,q}^\mu$ (soft modes are ignored), and a collinear Wilson line

$$W_n(x) = \left[\sum_{\text{perms}} \exp\left(-g_s \frac{1}{\bar{\mathcal{P}}} \bar{n} \cdot A_{n,q}(x) \right) \right]. \tag{3.6}$$

The subscripts on the collinear fields are the light-cone direction n^μ, and the large components of the light-cone momentum $(\bar{n} \cdot q, q_\perp)$. We use the operator $\mathcal{P}^\mu$ to project out the momentum label [7], $\bar{n} \cdot \mathcal{P}\xi_{n,p} \equiv \bar{\mathcal{P}}\xi_{n,p} = \bar{n} \cdot p\xi_{n,p}$. In the usoft sector there is a usoft fermion

field q_{us}, a usoft gluon field A_{us}^μ, and a usoft Wilson line Y. Using the transformation properties for each of these fields under collinear and usoft gauge transformations [8], we can build invariant operators. The collinear-gauge invariant field strength is

$$G_n^{\mu\nu} \equiv -\frac{i}{g_s} W^\dagger [i\mathcal{D}_n^\mu + g_s A_{n,q}^\mu, i\mathcal{D}_n^\nu + g_s A_{n,q'}^\nu]W, \tag{3.7}$$

where

$$i\mathcal{D}_n^\mu = \frac{n^\mu}{2}\bar{\mathcal{P}} + \mathcal{P}_\perp^\mu + \frac{\bar{n}^\mu}{2}in\cdot D, \tag{3.8}$$

and $iD^\mu = i\partial^\mu + g_s A_{us}^\mu$ is the usoft covariant derivative. RPI requires the label operators and the usoft covariant derivatives, which scale differently with λ, to appear in the linear combination appearing in $i\mathcal{D}_n^\mu$. The leading piece of $G_n^{\nu\mu}$ is order λ and can be written as $\bar{n}_\nu G_n^{\nu\mu} = i[\bar{\mathcal{P}}, B_\perp^\mu]$, where

$$B_\perp^\mu = \frac{1}{g_s} W^\dagger (\mathcal{P}_\perp^\mu + g_s(A_{n,q}^\mu)_\perp)W. \tag{3.9}$$

The subscript $\perp$ on $B_\perp^\mu$ indicates that μ must be a perpendicular direction.

We next construct the operators necessary to describe color-singlet $^3S_1$ production at the end point. A $c\bar{c}$ pair in a color-singlet $^3S_1$ configuration must be accompanied by a colorless jet of quarks and gluons. The leading operator must have two gluon field operators to create the collinear gluons in the final state. Thus, we should construct the operator out of two $B_\perp$ fields in color singlet configuration. Taking gauge-invariance into consideration, the only operator is

$$\mathcal{O}_{\mu\,gg}(1,{}^3S_1) = \chi_{-\mathbf{p}}^\dagger \Lambda \cdot \boldsymbol{\sigma}^\delta \psi_\mathbf{p} \mathrm{Tr}\big\{ B_\perp^\alpha\, \Gamma_{\alpha\beta\delta\mu}^{(1,{}^3S_1)}(\bar{\mathcal{P}}, \bar{\mathcal{P}}^\dagger)\, B_\perp^\beta \big\}. \tag{3.10}$$

Here Λ is an operator which boosts J/ψ from its rest frame to an arbitrary frame.

At leading order, the coefficient is determined by requiring the SCET matrix element of Eq. (3.10) to reproduce the lowest order QCD diagrams for $e^+e^- \to c\bar{c} + gg$, shown in Fig. 12. Matching at tree level, we obtain

$$\Gamma_{\alpha\beta\mu\delta}^{(1,{}^3S_1)} = \frac{32\pi}{3}\frac{e_c e\alpha_s}{M^2}\frac{r}{1-r} g_{\alpha\beta}^\perp \Big(g_{\mu\delta} - \frac{1-r}{2}n_\mu n_\delta\Big), \tag{3.11}$$

where $r = 4m_c^2/s$ and $g_\perp^{\mu\nu} = g^{\mu\nu} - (n^\mu\bar{n}^\nu + n^\nu\bar{n}^\mu)/2$. We can also have a jet made up of a quark-antiquark pair. Again, taking gauge-invariance into account, the only operator is

$$\mathcal{O}_{\mu\,\bar{q}q}(1,{}^3S_1) = \chi_{-\mathbf{p}}^\dagger \Lambda \cdot \boldsymbol{\sigma}^\delta \psi_\mathbf{p} \bar{\xi}_{n,p} W_n \Gamma_{\delta\mu}^{(1,{}^3S_1)}(\bar{\mathcal{P}}, \bar{\mathcal{P}}^\dagger) W_n^\dagger \xi_{n,p}. \tag{3.12}$$

+ cross terms
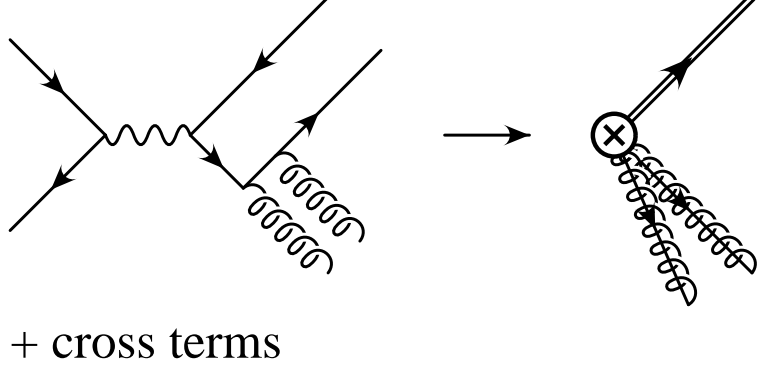
Figure 12: Matching the production amplitude for $e^+e^- \to c\bar{c} + gg$ in QCD and SCET. Collinear gluons are represented by a spring with a line through it.

The leading order Wilson coefficient is zero. However, since this operator occurs at the same order in λ, it can be generated through mixing. Just as in the case of Ref. [75], the mixing is small, and we will neglect this term for now.

At leading order in the SCET power counting the cross section in the endpoint can be expressed in a factored form to all orders in α_s

$$2E_\psi \frac{d\sigma}{d^3p_\psi} = \frac{e^2}{16\pi^3 s^3} L^{\mu\nu} H_{\mu\nu} \int dl^+ S(l^+, \mu) J_\omega(l^+ - \sqrt{s}(1 - \hat{x})),\qquad(3.13)$$

where J is the collinear jet function, S is the usoft function and $H_{\mu\nu}$ is the hard coefficient. We shall now prove this factorization theorem. Using the optical theorem, the production cross section can be written as

$$\begin{aligned}
2E_\psi \frac{d\sigma}{d^3p_\psi} &= \frac{e^2}{16\pi^3 s^3} L^{\mu\nu} \sum_X \langle 0|J_\nu^\dagger(0)|J/\psi + X\rangle \langle J/\psi + X|J_\mu(0)|0\rangle (2\pi)^4 \delta^4(q - p_\psi - p_X) \\
&= \frac{e^2}{16\pi^3 s^3} L^{\mu\nu} \int d^4y\, e^{-iq\cdot y} \sum_X \langle 0|J_\nu^\dagger(y)|J/\psi + X\rangle \langle J/\psi + X|J_\mu(0)|0\rangle \\
&\equiv \frac{e^2}{16\pi^3 s^3} L^{\mu\nu} \mathrm{Im} T_{\mu\nu},\qquad(3.14)
\end{aligned}$$

where the sum includes integration over the phase space of X. The lepton tensor is

$$L^{\mu\nu} = p_1^\mu p_2^\nu + p_1^\nu p_2^\mu - g^{\mu\nu} p_1 \cdot p_2,\qquad(3.15)$$

48

where $p_{1,2}$ are the momenta of the electron and positron, respectively, and

$$T_{\mu\nu} = -i \int d^4 y e^{-iqy} \sum_X \langle 0|J_\mu^\dagger(y)|J/\Psi + X\rangle\langle J/\Psi + X|J_\nu^\dagger(0)|0\rangle \,. \qquad (3.16)$$

The first step is to match the QCD current J_μ in Eq. (3.14) to leading order in λ,

$$J^\mu = \sum_\omega e^{-i(Mv - \bar{\mathcal{P}}n/2)\cdot y} \Gamma^{\alpha\beta\mu\delta} \tilde{J}_{\alpha\beta\delta}(\omega) \,, \qquad (3.17)$$

where the effective current is

$$\tilde{J}^{\alpha\beta\delta} = \psi_p^\dagger(\Lambda \cdot \boldsymbol{\sigma})^\delta \chi_{-p}\{\mathrm{Tr}[B_\perp^\alpha \delta_{\omega\mathcal{P}_-} B_\perp^\beta]\} \,, \qquad (3.18)$$

and $\Gamma_{\alpha\beta\mu\delta}^{(1,^3S_1)}(\omega)$ is given in Eq. (3.11). Substituting Eq. (3.17) into Eq. (3.16) and using $q^\mu - Mv^\mu + \bar{\mathcal{P}}n^\mu/2 \approx \sqrt{s}(1-\hat{x})\bar{n}^\mu/2$ gives

$$T_{\mu\nu} = \sum_{\omega,\omega'} \Gamma_{\alpha'\beta'\delta'\mu}^\dagger \Gamma_{\alpha\beta\delta\nu} T_{\mathrm{eff}}^{\alpha\alpha'\beta\beta'\delta\delta'}(\omega, \omega', \hat{x}, \mu) \,, \qquad (3.19)$$

where

$$T_{\alpha\alpha'\beta\beta'\delta\delta'}^{\mathrm{eff}} = -i \int d^4 y e^{-i\sqrt{s}(1-\hat{x})\bar{n}\cdot y} \sum_X \langle 0|\tilde{J}_{\alpha'\beta'\delta'}^\dagger(\omega')|J/\psi + X\rangle\langle J/\psi + X|\tilde{J}_{\alpha\beta\delta}(\omega)|0\rangle \,. \qquad (3.20)$$

Next we decouple the usoft gluons in T_{eff} using the field redefinition [8]

$$A_{n,q}^\mu = Y A_{n,q}^{(0)\mu} Y^\dagger \quad \rightarrow \quad W_n = Y W_n^{(0)} Y^\dagger \,, \qquad (3.21)$$

where the first identity implies the second. The collinear fields with the superscript (0) do not interact with usoft fields to lowest order in λ. In the color-singlet contribution all usoft Wilson lines Y cancel due to the identity $Y^\dagger Y = 1$. Furthermore, the J/ψ does not contain any collinear quanta, so using

$$\sum_{X_u} |J/\psi + X_u\rangle\langle J/\psi + X_u| = a_\psi^\dagger \sum_{X_u} |X_u\rangle\langle X_u|a_\psi = a_\psi^\dagger a_\psi, \qquad (3.22)$$

$$\sum_{X_c} |X_c\rangle\langle X_c| = 1, \qquad (3.23)$$

where $a_\psi^\dagger a_\psi$ projects onto final states containing a J/ψ, we can write

$$T_{\text{eff}}^{\alpha\alpha'\beta\beta'\delta\delta'} = \int d^4y \, e^{-i\sqrt{s}/2(1-\hat{x})\bar{n}\cdot y} \langle 0|\chi_{-\mathbf{p}}^\dagger(\Lambda\cdot\boldsymbol{\sigma})^{\delta'}\psi_{\mathbf{p}}(y) \, a_\psi^\dagger a_\psi \, \psi_{\mathbf{p}}^\dagger(\Lambda\cdot\boldsymbol{\sigma})^\delta\chi_{-\mathbf{p}}(0)|0\rangle \quad (3.24)$$

$$\times \, \langle 0|\{\text{Tr}[B_\perp^{\alpha'}\delta_{\omega'P_-}B_\perp^{\beta'}](y)\}\{\text{Tr}[B_\perp^\alpha\delta_{\omega P_-}B_\perp^\beta](0)\}|0\rangle.$$

We can use spin symmetry to simplify the usoft matrix element,

$$\Lambda_i^{\delta'}\Lambda_j^\delta\langle 0|\chi_{-\mathbf{p}}^\dagger\boldsymbol{\sigma}^i\psi_{\mathbf{p}}(y) \, a_\psi^\dagger a_\psi \, \psi_{\mathbf{p}}^\dagger\boldsymbol{\sigma}^j\chi_{-\mathbf{p}}(0)|0\rangle =$$
$$\frac{1}{3}\delta^{ij}\Lambda_i^\delta\Lambda_j^{\delta'}\langle 0|\chi_{-\mathbf{p}}^\dagger\boldsymbol{\sigma}^k\psi_{\mathbf{p}}(y) \, a_\psi^\dagger a_\psi \, \psi_{\mathbf{p}}^\dagger\boldsymbol{\sigma}^k\chi_{-\mathbf{p}}(0)|0\rangle. \quad (3.25)$$

Then we can use the identity $\delta^{ij}\Lambda_i^\delta\Lambda_j^{\delta'} = (v^\delta v^{\delta'} - g^{\delta\delta'})$, where v^δ is the four-velocity of the J/ψ, to further simplify the result.

We can define a collinear jet function from the collinear matrix element,

$$\langle 0|\{\text{Tr}[B^{\alpha'}\delta_{\omega'P_-}B^{\beta'}](y)\}\{\text{Tr}[B^\alpha\delta_{\omega P_-}B^\beta](0)\}|0\rangle \equiv \quad (3.26)$$
$$2\pi i(g_\perp^{\alpha\alpha'}g_\perp^{\beta\beta'} + g_\perp^{\alpha\beta'}g_\perp^{\beta\alpha'})\delta_{\omega\omega'}\int\frac{dk^+}{2\pi}\delta^{(2)}(y^\perp)\delta(y^+)e^{-\frac{i}{2}k^+y^-}J_\omega(k^+,\mu).$$

The jet function, $J_\omega(k^+,\mu)$, is only a function of one component of the usoft momentum, k^+, which follows from the collinear Lagrangian containing only the $n\cdot\partial$ derivative [8]. We can also define a usoft function

$$S(l^+,\mu) \equiv \int\frac{dy^-}{4\pi}e^{-il^+y^-}\frac{\langle 0|\chi_{-p}^\dagger\boldsymbol{\sigma}^k\psi_p(y^-)a_\psi^\dagger a_\psi\psi_p^\dagger\boldsymbol{\sigma}^k\chi_{-p}(0)|0\rangle}{4m_c\langle\mathcal{O}_1^\psi(^3S_1)\rangle}. \quad (3.27)$$

Combining Eqs. (3.19, 3.20, 3.26, 3.27), we can get the factorization theorem:

$$T_{\mu\nu} = H_{\mu\nu}\int dl^+ S(l^+,\mu)J_\omega(l^+ - \sqrt{s}(1-\hat{x})), \quad (3.28)$$

with

$$H_{\mu\nu} \equiv \frac{m_c}{6\pi}\langle\mathcal{O}_1^\psi(^3S_1)\rangle(v^\delta v^{\delta'} - g^{\delta\delta'})(g_\perp^{\alpha\alpha'}g_\perp^{\beta\beta'} + g_\perp^{\alpha\beta'}g_\perp^{\beta\alpha'})\Gamma_{\alpha'\beta'\mu\delta'}^\dagger\Gamma_{\alpha\beta\nu\delta}. \quad (3.29)$$

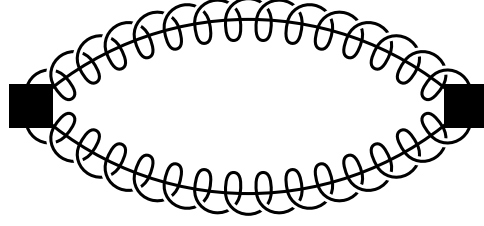Plugging Eq. (3.28) back into Eq. (3.14), proves the result Eq. (3.13).

50

Figure 13: Feynman diagram for the leading order jet function.

Changing variables from p_ψ to $z = E_{c\bar{c}}/E_{c\bar{c}}^{max}$ with $E_{c\bar{c}}^{max} = \sqrt{s}(1+r)/2$ and integrating over $\cos\theta$, we finally get

$$
\begin{aligned}
\frac{d\sigma}{dz} &= \frac{256\pi}{81} \frac{\alpha^2\alpha_s^2 e_c^2}{s^2 m_c} \frac{(1+r)(2r+1)}{(1-r)} \langle \mathcal{O}_1^\psi(^3S_1)\rangle P[r,z] \int dl^+ S(l^+,\mu) J_\omega(l^+ - \sqrt{s}(1-\hat{x})) \\
&= \sigma_0 P[r,z] \int dl^+ S(l^+,\mu) J_\omega(l^+ - \sqrt{s}(1-\hat{x})) \,.
\end{aligned}
\tag{3.30}
$$

Here

$$
\sigma_0 = \frac{256\pi}{81} \frac{\alpha^2\alpha_s^2 e_c^2}{s^2 m_c} \frac{(1+r)(1+2r)}{1-r} \langle \mathcal{O}_1^\psi(^3S_1)\rangle
\tag{3.31}
$$

is the differential cross section at the endpoint predicted by NRQCD. And $P[r,z]$ is a phase space factor defined to be $\sqrt{(1+r)^2 z^2 - 4r}/(1-r)$. Note that $P[r,1] = 1$.

To leading order the jet function can be calculated easily. The Feynman diagram for the vacuum matrix element is shown in Fig. 13. By evaluating the one loop integral, we get

$$
\mathrm{Im} J_\omega(k^+) = \frac{1}{2} \int_{-1}^{1} d\xi \delta_{\omega,\sqrt{s}(1-r)\xi} \,.
\tag{3.32}
$$

Substituting it into differential cross section in Eq. (3.30) and summing over ω gives,

$$
\frac{d\sigma}{dz} = \sigma_0 P[r,z] \int dl^+ S(l^+,\mu) \Theta(l^+ - \sqrt{s}(1-\hat{x})) \,.
\tag{3.33}
$$

The color-singlet usoft function just shifts the endpoint from the partonic to the physical hadronic endpoint [74]. To show this, we first note that the usoft function can formally be written as

$$
S(\ell^+,\mu) = \frac{\langle 0|\chi_{-p}^\dagger \boldsymbol{\sigma}^k \psi_p \delta(in\cdot\partial - \ell^+) a_\Psi^\dagger a_\Psi \psi_p^\dagger \boldsymbol{\sigma}^k \chi_{-p}|0\rangle}{4m_c \langle \mathcal{O}_1^\psi(^3S_1)\rangle} \,.
\tag{3.34}
$$

51

Then by integrating over ℓ^+ in Eq. (3.33) we get

$$\frac{d\sigma}{dz} = \sigma_0 P[r,z] \frac{\langle 0|\chi^\dagger_{-p}\boldsymbol{\sigma}^k\psi_p\Theta[in\cdot\partial + \sqrt{s}(1-\hat{x})]a^\dagger_\Psi a_\Psi\psi^\dagger_p\boldsymbol{\sigma}^k\chi_{-p}|0\rangle}{4m_c\langle\mathcal{O}^\psi_1(^3S_1)\rangle}\,. \tag{3.35}$$

Finally, writing x in terms of z

$$z = \frac{sx + M^2_\psi/x}{s + M^2_\psi} \approx 1 - \frac{1-r}{1+r}(1-x), \tag{3.36}$$

$$x \approx 1 - \frac{1+r}{1-r}(1-z)\,, \tag{3.37}$$

and using the result in Ref. [78] we get

$$\frac{d\sigma}{dz} = \Theta(1-z)\sigma_0 P[r,z]\,. \tag{3.38}$$

Notice that as $z \to 1$, this coincides with the lowest order NRQCD result in the same limit.

3.3   RESUMMING SUDAKOV LOGARITHMS

One of the main strengths of using an effective field theory is the ability to sum logarithms using the renormalization group equations (RGEs). Large logarithms of the ratio of well-separated scales arise naturally in perturbation theory, which can cause a breakdown of the perturbative expansion. By matching onto an effective theory, the large scale is removed to be replaced by a running scale μ. After matching at the high scale, the operators are run to the low scale using the RGEs. This sums all large logarithms into an overall factor, and any logarithms that arise in the perturbative expansion of the effective theory are of order one.

For $e^+e^- \to J/\psi + X$, there are logarithms of $\log(1-z)$ that appear in the perturbation series. Near the endpoint, $z \to 1$, these become large, and need to be summed, which the RGEs will do for us. For the color-singlet $^3S_1$ contribution, unlike the color-octet process [73], these endpoint logarithms are single, not double, logarithms. A similar situation occurs for radiative Υ decay [44]. Double logarithms occur when there is an overlap of soft and collinear logs. For the color-singlet case, the soft logarithms do not occur. This can be seen by the

fact that the usoft Wilson lines canceled out of the color-singlet matrix element. Physically, the long-wavelength gluons do not couple to the tightly bound color-singlet $c\bar{c}$.

We have matched in the previous section onto the SCET color-singlet operator, which intergrates out the large scale μ_H, replacing it with a running scale μ. We now run the color-singlet operator from the hard scale to the collinear scale, which sums all logarithms of $1 - z$. To run the color-singlet operator given in Eq. (3.10), we calculate the counterterm for the operator, determine the anomalous dimension, and then use this in the RGEs. Luckily, the calculation of the anomalous dimension has already been done in Ref. [44], and we can lift the results from that paper. The result for the resummed, differential cross-section after running from the hard scale μ_H to the collinear scale μ_c is

$$\frac{d\sigma_{\text{resum}}}{dz} = \sigma_0 P[r, z]\Theta(1 - z) \int_0^1 d\eta \Big[\frac{\alpha_s(\mu_c)}{\alpha_s(\mu_H)}\Big]^{2\gamma(\eta)}, \qquad (3.39)$$

where γ is defined as

$$\gamma \equiv \frac{2}{\beta_0}\left[C_A\Big[\frac{11}{6} + (\eta^2 + (1 - \eta)^2)\Big(\frac{1}{1 - \eta}\ln\eta + \frac{1}{\eta}\ln(1 - \eta)\Big)\Big] - \frac{n_f}{3}\right]. \qquad (3.40)$$

To sum the large logarithms, we use the same hard scale as in Ref. [73], $\mu_H = (s/M)(1 - r)$ and the collinear scale $\mu_c \approx \sqrt{1 - z}\mu_H$ in the above expression.[2]

To be completely consistent, we should include the mixing of the gg jet with the $\bar{q}q$ jet. Since the matching onto the $\bar{q}q$ operator begins at a higher order than the gg operator, except for very close to $z = 1$ the mixing term is small [75]. The calculation of the mixing in SCET was first done in Ref. [75], and we just quote the results here. Once we included the mixing effect, the resummed differential cross section becomes

$$\frac{1}{\sigma_0}\frac{d\sigma_{\text{resum}}}{dz} = \frac{8}{9}P[r, z]\Theta(1 - z) \sum_{n\,\text{odd}} \left[\frac{1}{f_{5/2}^{(n)}}\Big(\gamma_+^{(n)}r(\mu_c)^{2\lambda_+^{(n)}/\beta_0} - \gamma_-^{(n)}r(\mu_c)^{2\lambda_-^{(n)}/\beta_0}\Big)^2 \right.$$
$$\left. + \frac{3f_{3/2}^{(n)}}{8[f_{5/2}^{(n)}]^2}\frac{\gamma_{gq}^{(n)2}}{\Delta^2}\Big(r(\mu_c)^{2\lambda_+^{(n)}/\beta_0} - r(\mu_c)^{2\lambda_-^{(n)}/\beta_0}\Big)^2\right], \quad (3.41)$$

---

[2]The hard scale μ_H that we use is different than the choice of Ref. [76]. However, numerically they are almost the same, and will not have a large effect on the results.

where $r(\mu)$ is defined as

$$r(\mu) = \frac{\alpha_s(\mu)}{\alpha_s(\mu_{\mathrm{H}})}, \tag{3.42}$$

and

$$f_{5/2}^{(n)} = \frac{n(n+1)(n+2)(n+3)}{9(n+3/2)}, \tag{3.43}$$

$$f_{3/2}^{(n)} = \frac{(n+1)(n+2)}{n+3/2}. \tag{3.44}$$

We also defined $\lambda_{\pm}^{(n)}$ and $\gamma_{\pm}^{(n)}$ as

$$\lambda_{\pm}^{(n)} = \frac{1}{2}\left[\gamma_{gg}^{(n)} + \gamma_{q\bar{q}}^{(n)} \pm \Delta\right], \tag{3.45}$$

$$\gamma_{\pm}^{(n)} = \frac{\gamma_{gg}^{(n)} - \lambda_{\mp}^{(n)}}{\Delta}, \tag{3.46}$$

with

$$\Delta = \sqrt{(\gamma_{gg}^{(n)} - \gamma_{q\bar{q}}^{(n)})^2 + 4\gamma_{gq}^{(n)}\gamma_{qg}^{(n)}}, \tag{3.47}$$

$$\gamma_{gg}^{(n)} = C_A\left[\frac{2}{n(n+1)} + \frac{2}{(n+2)(n+3)} - \frac{1}{6} - 2\sum_{i=2}^{n+1}\frac{1}{i}\right] - \frac{1}{3}n_f, \tag{3.48}$$

$$\gamma_{gq}^{(n)} = C_F\frac{1}{3}\frac{n^2+3n+4}{(n+1)(n+2)}, \tag{3.49}$$

$$\gamma_{qg}^{(n)} = 3n_f\frac{n^2+3n+4}{n(n+1)(n+2)(n+3)}, \tag{3.50}$$

$$\gamma_{q\bar{q}}^{(n)} = C_F\left[\frac{1}{(n+1)(n+2)} - \frac{1}{2} - 2\sum_{i=2}^{n+1}\frac{1}{i}\right]. \tag{3.51}$$

In Fig. 14, we plot the difference of the mixing result, Eq. (3.41), and the non-mixing result, Eq. (3.39), normalized to the mixing result. For this plot, we chose the scale $\mu_c = \sqrt{1-z}\mu_H$. The difference between the two is a fraction of a percent, except extremely close to the endpoint, where our results no longer hold. We can therefore use either the mixing or the non-mixing result, Eq. (3.39) or Eq. (3.41).

3.4 PHENOMENOLOGY

The result from the previous section, Eq. (3.39) or Eq. (3.41), summed up the leading logarithmic corrections that are important near the endpoint. Away from the endpoint, the logarithms that we have summed are not important and contributions that we neglected in the endpoint become important. We therefore would like to interpolate between the leading order color-singlet calculation away from the endpoint and the resummed result in the endpoint. To do this, we will define the interpolated differential rate as

$$\frac{1}{\sigma_0}\frac{d\sigma_{\text{int}}}{dz} = \left(\frac{1}{\sigma_0}\frac{d\sigma_{\text{LO}}^{\text{dir}}}{dz} - P[r,z] \right) + \frac{1}{\sigma_0}\frac{d\sigma_{\text{resum}}}{dz} \ . \tag{3.52}$$

The term in parentheses vanishes as $z \to 1$, leaving only the resummed contribution in that region.[3] Away from the endpoint the resummed contribution combines with the $-P[r,z]$ to give higher order in $\alpha_s(\mu_H)$ corrections.

For our figures, we will use $m_c = 1.4$ GeV and $\sqrt{s} = 10.58$ GeV. In Fig. 15, we compare the resummed, interpolated result, Eq. (3.52), to the leading-order $e^+e^- \to J/\psi gg$ color-singlet result [64]. We also show the scale dependence of the interpolated result. The dot-dashed curve corresponds to the leading-order color-singlet result. All curves are normalized to σ_0 given in Eq. (3.31). The solid curve is the interpolated result, plotted at a scale $\mu_c = \sqrt{(1-z)}\mu_H$. The dashed curve is the interpolated result at a scale $\mu_c = 2\sqrt{(1-z)}\mu_H$, while the dotted curve uses the scale $\mu_c = \sqrt{(1-z)}\mu_H/2$. As can be seen, there is not a large scale dependence.

As shown in Fig. 15, the resummed result is smaller than the leading order result. In order to better see the effects of the resummation, in Fig. 16, we plot the difference of the leading-order, color-singlet result and the interpolated result, normalized to the leading-order result. As can be seen, in the endpoint region there corrections become large. However, over most of phase space, the corrections are less than 10%.

---

[3]This choice of interpolating between the results is different than the one made in Ref. [76]. Given the fact that the function $P[r,z]$ is a phase-space factor, we believe our choice more accurately encompasses the deviation due to higher-order QCD corrections. The choice in interpolating factor is the largest difference between our result and the result of Ref. [76]. Note that the choice made in Eq. (3.52) switches from the leading-order result to the resummed result closer to the endpoint than the choice in Ref. [76].

The total color-singlet contribution also has the $J/\psi + c + \bar{c}$ final state, so we need to combine the results above with the color-singlet $e^+e^- \rightarrow J/\psi + c\bar{c}$ contribution [64]. In Fig. 17 we compare the total leading-order, color-singlet result (dotted line) to the total, resummed color-singlet result (solid line) for $(1/\sigma_0)d\sigma/dp_\psi$. Also shown as the dashed line is the $J/\psi + c + \bar{c}$ contribution. While the resummed result is slightly suppressed compared to the leading-order result, qualitatively the plots are the same. Note that this implies that the resummation of the color-singlet contribution is not big enough to explain the anomalously large contribution to J/ψ associated with extra $c\bar{c}$ found at the B factories [62, 63].

In Fig. 18, we plot the color-singlet prediction for $A(p_\psi)$. The dashed curve is the leading order, color-singlet result, and the solid curve is the interpolated result, including the $J/\psi + c + \bar{c}$ contribution. Since the resummation is independent of the angle, both curves drop to the same value at the endpoint,

$$A(p_\psi^{\max}) = \frac{s - m_\psi^2}{s + m_\psi^2}.$$

(3.53)

Away from the endpoint, the resummed color-singlet rate is slightly larger than the leading-order rate. However, to explain the data, we still need to include the color-octet contribution.

To make a prediction for the differential cross section, we need to combine the color-singlet results discussed in this chapter with the resummed color-octet results from Ref. [73]. Given the size of the corrections found in this chapter, the results are qualitatively the same as those presented in Ref. [73].

3.5 SUMMARY

In this chapter, we studied the color-singlet contribution to J/ψ production in e^+e^- collision near the kinematic end point by using a combination of SCET and NRQCD. The calculation consists of matching onto a color-singlet operator in SCET that integrates out the hard scale. By decoupling the usoft modes from the collinear modes using a field redefinition, we are able to show a factorization theorem for the differential cross section. The differential rate can be factorized into a hard piece, a collinear jet function, and an usoft function. As pointed out

by Ref. [78] the usoft function in this case can be calculated, resulting in just a shift from the partonic to the physical endpoint.

By running the resulting rate from the hard scale to the collinear scale, we sum the logarithms of the ratio of the hard and collinear scales, which correspond to large Sudakov logarithms of $1 - z$. Finally, we combine the SCET calculation with the leading order, color-singlet NRQCD result to make a prediction for the color-singlet contribution to the differential cross section over the entire allowed kinematic range. If we combine the results for the color-singlet calculation given in this chapter the resummed results for the color-octet calculation given in Ref. [73], we now have a consistent prediction over the entire kinematic range for the $e^+e^- \rightarrow J/\psi + X$ differential cross section.

To be consistent the resummation of the color-singlet presented here must be included. However, except for right near the endpoint the size of the corrections are small. The color-octet contributions, as can be seen from Ref. [73], are necessary to get a reasonable fit to the data and are larger than the color-singlet contribution over all of phase space. Therefore, while the quantitative picture changes slightly, the qualitative picture is the same with or without running as was presented in Ref. [73]. In particular, we still do not have an explanation for the unexpectedly large number of J/ψ being produced with extra charm. The solution to this puzzle will have to come from another source.
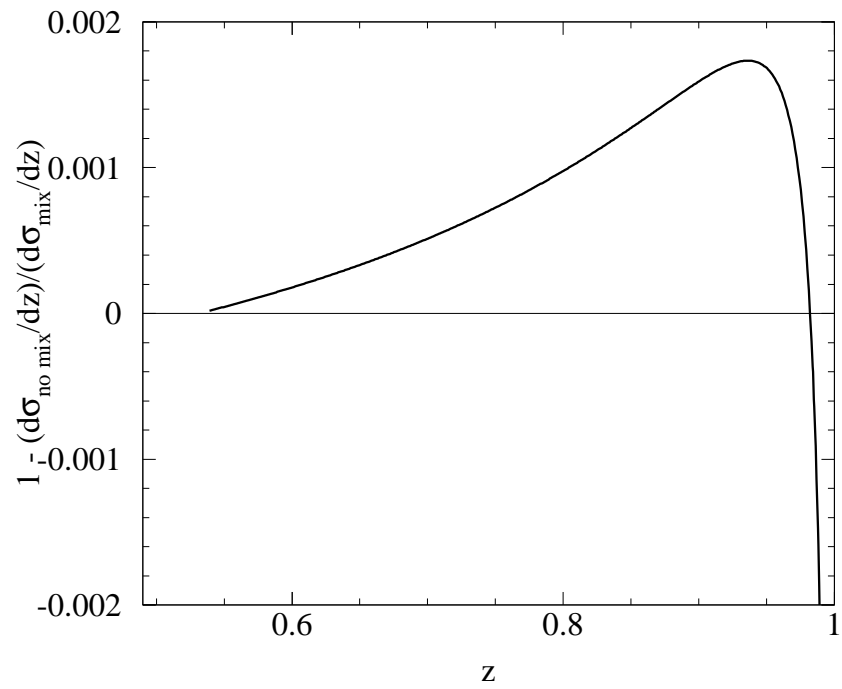
Figure 14: The difference between mixing and non-mixing $d\sigma_{\text{resum}}/dz$, normalized to the mixing result, calculated at the scale $\mu_c = \sqrt{1-z}\mu_H$.
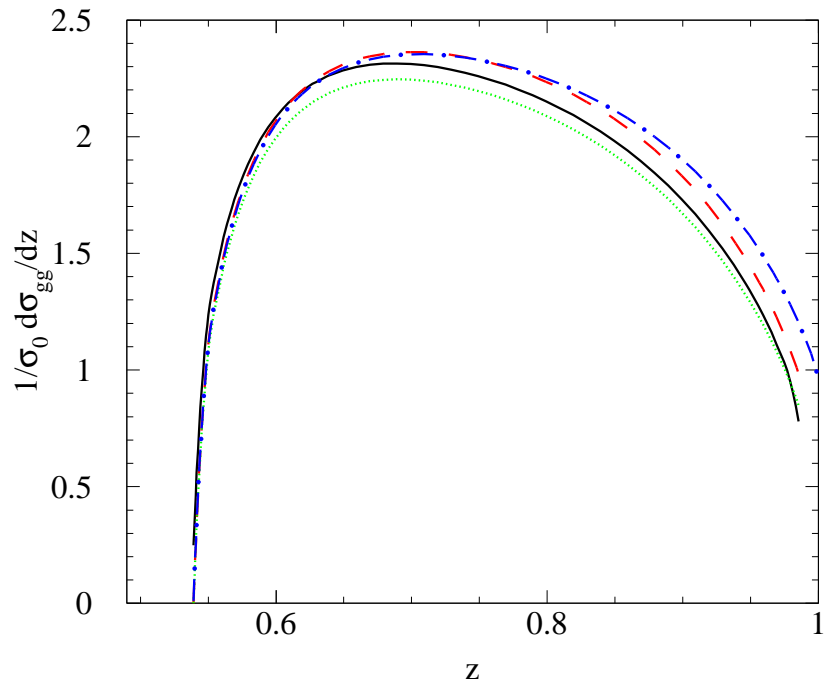
Figure 15: The color-singlet differential cross section . The dot-dashed curve is the leading-order NRQCD prediction. The solid curve is the interpolated result, Eq. (3.52) prediction at calculated at the scale $\mu_c = \sqrt{(1-z)}\mu_H$. The dashed curve is the interpolated result at the scale $\mu_c = 2\sqrt{(1-z)}\mu_H$, and the dotted curve is the interpolated result using the scale $\mu_c = \sqrt{(1-z)}\mu_H/2$.
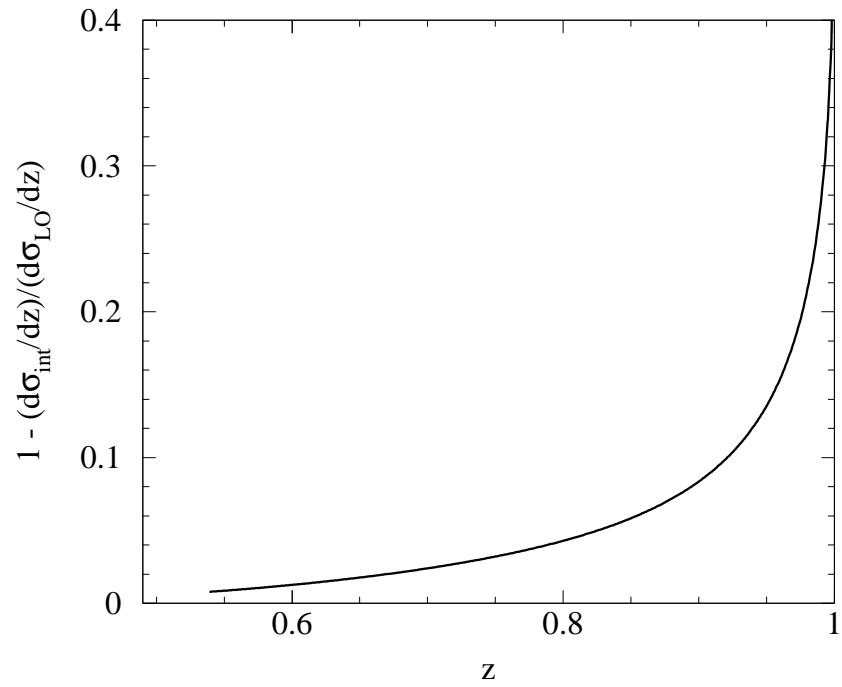
Figure 16: The difference of the leading-order NRQCD $e^+e^- \to J/\psi gg$ differential cross section and the interpolated result, Eq. (3.52), normalized to the leading-order result. The interpolated result was calculated at the scale $\mu_c = \sqrt{(1-z)}\mu_H$.
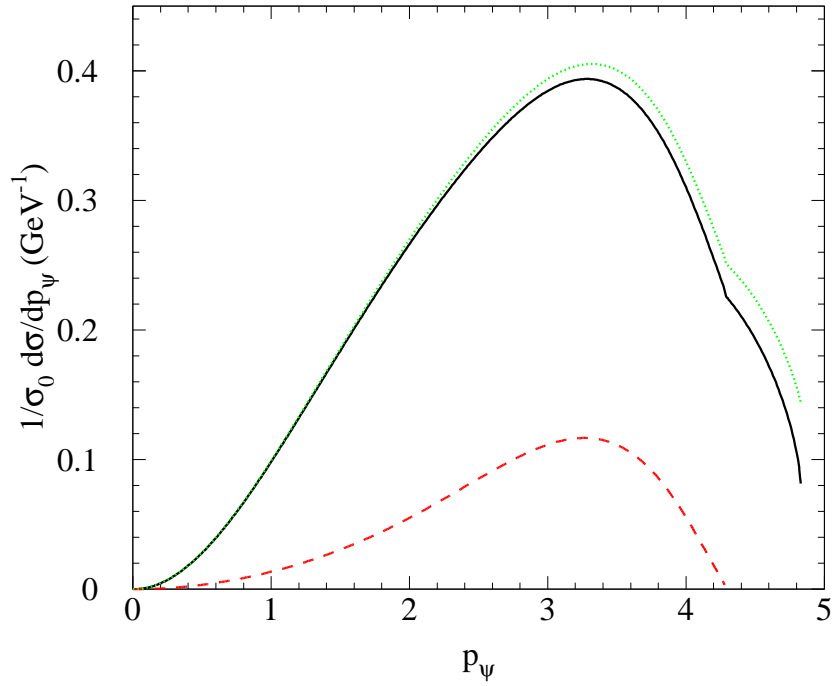
Figure 17: Comparison of the leading-order and resummed total color-singlet results. The dashed curve is the NRQCD prediction for $e^+e^- \to J/\psi c\bar{c}$. The dotted line is the total leading-order, color-singlet NRQCD prediction, while the solid curve is the total color-singlet prediction including the interpolated $e^+e^- \to J/\psi gg$ result. The resummed result was calculated at the scale $\mu_c = \sqrt{(1-z)}\mu_H$.

Figure 18: The color-singlet contribution to $A(p_\psi)$. The solid curve is the SCET prediction, with $\mu_c = \sqrt{(1-z)}\mu_H$ and the dashed curve is the lowest-order NRQCD prediction.

4.0 J/ψ PRODUCTION IN UPSILON DECAY

Now we turn to the problem mentioned in section 1.2, the J/ψ momentum spectrum in Upsilon decay. Recent experiments by the CLEO III detector at CESR indicate that the J/ψ spectrum produced in decay is in conflict with NRQCD calculations. Th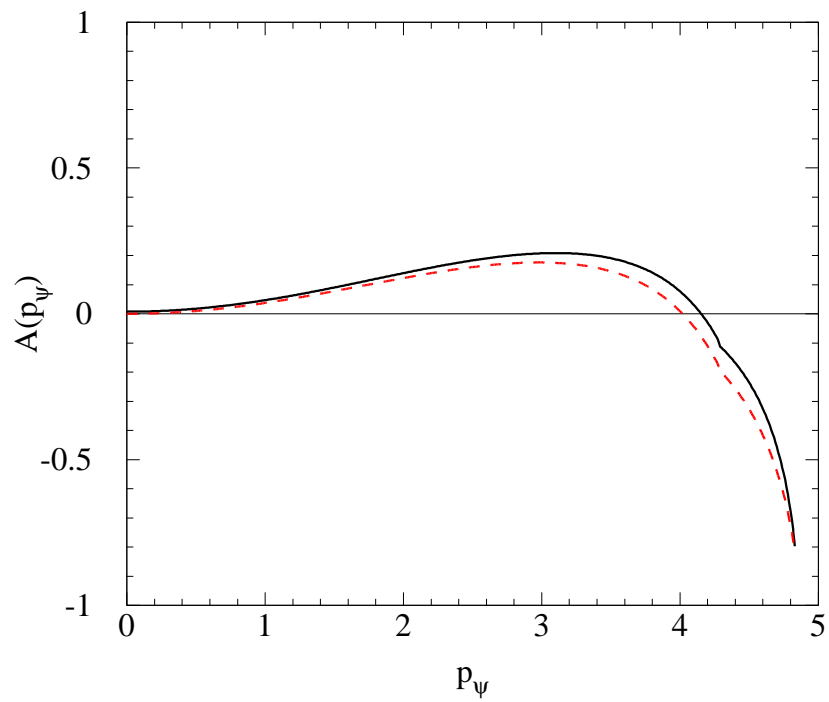e measured J/ψ momentum distribution is much softer than predicted by the color-octet mechanisms. The expected peak at the kinematic limit is not observed in the data. In this chapter we combine NRQCD with soft collinear effective theory to study the color-octet contribution to the $\Upsilon \to J/\psi X$ decay near phase space boundaries. We obtain a spectrum that is significantly softened when including the correct degrees of freedom in the endpoint region, giving better agreement with the data than previous predictions. This chapter is from a previous work in Ref. [79]

4.1 INTRODUCTION

NRQCD calculations have been made for the production of J/ψ in Υ decay through both color-singlet and color-octet configurations [82, 83]. Theoretical calculations predict that the color-singlet process $\Upsilon(1S) \to J/\psi c\bar{c}g + X$ features a soft momentum spectrum. Meanwhile, the theoretical estimates based on color-octet contribution indicates that the momentum spectrum peaks near the kinematic endpoint [83]. In contrast to the theoretical predictions, the experimentally measured momentum spectrum is significantly softer than predicted by the color-octet model and somewhat softer than the color-singlet case [33].

As mentioned in the last chapter, the NRQCD predictions break down in the endpoint region because the effective field theory does not contain the correct degrees of freedom to

describe the physics. NRQCD contains soft quarks and gluons, but it does not contain quarks and gluons moving collinearly. The correct effective theory to use in situations where there is both soft and collinear physics is Soft-Collinear Effective Theory (SCET) [5, 6, 7, 8]. SCET has the power to describe the endpoint regime by including the light energetic degrees of freedom. In addition, renormalization group equations of SCET can be used to resum large perturbative logarithmatic corrections. Nonperturbative martix element will occur naturally in deriving the factorization theorem using SCET.

In this chapter, we use SCET to study the color-octet contribution to the $\Upsilon \to J/\psi + X$ decay near the endpoint. We derive the factorization theorem in SCET for this process. We find that the spectrum is significantly softened when including perturbative up to leading logarithms (LL) and nonperturbative corrections near the endpoint, giving better agreement with the data than the previous predictions.

4.2   FACTORIZATION AND MATCHING

In this section, we briefly derive the SCET factorization theorem for $\Upsilon \to J/\psi + X$ near the endpoint. A more detailed derivation will be presented in the Appendix. The derivation is similar to radiative Υ decay [85], which we refer to for details. However, for the process that we are discussing here, it involves the decay of a heavy quarkonium into another heavy quarkonium, thus we should combine SCET with two independent NRQCD's for these two onia systems. The factorization for a similar process $B \to J/\psi + X_s$ has been discussed in Ref. [84].

Near the endpoint regime, a new factorization formula is required since the NRQCD does not include all the relevant physical degrees of freedom and thus the factorization theorem breaks down. This can easily be seen when we analyze the kinematics at the endpoint. To do so, we work in the centre-of-mass (COM) frame, and introduce light-cone coordinates.

By introducing the parameter $x = (E_\psi + p_\psi)/M_\Upsilon$, we have

$$p_\Upsilon^\mu = \frac{M_\Upsilon}{2} n^\mu + \frac{M_\Upsilon}{2} \bar{n}^\mu + k_\Upsilon^\mu,$$

$$p_\psi^\mu = \frac{M_\psi^2}{2 x M_\Upsilon} n^\mu + \frac{x M_\Upsilon}{2} \bar{n}^\mu + k_\psi^\mu,$$

$$p_X^\mu = \frac{M_\Upsilon}{2} \left[\left(1 - \frac{r}{x} \right) n^\mu + (1 - x) \bar{n}^\mu \right] + k_X^\mu. \tag{4.1}$$

Here $n = (1, 0, 0, 1)$ and $\bar{n} = (1, 0, 0, -1)$, we have defined $r = m_c^2 / m_b^2$, and we also assumed that $M_\psi = 2m_c$ and $M_\Upsilon = 2m_b$. k_Υ^μ and k_ψ^μ are the residual momentum of the $Q\bar{Q}$ pair inside the Υ and J/ψ respectively. Near the kinematic endpoint, the variable $x \to 1$ and thus the jet invariant mass approaches zero. In NRQCD, an expansion of k^μ / m_X is performed and hence the jet mode is integrated out, which is only valid when it has a large invariant mass, i.e., away from the endpoint. As $x \to 1$, the jet energy becomes large and the invariant mass becomes small, with k^μ / m_X of order 1. Hence we must keep k^μ / m_X to all orders. As a result, the standard NRQCD factorization breaks down at the endpoint. SCET is the appropriate framework for properly including the collinear modes needed in the endpoint in order to make reasonable predictions.

To derive the factorization theorem in SCET, we start from the optical theorem in which the decay rate can be written as

$$2E_\psi \frac{d\Gamma}{d^3 p_\psi} = \frac{1}{16\pi^3 M_\Upsilon} \sum_X \int d^4 y\, e^{-iq\cdot y} \langle \Upsilon | \mathcal{O}^\dagger(y) | J/\psi + X \rangle \langle J/\psi + X | \mathcal{O}(0) | \Upsilon \rangle, \tag{4.2}$$

where the summation includes integration over phase space of X. The SCET operator $\mathcal{O}$ is

$$\mathcal{O} = \sum_i \sum_\omega e^{-i(M_\Upsilon v + \bar{\mathcal{P}} \frac{n}{2}) \cdot y} C_i(\mu, \omega) \mathcal{J}_i(\omega), \tag{4.3}$$

where the Wilson coefficient C_i is obtained by matching from QCD to SCET at some hard scale $\mu = \mu_H$ and the SCET current function $\mathcal{J}_i(\omega)$ is contrained by the gauge invariance. For instance, in our case, to leading order the non-vanshing SCET current will be of the form

$$\mathcal{J}(\omega) = \Gamma_{abc}^{\alpha\beta\mu\nu} \left[B_{\alpha,\omega_1}^{a\perp} B_{\beta,\omega_2}^{b\perp} \right] \left[\chi_{\bar{b}}^\dagger (\Lambda_1 \cdot \sigma)_\nu \psi_b \right] \left[\chi_{\bar{c}}^\dagger (\Lambda_2 \cdot \sigma)_\mu T^c \psi_c \right]. \tag{4.4}$$
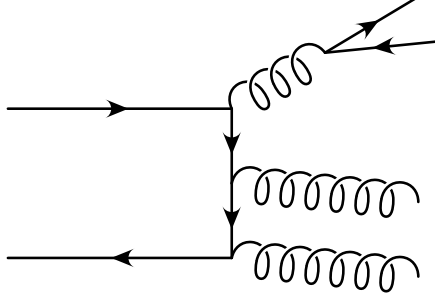
$$+ \text{ perms}$$

Figure 19: QCD production amplitude for $\Upsilon \to J/\psi + X$. The J/ψ is produced in a color-octet and becomes a color-singlet by emitting a soft gluon. There is another contribution to this process with only one gluon emitted, which is suppressed by an order of α_s.

Here $\Gamma_{abc}^{\alpha\beta\mu\nu}$ is a hard coefficient containing the color and spin structures that is obtained by matching onto the QCD Feynman diagrams shown in fig. 19. The matching gives

$$\Gamma_{abc}^{\alpha\beta\mu\nu} = \frac{2ig^4}{N_c} \frac{1}{1-r} \frac{M_\psi}{M_\Upsilon} \frac{1}{M_\psi^2} d_{abc} g_\perp^{\alpha\beta} \left(g_\perp^{\mu\nu} + \bar{n}^\mu n^\nu \right) , \tag{4.5}$$

where we have chosen the coefficient so that the Wilson coeffcient $C(\mu, \omega)$ is 1 at the hard scale μ_H. The Λ's boost the J/ψ or Υ from the COM frame to a frame where those quarkonia have arbitrary four-momentum. ψ and χ are the heavy quark and antiquark fields that create or annihilate the constituent heavy (anti-)quarks inside the quarkonia. As defined in the previous chapter, the collinear gauge invariant field strength is built out of the collinear gauge field $A_{n,q}^\mu$

$$B_\perp^\mu = \frac{-i}{g_s} W_n^\dagger \left(\mathcal{P}_\perp^\mu + g_s (A_{n,q}^\mu)_\perp \right) W_n , \tag{4.6}$$

where

$$W_n = \sum_{\text{perms}} \exp \left(-g_s \frac{1}{\bar{\mathcal{P}}} \bar{n} \cdot A_{n,q} \right) \tag{4.7}$$

66

is the collinear Wilson line. As a reminder, the operator $\mathcal{P}$ picks out the large momentum label [7].

The SCET operator $\mathcal{O}$ in Eq. (4.4) takes the form

$$\mathcal{O} = e^{-i(M_\Upsilon v + \bar{\mathcal{P}}\frac{n}{2})\cdot y}\, \Gamma^{\alpha\beta\mu\nu}_{abc}\, \mathcal{J}^{ab}_{\alpha\beta}\mathcal{O}^\Upsilon_\nu[\mathbf{1}^3S_1]\, \mathcal{O}^{c\psi}_\mu[\mathbf{8}^3S_1]\,, \tag{4.8}$$

where

$$\mathcal{J}^{ab}_{\alpha\beta} = B^{a\perp}_{\alpha,\omega_1} B^{b\perp}_{\beta,\omega_2}\,, \tag{4.9}$$

$$\mathcal{O}^\Upsilon_\nu[\mathbf{1}^3S_1] = \psi^\dagger_b\,(\Lambda_1\cdot\sigma)_\nu\,\chi_{\bar{b}}\,, \tag{4.10}$$

$$\mathcal{O}^{c\psi}_\mu[\mathbf{8}^3S_1] = \psi^\dagger_c\,(\Lambda_2\cdot\sigma)_\mu\,T^c\chi_{\bar{c}}\,. \tag{4.11}$$

Inserting the operator into Eq. (4.2), the $\mathcal{O}^\dagger(y)$ picks up an additional phase and the differential rate becomes

$$\begin{aligned}
2E_\psi\frac{\mathrm{d}\Gamma}{\mathrm{d}^3p_\psi} &= \frac{1}{16\pi^3 M_\Upsilon}\sum_X\int \mathrm{d}^4y\, e^{-iM_\Upsilon/2(1-x)\cdot\bar{n}\cdot y}\, \Gamma^{\alpha\beta\mu\nu\dagger}_{abc}\,\Gamma^{\alpha'\beta'\mu'\nu'}_{a'b'c'}\\
&\quad \times\langle\Upsilon|\,\mathcal{J}^{ab\dagger}_{\alpha\beta}\,\mathcal{O}^{\Upsilon\dagger}_\nu[\mathbf{1}^3S_1]\,\mathcal{O}^{c\psi\dagger}_\mu[\mathbf{8}^3S_1](y)|J/\psi + X\rangle\\
&\quad \langle J/\psi + X|\,\mathcal{J}^{a'b'}_{\alpha'\beta'}\mathcal{O}^\Upsilon_{\nu'}[\mathbf{1}^3S_1]\,\mathcal{O}^{c'\psi}_{\mu'}[\mathbf{8}^3S_1](0)|\Upsilon\rangle\\
&\equiv \Gamma^{\alpha\beta\mu\nu\dagger}_{abc}\,\Gamma^{\alpha'\beta'\mu'\nu'}_{a'b'c'}\,\mathcal{A}^{abc,a'b'c'}_{\alpha\beta\mu\nu,\alpha'\beta'\mu'\nu'}\,. \tag{4.12}
\end{aligned}$$

In the exponent of Eq. (4.12), we have used $q^\mu - M_\Upsilon v^\mu + \bar{\mathcal{P}}n^\mu/2 \approx M_\Upsilon/2(1-x)\bar{n}^\mu$. As mentioned in Section 4.2, we can decouple the usoft modes from the collinear degrees of freedom using the field redefinition [8]

We can decouple the usoft modes from the collinear degrees of freedom by making the field redefinition [8]

$$A^\mu_{n,q} \to Y A^\mu_{n,q} Y^\dagger\,, \tag{4.13}$$

which modifies $\mathcal{O}^{c\psi}_\mu[\mathbf{8}^3S_1]$ to

$$\mathcal{O}^{c\psi}_\mu \to Y\tilde{Y}\mathcal{O}^{c\psi}_\mu\tilde{Y}^\dagger Y^\dagger \equiv \tilde{\mathcal{O}}^{c\psi}_\mu\,, \tag{4.14}$$

where $Y(\tilde{Y})$ is the usoft Wilson line made out of the usoft gauge fields. In such a way, we can separate the collinear physics from the usoft, which leads to

$$
\begin{aligned}
\mathcal{A}^{abc,a'b'c'}_{\alpha\beta\mu\nu,\alpha'\beta'\mu'\nu'} &= \frac{1}{16\pi^3 M_\Upsilon} \int \mathrm{d}^4y \, e^{-iM_\Upsilon/2(1-x)\bar{n}\cdot y} \\
&\times \langle\Upsilon| \mathcal{O}^{\Upsilon\dagger}_\nu[\mathbf{1}^3 S_1] \tilde{\mathcal{O}}^{c\psi\dagger}_\mu[\mathbf{8}^3 S_1](y) \, a^\dagger_\psi a_\psi \, \mathcal{O}^\Upsilon_{\nu'}[\mathbf{1}^3 S_1] \tilde{\mathcal{O}}^{c'\psi}_{\mu'}[\mathbf{8}^3 S_1](0) |\Upsilon\rangle \\
&\times \langle 0| \mathcal{J}^{ab\dagger}_{\alpha\beta}(y)\mathcal{J}^{a'b'}_{\alpha'\beta'}(0)|0\rangle \,,
\end{aligned} \tag{4.15}
$$

where we have introduced an interpolating field, a_ψ, for the J/ψ and used the completeness of states in the usoft and collinear sectors

$$
\sum_{X_u} |J/\psi + X_u\rangle\langle J/\psi + X_u| = a^\dagger_\psi \sum_{X_u} |X_u\rangle\langle X_u| a_\psi = a^\dagger_\psi a_\psi, \tag{4.16}
$$

$$
\sum_{X_c} |X_c\rangle\langle X_c| = 1. \tag{4.17}
$$

The the usoft Wilson lines only come with the color-octet J/ψ operator, $\mathcal{O}^{c\psi}_\mu[\mathbf{8}^3 S_1]$. The Υ is a very compact bound state, due to the large b-quark mass. In a multipole expansion, long wavelength gluons interacts with the Υ color charge distribution through its color dipole moment since the state itself is color neutral. In the theoretical limit of very heavy bottom quark, this coupling to the dipole vanishes [84]. The order of the corrections can be estimated by means of the "vacuum-saturation approximation" [58]. A complete set of light-hadronic states $\sum_X |X\rangle\langle X|$ can be inserted between the Υ operator and the J/ψ operator. Notice that the Υ operator is in color-singlet configuration. therefore the sum over states is saturated by the QCD vacuum $|0\rangle$ with corrections of order v^4 [58]. These arguments allow us to factorize the matrix element into the convolution of the shape functions for Υ in color-singlet configuration and J/ψ in color-octet one. Thus we are able to write

$$
\begin{aligned}
\mathcal{A}^{abc,a'b'c'}_{\alpha\beta\mu\nu,\alpha'\beta'\mu'\nu'} &\approx \frac{1}{16\pi^3 M_\Upsilon} \int \mathrm{d}^4y \, e^{-iM_\Upsilon/2(1-x)\bar{n}\cdot y} \\
&\times \langle\Upsilon| \mathcal{O}^{\Upsilon\dagger}_\nu[\mathbf{1}^3 S_1](y) \, \mathcal{O}^\Upsilon_{\nu'}[\mathbf{1}^3 S_1](0) |\Upsilon\rangle \\
&\times \langle 0| \tilde{\mathcal{O}}^{c\psi\dagger}_\mu[\mathbf{8}^3 S_1](y) \, a^\dagger_\psi a_\psi \, \tilde{\mathcal{O}}^{c'\psi}_{\mu'}[\mathbf{8}^3 S_1]|0\rangle \\
&\times \langle 0| \mathcal{J}^{ab\dagger}_{\alpha\beta}(y)\mathcal{J}^{a'b'}_{\alpha'\beta'}(0)|0\rangle \,.
\end{aligned} \tag{4.18}
$$

Following this procedure, the decay rates can be written as a convolution of soft shape functions and the jet function with an overall hard coefficient. By introducing $z = E_\psi/m_b$ and using $p_\psi^2 \mathrm{d}p_\psi/(2E_\psi) = m_b^2\sqrt{z-4r}\mathrm{d}z/2$, we get the decay rate of the form

$$\frac{\mathrm{d}\Gamma}{\mathrm{d}z} = \Gamma_0 P[z,r] \sum_\omega |C(\omega,\mu)|^2 \int \mathrm{d}k^+ \int \mathrm{d}l^+ J_\omega(k^+) S_\psi(l^+) S_\Upsilon(M_\Upsilon(1-x) - k^+ - l^+) , \quad (4.19)$$

where $P[z,r] = 8\pi\sqrt{z^2-4r}/(1-r)$ is a kinematic factor and

$$\Gamma_0 = \frac{\pi\alpha_s^4}{18} \frac{N_c^2-4}{N_c^3} \frac{2+r}{1-r} \frac{1}{m_b^2 m_c^3} \langle \Upsilon|\mathcal{O}_\Upsilon^{\mathbf{1}}[^3S_1]|\Upsilon\rangle \langle \mathcal{O}_\psi^{\mathbf{8}}[^3S_1]\rangle . \quad (4.20)$$

We have used spin symmetry [86]

$$\Lambda_i^\delta \Lambda_j^{\delta'} \langle \ldots \sigma^i \ldots \sigma^j \ldots \rangle = \frac{1}{3}\delta^{ij}\Lambda_i^\delta\Lambda_j^{\delta'} \langle \ldots \sigma^k \ldots \sigma^k \ldots \rangle , \quad (4.21)$$

to simplify the matrix elements, and applied the identity $\delta^{ij}\Lambda_i^\delta\Lambda_j^{\delta'} = (v^\delta v^{\delta'} - g^{\delta\delta'})$, where v^δ is the four-velocity of the Υ or J/ψ.

The shape function for J/ψ is defined as

$$S_\psi(l^+) = \int \frac{\mathrm{d}y^-}{4\pi} e^{-\frac{i}{2}l^+y^-} \frac{\langle 0| \left[\chi_{\bar{c}}^\dagger \sigma_i Y \tilde{Y} T^k \tilde{Y}^\dagger Y^\dagger \psi_c(y^-) a_\psi^\dagger a_\psi \psi_c^\dagger \sigma_i Y \tilde{Y} T^k \tilde{Y}^\dagger Y^\dagger \chi_{\bar{c}} \right] |0\rangle}{4m_c\langle \mathcal{O}_\psi^{\mathbf{8}}[^3S_1]\rangle} , \quad (4.22)$$

where we have made the field redefinition in Eq. (4.13) for the two collinear gluons in the final state by introducing two different usoft Wilson lines Y and $\tilde{Y}$. For Υ we have the shape function

$$S_\Upsilon(l^+) = \int \frac{\mathrm{d}y^-}{4\pi} e^{-\frac{i}{2}l^+y^-} \frac{\langle \Upsilon|\chi_{\bar{b}}^\dagger \sigma_i \psi_b(y^-)\psi_b^\dagger \sigma_i \chi_{\bar{b}}|\Upsilon\rangle}{4m_b\langle \Upsilon|\mathcal{O}_\Upsilon^{\mathbf{1}}[^3S_1]|\Upsilon\rangle} , \quad (4.23)$$

respectively. Both shape functions are normalized so that $\int \mathrm{d}l^+ S_{\psi,\Upsilon}(l^+) = 1$.

The jet function is given by

$$\begin{aligned}
&\langle 0| \left[B_\alpha^{a\perp} B_\beta^{b\perp}(y) B_{\alpha'}^{a'\perp} B_{\beta'}^{b'\perp}(0) \right] |0\rangle \\
&= \frac{i}{2} (g_{\alpha\alpha'}g_{\beta\beta'}\delta^{aa'}\delta^{bb'} + g_{\alpha\beta'}g_{\beta\alpha'}\delta^{ab'}\delta^{ba'}) \delta_{\omega\omega'} \int \frac{\mathrm{d}k^+}{2\pi}\delta^{(2)}(y^\perp)\,\delta(y^+)e^{-\frac{i}{2}k^+y^-} J_\omega(k^+) ,
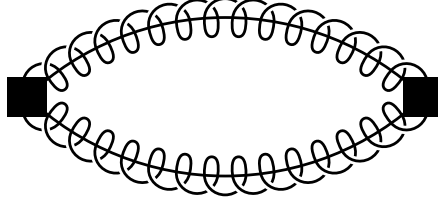\end{aligned}$$
$$(4.24)$$

Figure 20: Feynman diagram for the leading-order jet function. The spring with a line through it represents a collinear gluon.

which is the same as the jet function defined in the previous chapter except for the color structure. To leading order, the jet function can be calculated by evaluating the diagram shown in Fig. 20 , which gives

$$
J_\omega(k^+) = \frac{1}{8\pi}\Theta(k^+) \int_0^1 \mathrm{d}\xi \, \delta_{\xi,(\bar{n}Q+\omega)/(2\bar{n}Q)} \,, \tag{4.25}
$$

where Q is the total four momentum carried by the jets.

The J/ψ shape function can formally be written as

$$
S_\psi(l^+) = \frac{\langle 0| \left[\chi_{\bar{c}}^\dagger \sigma_i Y \tilde{Y} T^k \tilde{Y}^\dagger Y^\dagger \, \psi_c \, \delta(in \cdot \partial - l^+) a_\psi^\dagger a_\psi \, \psi_c^\dagger \sigma_i Y \tilde{Y} T^k \tilde{Y}^\dagger Y^\dagger \, \chi_{\bar{c}} \right] |0\rangle}{4 m_c \langle \mathcal{O}_\psi^{\mathbf{8}}[^3S_1] \rangle} \,, \tag{4.26}
$$

and to lowest order in v^2, $S_\Upsilon(l^+) \to \delta(l^+)$. By integrating over k^+ and l^+ in Eq. (4.19), we find the tree level decay rates become

$$
\frac{\mathrm{d}\Gamma}{\mathrm{d}z} = \Gamma_0 \tilde{P}[z,r]\Theta(1-x) \,, \tag{4.27}
$$

with $\tilde{P}[z,r] = P[z,r]/8\pi$. This can easily be seen to reproduce the tree level calculation of NRQCD [83].

4.3 RUNNING

Effective field theories provide a powerful tool to sum logarithms by using the renormaliza-
tion group equations (RGEs). Logarithms of the ratio of different scales arise naturally in
perturbation theory, which can cause a breakdown of the perturbative expansion when those
scales are well separated. By matching onto an effective theory, the large scale is removed
to be replaced by a running scale μ and the effective operators are run from a high scale to
the low scale using the RGEs, which sum all large logarithms of the ratio of scales into an
overall factor.

In our case, there are logarithms of the form $\log(1-x)$ that will appear in the perturbation
series. Near the endpoint, $x \to 1$, these become large, and must be resummed. In this section,
we will apply the RGEs of SCET to sum these large logarithms.

In the previous section, we have matched QCD onto the SCET operator by intergrating
out the hard scale μ_H, replacing it with a running scale μ. We now run the operator from
this hard scale to the collinear scale. To do so, we calculate the counterterm for the operator
to determine the anomalous dimension, and then use this in the RGEs.

The one-loop corrections to the SCET operator in Eq. (4.4) is given by the graphs in
Fig. 21. Evaluating these diagrams gives the divergent term

$$
\begin{aligned}
\mathcal{A}_{1-\text{loop}} \;=\; & \sum_{\omega} \frac{\alpha_s C_A}{4\pi} \left\{ \left[\frac{1}{\epsilon^2} + \frac{1}{\epsilon} \left(2 + \log \frac{\mu^2}{\bar{n}{\cdot}Q^2/r} \right) \right] \right. \\
& \left. + \frac{1}{\epsilon} \left[\frac{\omega(\bar{n}{\cdot}Q + \omega)}{\bar{n}{\cdot}Q(\bar{n}{\cdot}Q - \omega)} \log \frac{\bar{n}{\cdot}Q + \omega}{2\bar{n}{\cdot}Q} - \frac{\omega(\bar{n}{\cdot}Q - \omega)}{\bar{n}{\cdot}Q(\bar{n}{\cdot}Q + \omega)} \log \frac{\bar{n}{\cdot}Q - \omega}{2\bar{n}{\cdot}Q} \right] \right\} \times \mathcal{A}_0 \,.
\end{aligned}
\tag{4.28}
$$

The calculation lets us estimate the hard scale be $\mu_H = \bar{n}{\cdot}Q/\sqrt{r}$ which will minimize the
logarithm. The divergent piece must be canceled by $Z_{\mathbf{8}} Z_3 / Z_{\mathcal{O}} - 1$, where $Z_{\mathcal{O}}$ is the couterterm
for the operator in SCET, Z_3 is the gluon wave function counterterm

$$
Z_3 = 1 + \frac{\alpha_s}{4\pi} \frac{1}{\epsilon} \left(\frac{5}{3} C_A - \frac{4 n_F}{3} T_F \right) \,,
\tag{4.29}
$$

and $Z_{\mathbf{8}}$ is the counterterm of color-octet J/ψ operator

$$
Z_{\mathbf{8}} = 1 + \frac{\alpha_s C_A}{4\pi\epsilon} \,.
\tag{4.30}
$$

This leads to

$$
\begin{aligned}
Z_{\mathcal{O}} - 1 &= \sum_{\omega} \frac{\alpha_s C_A}{4\pi} \left\{ \left[\frac{1}{\epsilon^2} + \frac{1}{\epsilon} \left(\log \frac{\mu^2}{\bar{n} \cdot Q^2/r} \right) + \frac{1}{\epsilon} \left(\frac{14}{3} - \frac{4n_F}{3} \frac{T_F}{C_A} \right) \right] \right. \\
&\left. + \frac{1}{\epsilon} \left(+\frac{\omega(\bar{n} \cdot Q + \omega)}{\bar{n} \cdot Q(\bar{n} \cdot Q - \omega)} \log \frac{\bar{n} \cdot Q + \omega}{2\bar{n} \cdot Q} - \frac{\omega(\bar{n} \cdot Q - \omega)}{\bar{n} \cdot Q(\bar{n} \cdot Q + \omega)} \log \frac{\bar{n} \cdot Q - \omega}{2\bar{n} \cdot Q} \right) \right\} .
\end{aligned}
$$

(4.31)

From Eq. (4.31), we can extract the anomalous dimension of the operator through the standard method. Using the anomalous dimension in the RGE for the color-octet Wilson coefficient and running from the hard scale down to the collinear scale gives

$$
|C(\xi, \mu_c)|^2 = \left[\frac{\mu_c^2}{\bar{n} \cdot Q^2/r} \right]^{-\frac{2C_A}{b_0}} \left[\frac{\alpha_s(\mu_c^2)}{\alpha_s(\bar{n} \cdot Q^2/r)} \right]^{-\frac{8\pi C_A}{\alpha_s(\bar{n} Q^2/r) b_0^2}} \left[\frac{\alpha_s(\mu_c^2)}{\alpha_s(\bar{n} \cdot Q^2/r)} \right]^{4\eta[\xi]} ,
$$

(4.32)

where

$$
\eta[\xi] = \frac{C_A}{2b_0} \left[\left(\frac{14}{3} - \frac{4n_F}{3} \frac{T_F}{C_A} \right) - (2\xi - 1) \left(\frac{1 - \xi}{\xi} \log(1 - \xi) - \frac{\xi}{1 - \xi} \log \xi \right) \right] ,
$$

(4.33)

with $\xi = (\bar{n} \cdot Q + \omega)/(2\bar{n} \cdot Q)$, $b_0 = 11C_A/3 - 2n_F/3$, and the collinear scale $\mu_c^2 \approx m_X^2$.

At the collinear scale, the jet mode can be regarded as large and can be integrated out. The decay rate can be further run down to the soft scale μ_s. To do this, we first note that the decay rate can be modified to

$$
\frac{d\Gamma}{dz} = \Gamma_0 \tilde{P}[z, r] \int_0^1 d\xi |C(\xi, \mu_c)|^2 \int dl^+ dl^{+\prime} \Theta(M_\Upsilon(1 - x) - l^+) \mathcal{U}_s(l^+ - l^{+\prime}, \mu_c, \mu_s) S_\psi(l^{+\prime}, \mu_s) ,
$$

(4.34)

since in Ref. [78], it was shown that

$$
\begin{aligned}
\langle \Upsilon | \chi_{\bar{b}}^\dagger \sigma_i \psi_b \, \Theta(in \cdot \partial + M_\Upsilon(1 - x) - l^+) \, \psi_b^\dagger \sigma_i \chi_{\bar{b}} | \Upsilon \rangle &= \\
\Theta(M_\Upsilon(1 - x) - l^+) \langle \Upsilon | \chi_{\bar{b}}^\dagger \sigma_i \psi_b \, \psi_b^\dagger \sigma_i \chi_{\bar{b}} | \Upsilon \rangle . &\ (4.35)
\end{aligned}
$$

Here we introduced an evolution kernel $\mathcal{U}_s$ as in Ref. [87]. The soft shape function has evolution through $\mathcal{U}_s$ which will sum the large logarithms between μ_s and μ_c.

The evolution kernel can be calculated explicitly [87], once we figure out the anomalous dimension for the soft shape function. To one-loop order, calculating the diagrams in fig. 22, we get

$$Z_{S_\psi} - 1 = \frac{\alpha_s}{2\pi} C_A \left[\left(-\frac{1}{\epsilon^2} - \frac{1}{\epsilon} \log \frac{\mu^2}{r M_\Upsilon^2} + \frac{1}{\epsilon} \right) \delta(k^+) + \frac{2}{\epsilon} \frac{1}{M_\Upsilon} \left(\frac{M_\Upsilon \Theta(k^+)}{k^+} \right)_+ \right]. \quad (4.36)$$

Therefore we $\mathcal{U}_s$ is

$$\mathcal{U}_s(l^+ - l^{+'}) = \frac{e^{\tilde{K}} (e^{\gamma_E})^{\tilde{\omega}}}{\mu_s \Gamma(-\tilde{\omega})} \left[\frac{\mu_s^{1+\tilde{\omega}} \Theta(l^+ - l^{+'})}{(l^+ - l^{+'})^{1+\tilde{\omega}}} \right]_+, \quad (4.37)$$

with $\tilde{\omega}$ is defined as

$$\tilde{\omega} = -\frac{2C_A}{\pi} \int_{\alpha_s(\mu_s)}^{\alpha_s(\mu_c)} \frac{\alpha \, d\alpha}{\beta[\alpha]} = \frac{4C_A}{b_0} \log \frac{\alpha_s(\mu_c)}{\alpha_s(\mu_s)}, \quad (4.38)$$

where $\beta[\alpha_s] = -(11 C_A/3 - 2 n_F/3) \alpha_s^2/(2\pi)$. Note that $\tilde{\omega} < 0$. We defined a function $\tilde{K}_\gamma$

$$\tilde{K}_\gamma = \frac{C_A}{\pi} \int_{\alpha_s(\mu_s)}^{\alpha_s(\mu_c)} \frac{\alpha \, d\alpha}{\beta[\alpha]} (1 + \log r) = -\frac{2C_A}{b_0} (1 + \log r) \log \frac{\alpha_s(\mu_c)}{\alpha_s(\mu_s)}, \quad (4.39)$$

which is related to $\tilde{K}$ in Eq. (4.37) by

$$\begin{aligned}
\tilde{K} &= \tilde{K}_\gamma - \frac{2C_A}{\pi} \int_{\alpha_s(\mu_s)}^{\alpha_s(\mu_c)} \frac{\alpha \, d\alpha}{\beta[\alpha]} \int_{\alpha_s(\mu_s)}^{\alpha} \frac{d\alpha'}{\beta[\alpha']} \\
&= \tilde{K}_\gamma + \frac{8\pi C_A}{b_0^2 \alpha_s(\mu_c)} \left(\frac{\alpha_s(\mu_c)}{\alpha_s(\mu_s)} - 1 - \frac{\alpha_s(\mu_c)}{\alpha_s(\mu_s)} \log \frac{\alpha_s(\mu_c)}{\alpha_s(\mu_s)} \right).
\end{aligned} \quad (4.40)$$

The soft scale is $\mu_s^2 \sim r M_\Upsilon^2 (1-x)^2$.

Gathering all the pieces we have, we find the resumed decay rate

$$\begin{aligned}
\frac{d\Gamma}{dz} = \quad & \Gamma_0 \tilde{P}[z,r] \left[\frac{\mu_c^2}{\bar{n} \cdot Q^2/r} \right]^{-\frac{2C_A}{b_0}} \left[\frac{\alpha_s(\mu_c^2)}{\alpha_s(\bar{n} \cdot Q^2/r)} \right]^{-\frac{8\pi C_A}{\alpha_s(\bar{n} Q^2/r) b_0^2}} \int_0^1 d\xi \left[\frac{\alpha_s(\mu_c^2)}{\alpha_s(\bar{n} \cdot Q^2/r)} \right]^{4\eta[\xi]} \\
& \times \frac{e^{\tilde{K}} (e^{\gamma_E})^{\tilde{\omega}}}{\mu_s \Gamma(-\tilde{\omega})} \int dl^+ dl^{+'} \Theta(M_\Upsilon(1-x) - l^+) \left[\frac{\mu_s^{1+\tilde{\omega}} \Theta(l^+ - l^{+'})}{(l^+ - l^{+'})^{1+\tilde{\omega}}} \right]_+ S_\psi(l^{+'}, \mu_s) \quad (4.41)
\end{aligned}$$

4.4 PHENOMENOLOGY

The decay rate from the previous section, Eq. (4.41), summed up the leading logarithmic corrections which are important near the kinematic endpoint. Away from that region, the logarithms that we have summed are not important and contributions that we neglected in the endpoint become important. We therefore would like to interpolate between the leading order color-octet contribution in NRQCD away from the endpoint and the resummed result near the endpoint. We choose the interpolated differential rate as

$$\frac{\mathrm{d}\Gamma}{\mathrm{d}y} = (1-y)\left(\frac{\mathrm{d}\Gamma}{\mathrm{d}y}\right)_{\mathrm{NRQCD}} + y\left(\frac{\mathrm{d}\Gamma}{\mathrm{d}y}\right)_{\mathrm{SCET}}, \tag{4.42}$$

to guarantee the interpolated decay rate be positive. Here, in order to compare with the data, we have used the scaled momentum defined as $y = p_\psi/p_\psi^{max}$. We see that as $y \to 1$ the first term vanishes, leaving only the SCET contribution in the endpoint region.

To proceed, we need the soft shape function of J/ψ that appears in Eq. (4.41). We will apply a modified version of a model used in the decay of B mesons [88],

$$f(\hat{l}^+) = \frac{1}{\Lambda}\frac{a^{ab}}{\Gamma(ab)}(\eta-1)^{ab-1}\,e^{-a(\eta-1)}\Theta(\eta-1)\,, \tag{4.43}$$

with $\eta = \hat{l}^+/\Lambda$. Here $\Lambda = M_\psi - M$ is of order Λ_{QCD}, and a and b are adjustable parameters of order 1. In our case, we choose $a = 1$ and $b = 2$. Λ was determined so that the first and the second moments of the shape function

$$\begin{aligned}
m_1 &= \int_\Lambda^\infty \mathrm{d}\hat{l}^+\, f(\hat{l}^+) = \Lambda(b+1)\,, \\
m_2 &= \int_\Lambda^\infty \mathrm{d}\hat{l}^+(\hat{l}^+)^2\, f(\hat{l}^+) = \Lambda^2\left(\frac{b}{a} + (b+1)^2\right),
\end{aligned} \tag{4.44}$$

take the value 890MeV and $(985\mathrm{MeV})^2$ respectively.

We show the results of resumming in fig. 23. The short dashed line is the NRQCD decay rate only and the dotted line is the NRQCD decay rate convoluted with the shape function. The thin line includes only the perturbative resummed interpolated decay rates without the convolution with the soft shape function. The solid thick line presenting our final result is the interpolated decay rate convoluted with the shape function in Eq. (4.43). As can be

74

seen, the shape function and the perturbative resummation both result in a softer spectrum. The combination of the two is softer still.

In fig. 24, we compare our results with the experimental data from CLEO [33]. We use the values $m_c = 1.5$ GeV, $m_b = 4.9$ GeV, and $\Lambda_{\text{QCD}} = 0.2$ GeV so that $\alpha_s(2m_b) = 0.1793$. The solid line represents the color-octet interpolated decay rate convoluted with the shape function. The NRQCD matrix element was chosen to be $\langle \Upsilon | \mathcal{O}_\Upsilon^{\mathbf{1}}[^1S_0] | \Upsilon \rangle = 2.3 \text{GeV}^3$. For comparison, we have used in the plot the same value for the overall strong coupling evaluated at the scale $2m_c$ as in Ref. [83]. The shaded band is obtained by varying the NRQCD color-octet matrix element from 0.003 GeV^3 to 0.014 GeV^3. Since the numerical value of the matrix element $\langle \mathcal{O}_\psi^{\mathbf{8}}[^3S_1] \rangle$ is fixed by experimental data, it has large uncertainties coming both from experiments and theoretical higher order corrections. For comparison, we also show the color-singlet contribution as the dashed line [33, 82]. The complete spectrum involves a combination of the color-octet contribution we calculated here, and the color-singlet component [33, 82] shown in the figure.

The differential rate predicted by the color-octet model is peaked near the end-point region. When convoluted with the shape function, the momentum distribution is shifted to the left but still is close to the kinematic limit. Once we resum the large leading logarithms under the framework of SCET, interpolate the result with the NRQCD prediction, and then convolute with the soft shape function, we find that spectrum is significantly softened near the endpoint and the peak is pushed further to the left, in better agreement with the data. We note here that if we use a high scale for the overall coupling constant, the color-octet contribution will be much smaller. In order to make a consistent comparison of theory to data, one needs to treat the endpoint of the color-singlet contribution in SCET and NRQCD, which we have not done here and will leave for future work. In the perturbative expansion, the color-singlet process is suppressed relative to the color-octet one by an factor of α_s. However, there is a large enhancement due to kinematic factors in the diagram, which can be as large as 360 and provides a huge enhancement to compensate the perturbative suppression [82].

4.5 SUMMARY

In this chapter we studied the color-octet contribution to $\Upsilon \to J/\psi + X$ near the kinematic endpoint. In this regime, the usual NRQCD factorization formalism breaks down due to large perturbative and nonperturbative corrections. We combined the usual NRQCD effective theory with SCET, which contains the correct physical degrees of freedom, to derive a factorizatioin theorem for the differential decay rate, $d\Gamma/dy$, valid in the endpoint region. This also allows us to resum large logarithms which appear in the endpoint by running the rate from the hard scale to the collinear scale and then to the soft scale using the RGE of the effective theory. At the soft scale, we are left with NRQCD shape functions. Using models for the color-octet shape function, and interpolating away from the endpoint to the leading order NRQCD prediction, we are able to make predictions about the color-octet contribution to the decay rate over the entire kinematic region.

Though a quantitative comparison to data can be made only when including both the color-singlet and color-octet terms, some qulitative conclusions can still be drawn here. We note that once we sum the large leading logarithms using the framework of SCET and convolute with the soft shape function, the spectrum is significantly softened near the endpoint and the peak is broadened and shifted to the left. This effect greatly improves the agreement between the data constraints and the theoretical predictions.

We note here that the hard scale we have chosen in our final results is $2m_c$ the same as in [83]. This scale is much smaller than what we expected from our one loop order corrections. If we used the hard scale μ_H decided by our calculations, the color-octet contribution will be further suppressed. As a result, we expected that the dominant contribution for this process will be from color-singlet rate. Once including higher order effects as well as the feed-down of $\psi(2S)$ and χ_{cJ} to J/ψ [33], the color-singlet decay rate should also be softened. We expected that combining color-singlet and octet contributions will give a good fit to the data.
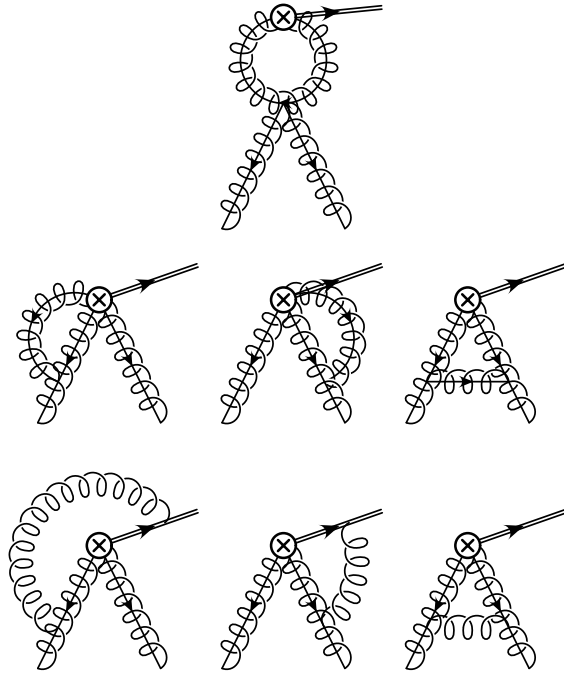
Figure 21: One-loop order diagrams needed to calculate the counterterm to the color-octet operator.The double line presents the J/ψ fields in color-octet configuration while the spring lines are the soft gluons.
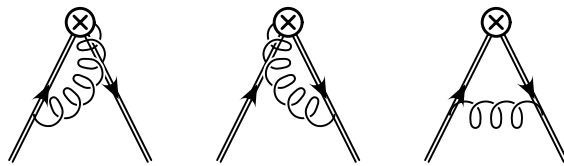

Figure 22: One loop corrections to the J/ψ soft shape function defined in Eq. (4.22).
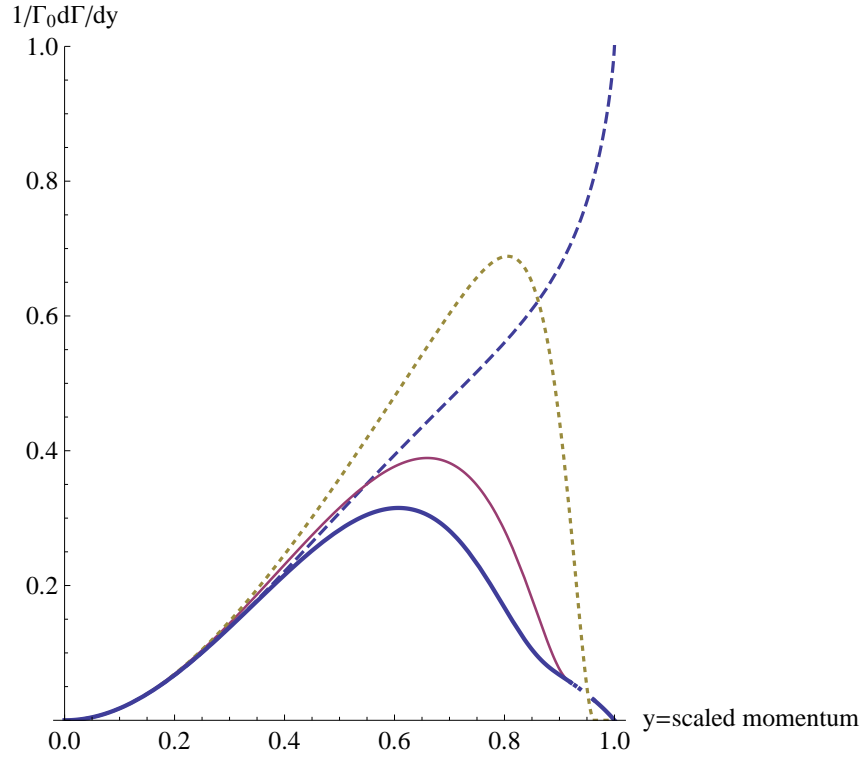
Figure 23: Comparison between the NRQCD results and SCET predictions normalized to the NRQCD decay rate at the end-point. Here $y = p_\psi/p_\psi^{max}$ is the scaled momentum. The short dashed line is the NRQCD decay rate only and the dotted line is the NRQCD decay rate convoluted with the shape function. The solid thin line includes only the perturbative resummed interpolated decay rates without convoluted with the soft shape function. The solid thick line presents the interpolated decay rates convoluted with the shape function.
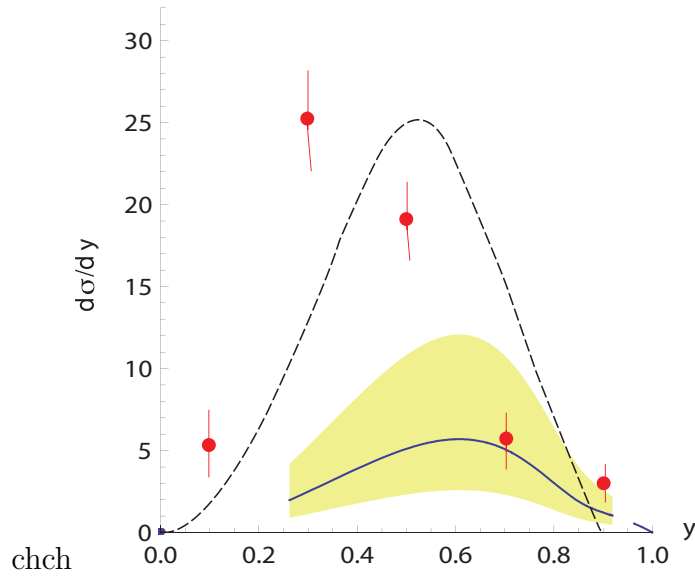
Figure 24: Comparison of the color-octet contribution to the differential rate to the data from CLEO [33]. The solid thick line presents the interpolated decay rates convoluted with the shape function with a choice of $\langle \mathcal{O}_\psi^{\mathbf{8}}[^3S_1] \rangle = 6.6 \times 10^{-3} \mathrm{GeV}^3$ [16]. The shaded band is obtained by varying $\langle \mathcal{O}_\psi^{\mathbf{8}}[^3S_1] \rangle$ from $0.003 \mathrm{GeV}^3$ to $0.014 \mathrm{GeV}^3$ [89]. Here, we also show the color-singlet contribution in long dashed line [33, 82]. The complete spectrum will involve a combination of both the color-octet and color-singlet contributions.

5.0 CONCLUSIONS

In this thesis, we explore the possibility to apply SCET to heavy quarkonium decay and production precesses. Conventional approach to these topics is rooted in the NRQCD mechanism including the NRQCD factorization theorm. However, as we have seen in this thesis, NRQCD alone is not sufficient to give a full explanation for the quarkonium decay or production spectrum over the entire kinematic range. In specific regions, especially near the phase space boundaries, collinear degrees of freedom emerges that are not captured by NRQCD and SCET comes into play. Focusing on J/ψ production in e^+e^- annihilation and Υ decay, we demonstrate the power of SCET in deriving the factorization theorems as well as resumming the large Sudakov logarithms for saving the perturbative calculations in quarkonium physics. it is hopefully clear that the predictions with SCET are much better than the one with NRQCD only when comparing with the experimental data.

BIBLIOGRAPHY

[1] A. Pich, Rep. Prog. Phys. **58**, 563 (1995).

[2] A. V. Manohar and M. B. Wise, 'Heavy Quark Physics', Cambridge University Press, New York, 2000.

[3] G. T. Bodwin, E. Braaten and G. P. Lepage, Phys. Rev. D **46** 1914 (1992).

[4] K. Nakamura *et al.* (Particle Data Group), JPG **37**, 075021 (2010).

[5] C. W. Bauer, S. Fleming and M. Luke, Phys. Rev. D **63**, 014006 (2001).

[6] C. W. Bauer, S. Fleming, D. Pirjol and I. W. Stewart, Phys. Rev. D **63**, 114020 (2001).

[7] C. W. Bauer and I. W. Stewart, Phys. Lett. B **516**, 134 (2001).

[8] C. W. Bauer, D. Pirjol and I. W. Stewart, Phys. Rev. D **65**, 054022 (2002).

[9] L. D. Faddeev and V. N. Popov, Phys. Lett. B **25**, 29 (1967).

[10] D. J. Gross, F. Wilczek, Phys. Rev. Lett. **30**, 1343 (1973), H. D. Politzer, Phys. Rev. Lett. **30**, 1346 (1973).

[11] S. Bethke, Prog. Part. Nucl. Phys. **58**, 351 (2007).

[12] P. R. Feynman, Phys. Rev. Lett. **23**, 1415 (1969).

[13] L. D. Landau, Nucl. Phys. **13**, 181 (1959).

[14] S. Coleman and R. E. Norton, Nouvo Cimento **38**, 438 (1965).

[15] J. C. Collins, D. E. Soper and G. Sterman, arXiv:hep-ph/0409313 (2004).

[16] P. Cho and A. K. Leibovich, Phys. Rev. D **53**, 150 (1996).

[17] P. Cho and A. K. Leibovich, Phys. Rev. D **53**, 6203 (1996).

[18] E. Braaten and S. Fleming, Phys. Rev. Lett. **74**, 3327 (1995).

[19] M. Klasen, B. A. Khiehl, L. N. Mihaila and M. Steinhauser, Phys. Rev. Lett. **89**, 032001 (2002).

[20] T. Daniels *et al.* (CDF Collaboration), Fermilab-Conf-94/136-E (1994).

[21] J. Abdallah *et al.* (DELPHI Collaboration), Phys. Lett. B **565**, 76 (2003).

[22] T. Affolder *et al.* (CDF Collaboration), FERMILABPUB-00-090-E (2000).

[23] C. L. da Silva *et al.* (PHENIX Collaboration), Nucl. Phys. A **830**, 227C (2009).

[24] P. L. Cho and M. B. Wise, Phys. Lett. B **346** 129 (1995); A. K. Leibovich, Phys. Rev. D **56** 4412 (1997); M. Beneke and M. Kramer, Phys. Rev. D **55** 5269 (1997); E. Braaten, B. A. Kniehl and J. Lee, Phys. Rev. D **62** 094005 (2000).

[25] M. Beneke and I. Z. Rothstein, Phys. Lett. B **372**, 157 (1996); **389**, 769(E) (1996).

[26] M. Beneke and M. Kramer, Phys. Rev. D **55**, 5269 (1997).

[27] A. K. Leibovich, Phys. Rev. D **56**, 4412 (1997).

[28] E. Braaten, B. A. Kniehl and J. Lee, Phys. Rev. D **62**, 094005 (2000).

[29] N. Brambilla *et al.*, arXiv:1010.5827v2 (2010).

[30] S. Wolf, Phys. Rev. D **63**, 074020 (2001).

[31] B. Nemati *et al.* (CLEO Collaboration), Phys. Rev. D **55**, 5273 (1997).

[32] S. Catani and F. Hautmann, Nucl. Phys. Proc. Suppl. **39BC**, 359 (1995)

[33] R. A. Briere *et al.* (CLEO Collaboration), Phys. Rev. D **70**, 072001 (2004).

[34] C. W. Bauer, D. Pirjol and I. W. Stewart, Phys. Rev. D **67**, 071502 (2003).

[35] T. Becher, R. J. Hill and M. Neubert, Phys. Rev. D **69**, 054017 (2004).

[36] C. W. Bauer, M. D. Dorsten and M. P. Salem, Phys. Rev. D **69**, 114011 (2004).

[37] D. J. Dugan and B. Grinstein, Phys. Lett. B **255**, 583 (1991).

[38] J. Chay, C. Kim and Y. G. Kim and J. P. Lee, Phys. Rev. D **71**, 056001 (2005).

[39] A. V. Manohar, T. Mehen, D. Pirjol and I. W. Stewart, Phys. Lett. B **539**, 59 (2002).

[40] A. V. Manohar and I. W. Stewart, Phys. Rev. D **76**, 074002 (2007).

[41] C. Lee and G. Sterman, Phys. Rev. D **75**, 014022 (2007).

[42] A. Idilbi and T. Mehen, Phys. Rev. D **75**, 114017 (2007).

[43] C. W. Bauer, D. Pirjol and I. W. Stewart, Phys. Rev. Lett **87**, 201806 (2001).

[44] C. W. Bauer, C. W. Chiang, S. Fleming, A. K. Leibovich and I. Low, Phys. Rev. D **64**, 114014 (2001); S. Fleming and A. K. Leibovich, Phys. Rev. Lett. **90**, 032001 (2003); Phys. Rev. D **67**, 074035 (2003).

[45] S. D. Ellis, A. Hornig, C. Lee, C. K. Vermilion and J. R. Walsh, JHEP **11**, 101 (2010).

[46] T. Becher and M. Neubert, Phys. Rev. Lett. **102**, 162001 (2009).

[47] C. W. Bauer and M. D. Schwartz, Phys. Rev. D **76**, 074004 (2007).

[48] S. Fleming, A. K. Leibovich and T. Mehen, Phys. Rev. D **74**, 114004 (2006).

[49] I. W. Stewart, F. J. Tackmann and W. J. Waalewijn, Phys. Rev. D **81**, 094035 (2010).

[50] T. Becher and M. Neubert, arXiv:1007.4005 (2010).

[51] S. Mantry and F. Petriello, Phys. Rev. D **81**, 093007 (2010).

[52] M. Procura and I. W. Stewart, Phys. Rev. D **81**, 074009 (2010).

[53] X. Liu, arXiv:1011.3872v1 (2010).

[54] A. Jain, M. Procura and W. J. Waalewijn, arXiv:1101.4953v1 (2011).

[55] M. Beneke and V. A. Smirnov, Nucl. Phys. B **522**, 321 (1998).

[56] A. K. Leibovich and X. Liu, Phys. Rev. D **76**, 034005 (2007).

[57] J. J. Aubert *et al.* , Phys. Rev. Lett. **33**, 1404 (1974); J. E. Augustin *et al.*, Phys. Rev. Lett. **33**, 1406 (1974).

[58] G. T. Bodwin, E. Braaten and G. P. Lepage, Phys. Rev. D **51**, 1125 (1995) [Erratum-ibid. D **55**, 5853 (1995)].

[59] M. E. Luke, A. V. Manohar and I. Z. Rothstein, Phys. Rev. D **61**, 074025 (2000).

[60] P. L. Cho and M. B. Wise, Phys. Lett. B **346**, 129 (1995); A. K. Leibovich, Phys. Rev. D **56**, 4412 (1997); M. Beneke and M. Kramer, Phys. Rev. D **55**, 5269 (1997); E. Braaten, B. A. Kniehl and J. Lee, Phys. Rev. D **62**, 094005 (2000).

[61] T. Affolder *et al.* [CDF Collaboration], Phys. Rev. Lett. **85**, 2886 (2000).

[62] K. Abe *et al.* [Belle Collaboration], Phys. Rev. Lett. **89**, 142001 (2002)

[63] B. Aubert *et al.* [BABAR Collaboration], Phys. Rev. D **72**, 031101 (2005).

[64] P. L. Cho and A. K. Leibovich, Phys. Rev. D **54**, 6690 (1996).

[65] S. Baek, P. Ko, J. Lee and H. S. Song, J. Korean Phys. Soc. **33**, 97 (1998).

[66] A. V. Luchinsky, hep-ph/0301190; G. T. Bodwin, J. Lee and E. Braaten, Phys. Rev. D **67**, 054023 (2003); Phys. Rev. Lett. **90**, 162001 (2003); K. Y. Liu, Z. G. He and K. T. Chao, Phys. Lett. B **557**, 45 (2003); E. Braaten and J. Lee, Phys. Rev. D **67**, 054007 (2003); S. J. Brodsky, A. S. Goldhaber and J. Lee, Phys. Rev. Lett. **91**, 112001 (2003); B. L. Ioffe and D. E. Kharzeev, Phys. Rev. D **69**, 014016 (2004); K. Hagiwara, E. Kou, Z. H. Lin, C. F. Qiao and G. H. Zhu, Phys. Rev. D **70**, 034013 (2004); Y. J. Zhang and K. T. Chao, Phys. Rev. Lett. **98**, 092003 (2007); Z. G. He, Y. Fan and K. T. Chao, Phys. Rev. D **75**, 074011 (2007).

[67] K. Abe *et al.* [BELLE Collaboration], Phys. Rev. Lett. **88**, 052001 (2002);

[68] B. Aubert *et al.* [BABAR Collaboration], Phys. Rev. Lett. **87**, 162002 (2001).

[69] E. Braaten and Y. Q. Chen, Phys. Rev. Lett. **76**, 730 (1996).

[70] F. Yuan, C. F. Qiao and K. T. Chao, Phys. Rev. D **56**, 321 (1997).

[71] G. A. Schuler, Eur. Phys. J. C **8**, 273 (1999).

[72] J. H. Kuhn and H. Schneider, Phys. Rev. D **24**, 2996 (1981); Z. Phys. C **11**, 263 (1981); V. M. Driesen, J. H. Kuhn and E. Mirkes, Phys. Rev. D **49**, 3197 (1994); L. Clavelli, Phys. Rev. D **26**, 1610 (1982).

[73] S. Fleming, A. K. Leibovich and T. Mehen, Phys. Rev. D **68**, 094011 (2003).

[74] M. Beneke, I. Z. Rothstein and M. B. Wise, Phys. Lett. B **408**, 373 (1997).

[75] S. Fleming and A. K. Leibovich, Phys. Rev. D **70**, 094016 (2004).

[76] Z. H. Lin and G. h. Zhu, Phys. Lett. B **597**, 382 (2004).

[77] C. W. Bauer, S. Fleming, D. Pirjol, I. Z. Rothstein and I. W. Stewart, Phys. Rev. D **66**, 014017 (2002).

[78] I. Z. Rothstein and M. B. Wise, Phys. Lett. B **402**, 346 (1997).

[79] X. Liu, Phys. Lett. B **685**, 151 (2010).

[80] M. E. Luke, A. V. Manohar and I. Z. Rothstein, Phys. Rev. D **61** 074025 (2000).

[81] T. Affolder et al. [CDF Collabortion], Phys. Rev. Lett. **85** 2886 (2000).

[82] Shi-yuan Li, Qu-bing Xie and Qun Wang, Phys.Lett. B **482** 65 (2000).

[83] Kingman Cheung, Wai-Yee Keung and Tzu Chiang Yuan, Phys.Rev. D **54** 929 (1996).

[84] C. Bobeth, B. Grinstein, and M. Savrov, Phys. Rev. D **77** 074007 (2008).

[85] S. Fleming, A. K. Leibovich, Phys. Rev. D **67** 074035 (2003).

[86] E. Braaten and Y. Q. Chen, Phys. Rev. D **54** 3216 (1996).

[87] S. Fleming, A. H. Hoang, S. Mantry and I. W. Stewart, Phys. Rev. D **77** 114003 (2008).

[88] A. K. Leibovich, Z. Ligeti and M. B. Wise, Phys. Lett. B **539** 242 (2002).

[89] S. Fleming, O. F. Hernandez, I. Maksymyk and H. Nadeau, Phys. Rev. D **55** 4098 (1997).